PROBING MINERAL-BITUMEN LIBERATION USING RHEOLOGICAL MEASUREMENTS

by

LEOPOLDO GUTIERREZ

B.Sc., University of Concepcion, 2001

A THESIS SUBMITTED IN PARTIAL FULFILLMENT OF
THE REQUIREMENTS FOR THE DEGREE OF

MASTER OF APPLIED SCIENCE

in

THE FACULTY OF GRADUATE STUDIES
(Mining Engineering)

THE UNIVERSITY OF BRITISH COLUMBIA

(Vancouver)

May 2009

ABSTRACT

The rheology of oil sand slurries was investigated under different physicochemical conditions in an attempt to establish a correlation between bitumen liberation and slurry rheology. Synthetic mixtures of bitumen with fine quartz of varying bitumen content, as well as actual oil sand ores, were used in all the tests. All rheological measurements were conducted using a rotational viscometer connected to a fixture specifically designed for testing settling suspensions.

The results showed that for both synthetic mixtures and actual oil sand ores the viscosity of the slurries decreases with increasing bitumen liberation. It was found that at low bitumen contents (0 and 1 wt%) the pH of the slurries was the most important parameter that controlled the rheology of synthetic quartz-bitumen slurries. At higher bitumen contents (5 and 10 wt%), it was a combination of high temperature and high pH that gave the lowest viscosities and yield stresses of the model mixtures. The overall results were discussed in terms of aggregation-dispersion phenomena between bitumen and mineral particles. The effect of salts such as NaCl, $CaCl_2$ and KCl on the rheology of synthetic mixtures was found to be small compared to the effects of pH and temperature. Experiments performed on slurries where bitumen was added as an emulsion (no attachment to solids) showed that viscosity was significantly lower compared to a suspension in which bitumen coated the solid particles. Humic acids were tested also in slurries of synthetic bitumen-quartz mixtures at 10 wt% bitumen showing that they produce an important improvement in rheology when they are added at dosages of 100 g/t or higher.

These observations on synthetic ores could qualitatively be used to predict the rheology data for slurries of four actual oil sand ores. In this case, it was also found that the content of very fine particles (% fraction finer than 3 microns) was the most significant variable that clearly correlated with the viscosity of the oil sand ore slurries. Interestingly, under the conditions of high bitumen liberation (high pH and high temperature), no property of the ores (e.g., bitumen content, solids content, presence of material finer than 44 microns) other than the content of the very fine particles produced a pronounced relationship with the rheological results for the oil sand slurries.

TABLE OF CONTENTS

LIST OF TABLES

LIST OF FIGURES

ACKNOWLEDGEMENTS

First of all, I would like to thank Dr. Marek Pawlik for giving me the opportunity of coming to Canada and complete the degree of Master of Applied Sciences in Mining Engineering. Without his supervision and expertise this thesis would not have been completed.

This study was possible through the financial assistance in form of a collaborative research and development grant by the Natural Sciences and Engineering Research Council (NSERC) and Canada Natural Resources Limited (CNRL).

I am particularly thankful of my mate Esau Arinaitwe. His friendship, help and advice with every little detail since before to arrive to this department, were of main significance in completing this goal.

My deepest admiration to my wife Stefania and my daughter Emilia. Their love, encouragement and motivation gave me the force required to complete this thesis.

I would like to thank my parents, Manuel and Dina, and my sister Dina for their love and endless supporting in all the decisions I have taken in my life.

I am grateful of God for allowing me to have a healthy family, great parents, very good friends and for helping me in my whole life.

1 Introduction

1.1 Importance of this study

Processing of oil sand ores can be described as a sequence of seven inter-related stages: mining, conditioning, utilities, extraction, froth treatment, water management and upgrading (Masliyah et al., 2004). A common flow diagram of oil sands processing is shown in Figure 1.1. The first stage consists of mining ores which are afterward transported to a conditioning stage where oil sand lumps are crushed and mixed with warm or hot water, a process which can be carried out in devices such as mixing boxes, stirred tanks, cyclo-feeders or rotary breakers. The slurry is then treated in hydrotransport pipes where bitumen liberation from particles of sand takes place; chemical additives such as NaOH can be added at this point. Once bitumen liberation is achieved, the slurry is transported to an extraction stage where drops of bitumen are recovered by flotation and then upgraded and refined; tailings obtained are treated in order to recover water.

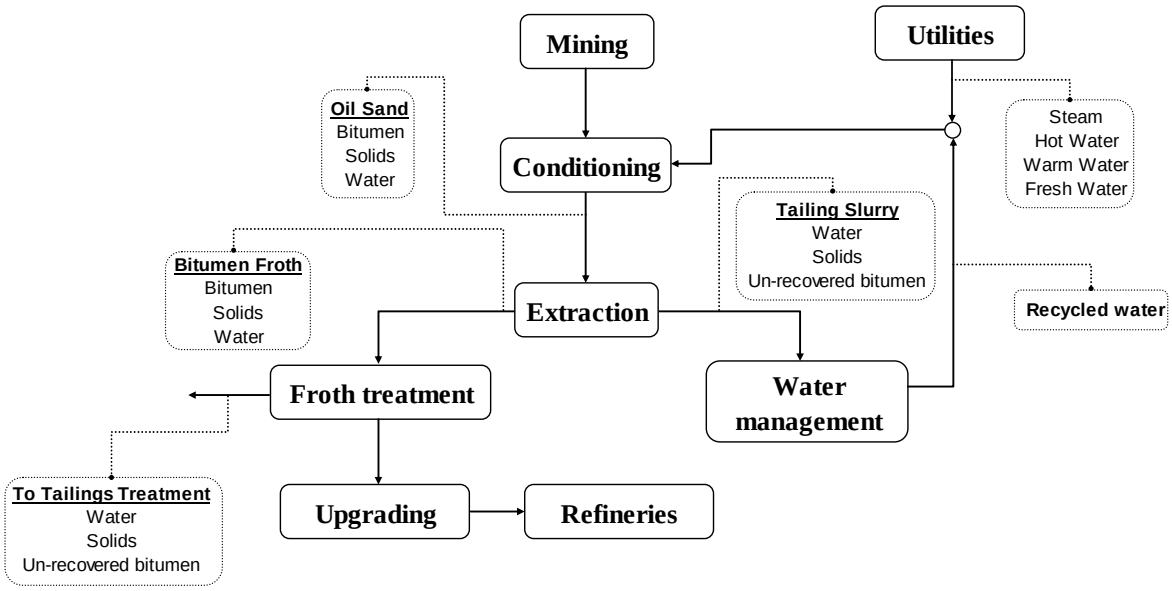

Figure 1.1: Common flow diagram of oil sands processing.

During the process of bitumen liberation the water located between the sand grains and bitumen is displaced, and the bitumen is released as droplets into the carrier fluid (Figure 1.2), which are afterward recovered by flotation.

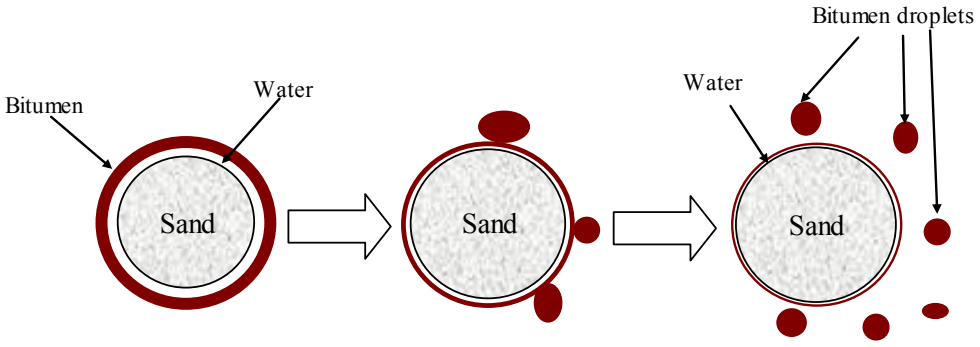

Figure 1.2: The process of liberation of bitumen from the particles of sand.

Masliyah et al. (2004) summarized the most relevant studies carried out in order to determine the variables that most affect bitumen liberation in oil sand ores. According to these authors temperature, pH, water chemistry, ore grade (bitumen content), clays content, particle size and, chemical additives are the most important parameters affecting bitumen liberation. In many works, interactions between bitumen and sand are measured through methods such as displacement of bitumen from glass slides, bitumen pickup tests in a bed of sand (Dai and Chung, 1995) and image analysis under mixing conditions (Wallwork et al., 2004).

It is generally accepted that the performance of every wet unit operation in mineral processing is affected by a rheological parameter. In processing of oil sand ores the hydrotransport stage is probably the most affected by the rheology of the pipelined slurries. Although rheology has such relevance, relationships between slurry rheology and processing of oil sand ores have never been adequately researched, perhaps due to the lack of bench-scale methods and instrumentation. Most of the available rheological studies in the field of oil sands have been conducted in order to understand the behavior of bitumen itself at different conditions.

The present work is focused on obtaining information related to the relationship between slurry rheology and bitumen-mineral interactions based on systematic rheological experiments with oil sand slurries.

1.2 Specific research objectives

To the author's knowledge, this thesis is the first systematic attempt to characterize the rheology of bitumen-mineral mixtures and oil sand ore slurries through bench scale tests. Therefore, the general focus of this study is on determining the effect of the most important physicochemical parameters (pH, temperature) - which are primarily used for process control during bitumen extraction - on the rheology of model and actual oil sand slurries. As an additional outcome, it will also be demonstrated that rheological measurements on oil sand suspensions can reliably be carried out using a rotational viscometer as long as some basic precautions are taken to eliminate the well-known problems with measurements on any solid-liquid suspension.

The specific objectives are:

-to identify the most significant physicochemical parameters (pH, temperature, water, salt type and concentration) that affect the rheology of oil sand ore slurries,

-to demonstrate the existence of a relationship between bitumen liberation from sand/quartz grains and the resulting rheological response,

-to characterize the general rheological behavior of oil sand ore slurries.

2 Literature review

2.1 Rheology of slurries

2.1.1 Definitions

By definition, rheology is the study of deformation and flow of matter (Barnes, 2000). As the slurry is subjected to shear stress, it begins to deform and flow according to some pattern. Shear rate, denoted by the symbol $\dot{\gamma}$, is the velocity gradient established in a slurry as a result of an applied shear stress and is expressed in units of reciprocal seconds, s^{-1}. Shear stress, denoted by the symbol τ, is the stress component and is expressed in units of force per unit area, Pa. From a rheological measurement in a concentric cylinder rheometer, a measurement of the apparent shear rate is obtained, however, in the rest of this thesis we will only use the expression "shear rate".

The ratio between shear stress and shear rate is called apparent viscosity (Equation 2.1) with units of Pa•s. Apparent viscosity is commonly used to characterize slurry rheology and represents the slurry viscosity at a particular shear rate.

$$\eta_{app} = \frac{\tau}{\dot{\gamma}} \qquad (2.1)$$

2.1.2 Flow behavior

The relationship between shear stress and shear rate is referred as a flow curve. The data necessary to plot a flow curve can be obtained from equilibrium and pseudo equilibrium rheological measurements. Equilibrium rheological measurements are done by applying a constant shear rate until shear stress values do not change with time, and then the data is plotted as a flow curve. On the other hand, pseudo-equilibrium rheological measurements are done by changing shear rate and recording the instantaneous shear stress obtained at every shear rate, without necessarily reaching equilibrium between shear stress and shear rate. All the rheological data presented in this thesis correspond to pseudo-equilibrium flow curves, however in order to describe the time dependency behavior of the slurries, all the experiments will be done considering an increase and decrease of the shear rate.

The most common relationships between shear stress and shear rate are shown in Figure 2.1. They can be classified in two main groups: those slurries which show a yield stress that must

be overcome to produce any deformation, and those slurries which do not need an initial energy to start flowing.

The most simple and well known type of behavior is described by the Newton's law. In this case, viscosity although varying with temperature and pressure, does not vary with deformation rate or time (Barnes, 2000) and is equal to the slope of the shear stress-shear rate curve. For Newtonian slurries viscosity is the only rheological parameter required for characterizing the rheological behavior. Slurries that do not follow the Newton's law are generally referred as non-Newtonian fluids.

The next simplest case is the Bingham plastic behavior for which no flow is displayed until the applied shear stress exceeds the yield stress, and thereafter shear stress is proportional to shear rate.

Another case is the pseudoplastic or shear thinning behavior that can exist both in the absence and in the presence of yield stress. These types of slurries show a reduction in apparent viscosity as the shear rate increases. In general, slurries showing asymmetric particle shapes are characterized by this behavior (Klein, 1992).

Dilatancy or shear thickening behavior is also possible in the presence or absence of yield stress. The most important characteristic of these slurries is that shear stress increases with shear rate. This type of behavior is less common than shear thinning and is very typical in quartz slurries (Scott, 1982) and in laterite slurries (Klein, 2009).

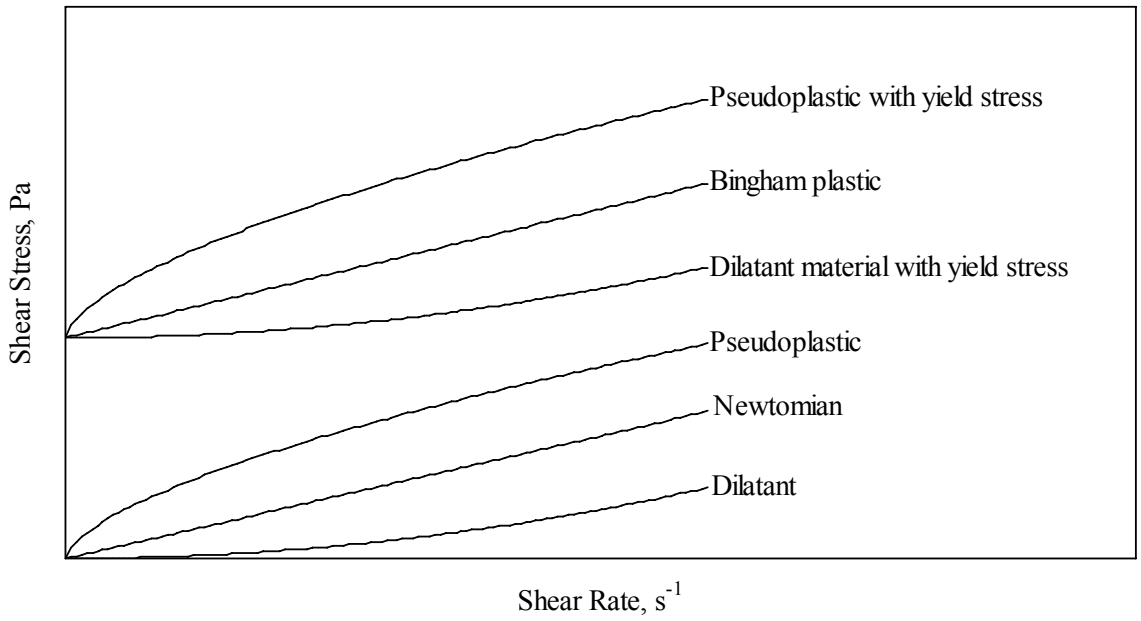

Figure 2.1: Common relationships between shear stress and shear rate.

2.1.3 Flow curve modelling

Several mathematical models have been developed in order to describe the different types of rheological behavior described in the last section.

The flow of Newtonian slurries can be described by the Newton's law of viscosity (Equation 2.2)

$$\tau = \mu\dot{\gamma} \qquad (2.2)$$

Where μ is the coefficient of viscosity.

The power-law or Ostwald-de Waele model (Barnes, 2000) is expressed by the Equation 2.3.

$$\tau = K\dot{\gamma}^{n} \qquad (2.3)$$

Where K is called the consistency parameter and n the power-law index.

In the power-law model, the constant K has units of Pas^n and the power-law index is dimensionless and usually its deviation from unity is a measure of non-Newtonian behavior. For n equal to 1 the model clearly represents the Newton's law. For n greater than 1 shear thickening flow is displayed and for n smaller than 1 the model describes shear thinning flow.

The Bingham plastic model (Equation 2.4) describes the simplest case in which a yield stress is applied before the fluid start flow. Once the yield stress is reached a linear relationship exists between shear stress and shear rate.

$$\tau = \tau_B + \eta_p\dot{\gamma} \qquad (2.4)$$

Where τ_B is the Bingham yield stress and η_p is the plastic viscosity.

The Herschel-Bulkley model (Equation 2.5) is a combination of the power-law and the Bingham plastic models. If the yield stress is zero the equation assumes the form of the power-law model and if the value of n is one, the equation assumes the form of the Bingham plastic model.

$$\tau = \tau_{HB} + K_{HB}\dot{\gamma}^{n} \qquad (2.5)$$

Where τ_{HB} is the Herschel-Bulkley yield stress and K_{HB} and n are as described for the power-law model. The Herschel-Bulkley model fits well the curvature at low shear rates and provides better estimates of the yield stress than Bingham model in this region. Yield stress values obtained from this model are comparable with those determined using direct measurement methods as vane methods (Klein, 1992).

In 1959 Casson proposed a two parameter model (Equation 2.6) based on physical arguments. He proposed that the slurry may form chain-like aggregates which are responsible of the fluid's viscosity. The formation of these aggregates is a result of the inter-particle forces (Casson, 1959).

$$\tau^{1/2} = \tau_{CY}^{1/2} + (\eta_C \dot{\gamma})^{1/2} \qquad (2.6)$$

Where τ_{CY} is the Casson yield stress and η_C is the limiting viscosity at high shear rates.

Some slurries exhibit time-dependent properties for which shearing at a constant rate results either in an increase in shear stress, which is called rheopexy, or in a decrease in shear stress, which is called thixotropy. Both types of behavior are typical of slurries with yield stress, being thixotropy more common than rheopexy. These types of behavior have usually been explained by the breakdown and formation of structure in the suspension which causes a change in viscosity with time. Some authors (Klein, 1992) have characterized the rate of structure breakdown by a rupture-formation kinetic model (Equation 2.7).

$$\frac{d\eta}{dt} = k_f \eta^m - k_r \eta^n \qquad (2.7)$$

Where, k_r and k_f are constants for structure rupture and formation; η is the apparent viscosity at time t; n and m are exponent parameters.

2.1.4 Surface chemistry and rheology

It is generally accepted that there is a direct relationship between the degree of particle aggregation of a concentrated slurry and its rheological behavior (Johnson et al., 2000; Zhou et al., 2001; Leong and Bober, 1990). It must be noted that aggregation is a result of particle-particle bonds due to attractive inter-particle forces that lead to coagulation, and that its opposite term is dispersion. Slurry viscosity is mainly determined by the degree of particle aggregation; when particles in the slurry are well dispersed the rheological behavior is Newtonian; when particles are aggregated the viscosity is increased and some non-Newtonian phenomena as yield stress, shear thinning and time dependency can appear. Scott (1982) suggests that the relatively high viscosity of the slurry is caused by entrapment of fluid into the aggregates, making the effective volumetric concentration of aggregates higher than that of the primary particles. If the effective aggregate concentration is used, the correlation between viscosity and solid concentration is the same for aggregates and for well dispersed particles.

It is well known that the aggregation phenomenon is strongly affected by particle surface charge. High surface charge means strong electrostatic repulsive forces acting between particles which prevent particles from aggregating. A reduction of surface charge to values close zero results in aggregation, a case in which three dimensional structures can be developed in a concentrated suspension producing yield stress.

The effect of surface charge on particle aggregation can be explained using the DLVO theory of colloid stability proposed independently by Derjaguin and Landau (1941) and Verwey and Overbeek (1948). In this theory, the net interaction energy acting between particles is determined by the energy balance of the van der Waals attractive forces, V_A, and the electrostatic repulsive forces, V_R. The net interaction energy, V_N, can be calculated by Equation 2.8:

$$V_N = V_A + V_R \qquad (2.8)$$

For very short distances d between particles, the attractive energy can be calculated by Equation 2.9.

$$V_A = -\frac{AD}{24d} \qquad (2.9)$$

Where, A is the Hamaker constant (typically of the order of 10^{-20} J) and D the particle diameter.

The repulsive energy in Equation 2.8 comes from the electrical charges that exist on particles when they are immersed in a liquid. The most important mechanisms of charging a particle are as follows (Kitchener, 1969):

- **Ionization of surface groups**: some solid surfaces contain acidic or basic groups which can be charged positively or negatively by adjusting the solution pH. In both cases the surface charge can be made zero by changing the pH, which is called point of zero charge (pzc).
- **Differential dissolution of ions from surfaces of soluble minerals**: when a particle of a soluble mineral is placed in water, dissolution takes place until the solubility product of the mineral is satisfied. If there is an excess of anions in the solution the particle surface will release cations into solution in order to satisfy the solubility product, which leads to a negative charge in the particle surface.
- **Isomorphous substitution**: some clays may exchange a structural ion with one of lower valency, producing a negatively surface charge.

- **Charged crystal surfaces**: an example of this mechanism is the case of kaolinite, which contains edges of alumina groups, positively charged (pH<8), and faces of silica groups, negatively charged.
- **Specific ion adsorption**: multivalent ions as well as surfactants and polymers may be specifically adsorbed. The sign of the surface charge depends on the charge of the absorbing entity.

Verwey and Overbeek (1948) proposed an approximate formula for the electrical energy applicable in cases where the electrical double layer around particles is extensive (Kitchener, 1969). Equation 2.10 shows this expression.

$$V_R = 2\pi\varepsilon R\Psi_0^2 \exp(-kd) \qquad (2.10)$$

Where Ψ_0 is the surface potential, ε is the dielectric constant of the medium, R is the radius of the particle and k is the Debye-Hückel parameter which is directly proportional to the square root of the ionic strength of the medium.

Finally, the total interaction energy can be expressed by Equation 2.11.

$$V_N = -\frac{AD}{24d} + 2\pi\varepsilon R\Psi_0^2 \exp(-kd) \qquad (2.11)$$

Figure 2.2 shows the value of V_N (from Equation 2.11) as a function of the separation distance between particles and surface potential. It must be pointed out that the positive total interaction energy means a repulsive force, and negative total interaction energy corresponds to a net attractive force. It can be seen that at a high surface potential, repulsive forces are dominant over a wide separation distance range, and attractive forces only appear when particles are very close; in this case creating an aggregate of two particles needs to overcome an energetic barrier. On the other hand, attractive forces are dominant at low surface potentials and there is a high probability of generating aggregates.

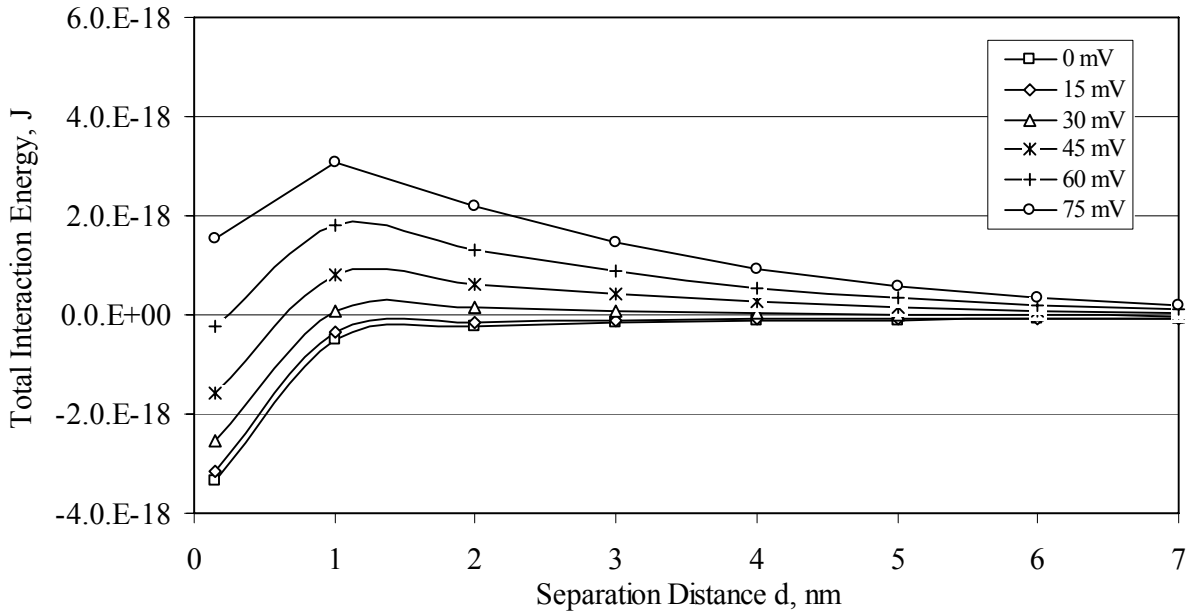

Figure 2.2: Total energy of interaction between two particles as a function of the separation distance and surface potential. Particle size 300 nm, permittivity of water 6.95×10^{-19} F/nm, Hamaker constant 2×10^{-20} J, Ionic strength (I) 0.02 mol/dm^3 ($k=3.2881 \times I^{0.5}$ where k is the Debye-Hückel parameter).

Even when the surface charge can be measured, what is commonly used to describe the colloidal behavior of particles is the zeta potential. The zeta potential can be defined as the work needed to bring a unit charge from infinity to some point at a distance d from the surface of the particle, where a compact layer of counter ions that cover the particle and move with it through the liquid carrier ends. By definition, the isoelectric point is the pH in which the zeta potential of a system is zero.

2.2 Rheology and surface chemistry of quartz

Savarmand et al. (2003) describe the behavior of silica at pH values greater than 2 by the equilibrium between silanol groups (-SiOH) and acid or base ions present in solution. According to these authors the addition of a base changes a fraction of neutral silanol groups to negative groups according to reaction 2.12.

$$-\mathrm{SiOH} + \mathrm{OH}^- \Leftrightarrow -\mathrm{SiO}^- + \mathrm{H_2O} \qquad (2.12)$$

Production of negative groups continues until the above equilibrium is reached. The decrease in pH from its natural value of around 6.5 has two effects; the first one is an increase in free ions in solution and the second and most important effect is the neutralization of some of the $-SiO^-$ groups to silanol according to reaction 2.13.

$$-\mathrm{SiO}^- + \mathrm{H_3O}^+ \Leftrightarrow -\mathrm{SiOH} + \mathrm{H_2O} \qquad (2.13)$$

Selected investigations regarding to rheology and surface chemistry of quartz suspensions are summarized in the following pages.

Scott (1982) studied the effect of surface charge on the rheology of concentrated aqueous quartz suspensions using particles 95 wt% finer than 8 μm. This author found that the zeta potential of quartz approaches 0 mV at pH 2.0 and that an increase in pH results in a decrease in zeta potential to about -70 mV at pH 10.0. No yield stress was observed under alkaline conditions, even at the highest solid concentration tested of 50 v/v%. At pH 6.4-7.2 yield stress was observed at 50 v/v%, and under acid conditions of pH 2.0-2.7 yield stress was observed at all solid concentrations tested which were between 10 and 52 v/v%. Rheological flow curves obtained from this study showed shear thickening behavior. Experimental results were compared with those obtained using the Thomas equation (relationship between viscosity and solid concentration) finding that when effective concentration is used the Thomas equation fit the experimental data well.

Lee et al. (1999) studied the rheological behavior and phase stability of concentrated silica slurries by examining the effects of particle size and temperature. Silica particles were stabilized by adsorption of a silane coupling agent, γ-methacryloxypropyl triethoxy silane (MPTES) and tests were done at a solid concentration range of 50-55 v/v%. The results showed a very significant level of shear thinning between shear rates of 0 and 450 s^{-1}. Shear thickening was

observed for shear rate values greater than 440 s^{-1}. An important reduction in viscosity was achieved as temperature was increased in 30 °C.

Using Couette and vane geometries, Savarmand et al. (2003) studied the effect of pH as well as the addition of electrolyte on the rheological behavior of concentrated aqueous slurries of nearly spherical silica particles of 0.29 μm. Slurries in deionized water without addition of any acid, base or electrolyte showed the largest apparent yield stress and shear viscosity. The addition of acid, base and KCl resulted in a significant decrease in yield stress as well as apparent viscosity. The lowest values of viscosity were obtained at high pH, and at the same pH the addition of KCl resulted in more aggregation and higher viscosities. These authors interpreted their results in light of the DLVO theory and the compression of the double layer around solid particles. Shear thickening was observed again for quartz suspension of 40 v/v% solids concentration. Measurements of the zeta potential were done in deionized water and in the presence of KCl; in the first case the zeta potential was close to zero at pH 2.0 and -35 mV at pH 6.0 while in the presence of 0.01M KCl the zeta potential was -15 mV at pH 2.0 and -35 mV at pH 6.0.

Ma and Pawlik (2005) investigated the effect of cesium, potassium, sodium and lithium on adsorption of natural guar gum onto particles of quartz of maximum size of 13.8 μm and mean size of 2.3 μm. According to this study, the zeta potential of quartz was more negative in the presence of sodium than in the presence of potassium which implies a lower degree of aggregation when sodium is in solution.

Fagan and Zukoski (1997) studied the rheological properties of aqueous slurries of silica particles of diameters ranging from 0.117 μm to 0.780 μm as a function of volume fraction, ionic strength and solution chemistry. Results obtained from this work show that dense aqueous slurries display similar behavior with yield stress in the limit of low shear rate, shear thinning as the stress was raised and, above a critical volume fraction, shear thickening. When the continuous phase viscosity was increased by suspending particles in a glycerin solution, no evidence of yield stress or ordering was observed. These suspensions became less viscous with increasing stress to a minimum viscosity, afterward thickening occurred in smooth transition.

Using a Couette geometry, Franks et al. (2000) studied the rheology of concentrated, nearly monodisperse and spherical silica and alumina slurries. They found that dispersed silica suspensions showed shear thickening above a critical shear rate. As pH is adjusted farther away from the isoelectric point, the critical shear rate increases. At pH far from the isoelectric point the

addition of salt decreases the critical shear rate. Thus, shear thickening not only depends upon hydrodynamic interactions but also on surface forces, in particular repulsive inter-particle forces. An increase of the magnitude and range of repulsive forces increases the shear stress at which shear thickening begins. Reducing the magnitude of repulsive forces allows particles to be more easily forced into clusters resulting in shear thickening.

Franks (2002) studied the behavior of the zeta potential and yield stress of silica slurries over a range of monovalent electrolyte concentrations. The counter-ions investigated were Li^+, Na^+, K^+ and Cs^+, while the co-ion was always Cl^-. Franks found that poorly hydrated ions like Cs^+ and K^+ adsorb in greater quantity onto the silica surface than well-hydrated ions like Li^+ and Na^+, and produce less negative zeta potentials at high pH. This author suggested that at high electrolyte concentrations and low pH the poorly hydrated ions adsorbed in a great enough quantity to reverse the sign of zeta potential from negative to positive. The specific adsorption of counter-ions shifts the isoelectric point (iep) to higher values, which is directly related to the hydration of the counter-ion. Rheological measurements showed that yield stress increases in the order $Li^+ < Na^+ < K^+ < Cs^+$. The magnitude of yield stress correlates well with the amount of adsorbed ions. The greatest yield stresses were observed with the least hydrated ions. According to Franks (2002) the values of yield stress measured at high pH and high salt concentrations are greater than those that can be accounted for from just van der Waals forces of electrostatic attraction. An attractive ion-ion correlation force is presumed responsible for the additional attraction necessary to explain the observed results.

Farrow et al. (1989) studied the rheological behavior of concentrated slurries of 70 wt% of relatively coarse particles of crushed quartz of a mean size of 11 μm, in solutions containing various metal chlorides. The apparent viscosity of these settling suspensions measured with a settling viscometer was compared with the zeta potential, degree of aggregation, sediment volume and degree of hydration of the metal cation. According to this study as salt concentration increases and suspensions coagulate, their viscosity increases. However, slurries that were completely aggregated showed large variations in apparent viscosity at 100 s^{-1}, depending on the particular metal cation in the salt solution. Viscosities increased in the order $Li^+ < Na^+ < K^+ < Cs^+$ and $Mg^{2+} < Ca^{2+} < Ba^{2+}$. These trends were attributed to an increase in attractive forces between colliding particles resulting from a decrease in the degree of hydration of particle surfaces as a result of adsorption of cations from solution.

Rodriguez and Araujo (2006) studied the effect of temperature on the zeta potential of quartz particles finer than 44 μm, specific surface area of 1.25 m^2/g, and using a solution of 0.01M NaCl. They found that the zeta potential became more negative as temperature was increased from 20 to 45 °C. At high pH the decrease rate with temperature for quartz was -2.3 mV/°C. At alkaline pH, it was found that an increase in temperature caused significant changes in the final zeta potential values. At low pH, temperature has a minor effect on the zeta potential. This same decreasing trend of the zeta potential with temperature was observed in previous works by Somasundaran and Kulkarni (1973), and Ramachandran and Somasundaran (1986).

2.3 Behavior of the bitumen-solid system

A typical oil sand ore, as those obtained from the Athabasca oil sands deposits in Alberta, usually contains 6-14 wt% bitumen, which is the oil component, 80-85 wt% mineral solids, which correspond to 90 wt% quartz and 10 wt% clays such as kaolinite, illite, and some montmorillonite, and finally water (Liu et al., 2004-2004b). It must be pointed out that kaolinite is the main type clay in oil sand ores (Tu et al., 2004).

For practical purposes oil sand ores are typically defined as "good processing ores" when bitumen content is greater than 10 wt% and the fraction of sand particles finer than 44 μm is smaller than 20 v/v%. On the other hand a "poor processing ore" has less than 10 wt% bitumen and the fraction of sand particles finer than 44 μm is greater than 20 v/v%.

The single most characteristic feature of the Alberta oil sands, and almost certainly the most fortunate, is that the mineral grains are water wet or hydrophilic. Otherwise the hot water extraction process would not work at all. The oil in the pores is not in direct contact with mineral grains because each grain of sand is surrounded by a film of water. Some authors postulate that the water film is stabilized by electrostatic forces arising from the electrical double layers at the water/sand and oil/water interfaces (Masliyah et al., 2004).

From a fundamental point of view, bitumen recovery from oil sands using the water-based extraction processes involves the following steps (Masliyah et al., 2004):

I. Lump size reduction which takes place in tumblers or hydrotransport pipelines. Hot or warm water is added at this point and the heated outer lump surface is sheared away from the lump. A reduction of bitumen viscosity is also obtained. Bitumen acts as the glue that holds an oil sand lump together.
II. Bitumen liberation from sand grains. The rate of bitumen liberation depends on the balance between forces pulling the bitumen away from the sand grains and forces of bitumen adhering to the grains. This step is affected by temperature, mechanical agitation, chemical additives and interfacial properties.
III. The liberated bitumen once disengaged from sand grains attaches to an available air bubble.
IV. The aerated bitumen floats and is consequently recovered as bitumen froth.

The entire bitumen extraction process is controlled by physical, chemical and hydrodynamic variables, with the interfacial properties being the most important factor in achieving a successful bitumen recovery from oil sand ores (Masliyah et al., 2004). It must be pointed out that the present work focuses on the bitumen liberation stage.

2.3.1 Bitumen-quartz interactions

Bitumen is a very viscous form of oil. Its electrokinetic behavior in aqueous emulsions and suspensions is mainly governed by the presence of polar groups. Some qualitative descriptions of surface charges at the bitumen/water interface have been offered. The ionizable surface group model can be adopted to explain the electrical properties of the bitumen/water interfaces (Masliyah et al., 2004). This model assumes that the charge of the bitumen/water interface comes from the dissociation of carboxylic groups; this would reasonably explain the effect of pH and calcium ions on bitumen displacement from sand grains.

From the point of view of oil sands processing, Masliyah et al. (2004) reported that the most important variables in achieving bitumen liberation from sand particles are: temperature, pH, presence of monovalent and divalent cations, and quality of oil sands ores (bitumen grade and particle size).

The following studies summarize the most important conclusions concerning the effect of temperature on the process of bitumen liberation.

Wallwork (2003) found that poor processing ores can reach better bitumen liberation at high temperature. The same author made further experiments in order to confirm his previous observations, finding that at a temperature of about 37 °C bitumen liberation from a glass slide is much faster than at 20 °C.

Wallwork et al. (2004) used a laboratory scale hydrotransport extraction system to investigate the effect of temperature on bitumen liberation. Their experiments showed that low temperatures have a negative impact on bitumen liberation for both high and low fines ores.

Dai and Chung (1995) studied bitumen-sand interaction as a function of pH, sand particle size, temperature and solvent addition. They found that increasing the temperature not only reduces the viscosity of bitumen to facilitate bitumen liberation, but also increases the electrostatic repulsion between sand and bitumen. This is confirmed by the DLVO theory and is in agreement with some batch extraction results that these authors obtained using actual oil sand ores.

Long et al. (2007) found that temperature affects nearly all properties of oil sands among which bitumen viscosity and bitumen-solids adhesion show an important impact on bitumen recovery. These authors suggest that there is a critical operational temperature of 35 ºC below which bitumen recovery severely deteriorates.

Regarding the effect of pH, Masliyah et al. (2004) summarized several studies on the micro-disintegration of oil sand lumps. When an aggregate from a good processing ore is immersed in NaOH solution at pH 11.8, bitumen liberation is faster than at lower pH. Measurements of the contact angle of bitumen in an aqueous phase were also used to evaluate bitumen liberation. In these studies a glass slide was coated with a bitumen layer and immersed in an aqueous solution containing chemicals and fine clays at a given pH (a small contact angle means good liberation). It was found that the solution pH has the most important effect in enhancing bitumen liberation from the glass slide at a given temperature.

Dai and Chung (1995) found that sand particles can be easily detached from a bitumen surface at pH higher than 6.0. At pH lower than 6.0, strong attachment between bitumen and sand was observed.

Liu et al. (2003), using direct force measurement between bitumen and silica, confirmed that bitumen liberation from sand grains is difficult at pH below 7.0 due to the strong adhesion forces between bitumen and silica.

Regarding the electrokinetic behavior of bitumen, Liu et al. (2003) also measured the zeta potential of bitumen as a function of pH in the presence of different amounts of calcium. From Figure 2.3, it is clear that the zeta potential of bitumen becomes increasingly more negative with increasing the solution pH, and that addition of calcium ions tends to move bitumen zeta potential closer to zero.

According to Liu et al. (2003, 2004b) the zeta potential for model silica fines and kaolinite clays responds to changes in pH and calcium addition in a similar manner as bitumen.

Liu et al. (2005) found that the Hamaker constant of interaction between two bitumen surfaces is around 100×10^{-21} J. These authors explained that hydrophobic forces lead to strong bitumen-bitumen interactions and that a way to reduce these forces would be to add surfactants to make bitumen less hydrophobic. It must be pointed out that the Hamaker constant for silica is around 0.5×10^{-20} J (Franks, 2002) and for alumina is around 5.2×10^{-20} J (Franks et al., 2000). Comparing values of the Hamaker constant of silica, alumina and bitumen it is possible to conclude that if pure particles of these solids were coated with bitumen, attraction forces between

bitumen-coated particles should be stronger and suspension viscosity should be higher compared to interactions and suspension viscosity for pure particles in the absence of bitumen.

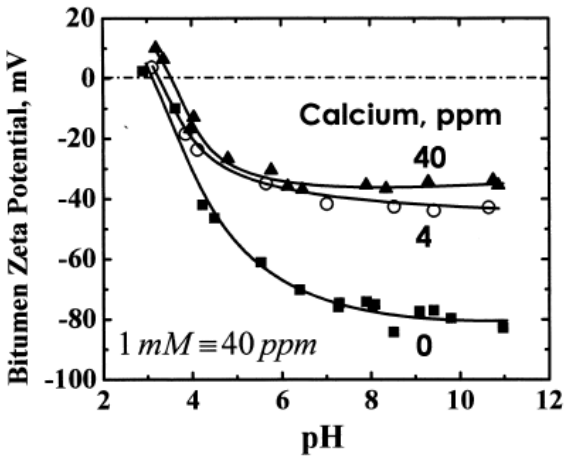

Figure 2.3: Variation of the zeta potential of bitumen with pH and calcium according to Masliyah et al., 2004. (With Permission)

When analyzing the interactions between bitumen and silica in oil sand slurries, both the colloidal and adhesion forces have to be considered (Masliyah et al., 2004). Colloidal forces are defined as forces acting before any contact between the interacting bodies, and adhesion forces appear when bodies bond together. A generalized diagram based on the measurement of interaction forces between bitumen and silica is given in Figure 2.4. It can be seen that at pH below 7.0, adhesion forces are very strong and at the same time repulsive forces are very weak, which would explain the experimentally observed coagulation of bitumen with silica at low pH. Therefore, it should be difficult for bitumen to be liberated from sand grains at a slurry pH below 7.0.

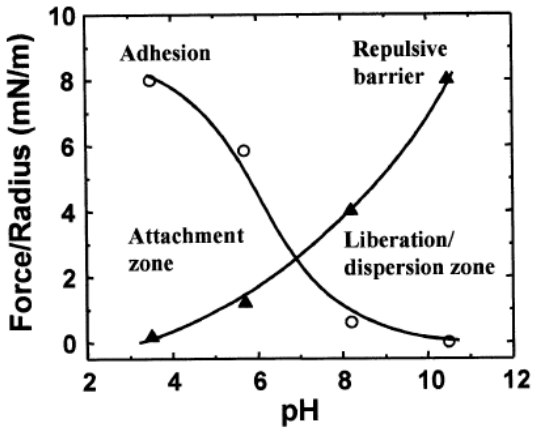

Figure 2.4: Coagulation and dispersion for bitumen-silica in the presence of 0.001M KCl. No calcium ions are present. (Masliyah et al., 2004). (With Permission)

Several studies investigated the effect of sodium, whose concentration in the extraction process may reach 1,000 ppm, on various interfacial phenomena involved in oil sands processing.

Masliyah et al. (2004) summarized studies from several authors whose results show that at pH 8.2 the addition of NaCl increases the contact angle (poor liberation) between a bitumen layer and a glass slide only when the concentration of the salt was near 16,000 ppm. However, with the addition of a Methyl Isobutyl Carbinol/kerosene mixture, the static contact angle could be restored to a value close to the case without NaCl addition (Basu et al., 1998). Other studies found that a sodium concentration below 10 mM would not cause coagulation, while a sodium concentration higher than 50–75 mM would reduce bitumen recovery; this theory was tested after finding that in some cases adding 5 mM of sodium ions as NaCl remarkably reduces bitumen recovery; in other cases, bitumen recovery was not affected up to 150 mM (3,450 ppm) of sodium ion addition (as $NaHCO_3$).

Concerning the effect of potassium ions, Wallace et al. (2004) found that high levels of soluble potassium in oil sand slurries, which appear to be a marker for degraded illite or smectitic clays, are associated with depressed bitumen recovery.

Masliyah et al. (2004) summarized some studies that show that in the presence of multivalent metal ions, zeta potential of silica changes in an unusual manner with pH, changing from negative to positive values when the slurry pH approaches or becomes higher than the pH for the formation of the corresponding metal monohydroxyl ions. Other works found that in the presence of calcium ions a strong coagulation between silica and bitumen is obtained at pH even greater than 10.5.

Liu et al. (2004) studied the effect of calcium ion and montmorillonite on both dynamic and static contact angles during bitumen droplet recession on a glass slide. Additions of calcium ion and montmorillonite clay increase the bitumen static contact angle as compared with the case without additives, thus indicating poor bitumen liberation from the glass slide. The presence of multivalent cations (e.g. Ca^{2+}) dramatically inhibit the ability of NaOH solution (pH = 11.8) to cause detaching of bitumen from the glass slide. These results suggest a negative impact of calcium on bitumen liberation and oil sand lumps processing. This finding is in agreement with suggestions made by other authors who observed that the presence of calcium ions significantly reduces the receding rate of bitumen/liquid/solid three phase contact line (Masliyah et al., 2004).

Kasongo et al. (2000) studied the effect of multivalent cations on the processability of different oil sand ores by using batch bitumen flotation tests in presence of 1 wt% clays (kaolinite, illite or montmorillonite) and/or 1 mM Ca^{2+} or Mg^{2+} ions as chloride salts. They found that the presence of calcium up to 40 ppm or clay at 1 wt% alone has a marginal effect on bitumen recovery, however, a sharp reduction in bitumen recovery was obtained when both calcium (> 30 ppm) and montmorillonite at 1 wt% were added together.

Dai and Chung (1995) studied the bitumen-sand interactions as a function of particle size. They found that bitumen-sand interactions are also particle-size dependent; the finer the particles, the stronger the attachment. The detachment of bitumen from coarse particles can be easily achieved by increasing the alkalinity of the solution, but not for fine particles, indicating that the particle size is one of the critical factors affecting bitumen liberation.

Using an on-line image analysis technique Luthra (2001) and Wallwork et al. (2003) evaluated the degree of bitumen liberation from oil sand ores. They found that a good processing ore containing a small amount of fines gave a much faster bitumen liberation rate than a poor processing ore containing a large amount of fines. These results suggest that one of the reasons for poor processability of high-fines ores may be related to the slow bitumen liberation rates.

The most successful image analysis techniques for analyzing bitumen liberation, such as those used by Wallwork (2003) and Luthra (2001), are applicable to slurry systems that give a clear contrast between bitumen and mineral/quartz particles, and such methods are most applicable to relatively dilute suspensions. However, more concentrated oil sand slurries containing a large fraction of fine non-settling particles are completely optically-opaque, and dispersion or aggregation phenomena in such systems can only be probed through rheological measurements.

2.3.2 Bitumen-clay interactions

Liu et al. (2002) used a novel technique to investigate the interactions between bitumen and clays in an aqueous solution from the measurement of zeta potential distributions to investigate the behavior of emulsified bitumen and montmorillonite clay suspensions in a 1 mM KCl and 1mM Ca^{2+} solution at pH 8.0. They found that montmorillonite particles are strongly attracted to bitumen surfaces. However, when measurements with kaolinite clays were conducted in the presence of calcium, two distinct peaks were observed. This result indicates that there is no coagulation between kaolinite clays and bitumen in the presence of calcium. Two peaks were

also obtained for two types of clays in the absence of calcium. This suggests that in the absence of calcium, there is no hetero-coagulation between bitumen and montmorillonite or kaolinite clays (Liu et al., 2002). It must be clarified that these experiments were done in an emulsified system where adhesion forces are not predominant.

Liu et al. (2004) studied colloidal interactions between bitumen and fines extracted directly from good and poor processing ores. They found that fines from poor processing ores are more hydrophobic than those from good processing ores, but their electrokinetic characteristics are essentially the same. Therefore, attachments of fines from a good processing ore to bitumen surfaces are negligible. Calcium addition showed little enhancement in coagulation of the fines with bitumen. They found also that there was a strong attachment of fines from poor processing ores to bitumen surfaces and significant modification in the zeta potentials of emulsified bitumen were observed for poor processing ores. In this case, calcium addition enhanced coagulation of fines with bitumen. According to these authors, electric double layer forces are the dominant component in the long range forces between bitumen and fines from good processing ores, while both electric double layer forces and hydrophobic forces are the dominant components of the long range forces between bitumen and fines from poor processing ores.

Wallace et al. (2004) found that when the minus 44 μm fines content of oil sands is higher than 10 v/v%, the first signs of a significant deterioration in extractability were noted. Above 20 v/v% fines, the incidence of very low recoveries increases dramatically.

Tu et al. (2004) found that particle size fraction below 3 μm and its ultra-fine component below 0.3 μm are of particular interest too.

2.3.3 Humic acids

Humic acids (HA) are the most widespread natural polyelectrolytes in all terrestrial and aquatic environments (Terashimaa et al., 2004). They originate from degradation of plant polymers. From the chemical point of view, HA are composed of a hydrophilic part (carboxylic acid groups are placed at ends of polymer segments) and a more hydrophobic part than the carboxylated segments, giving to the HA characteristics of an amphiphile (Gamboa et al., 2006). Humic acids behave like weak-acid polyelectrolytes and they can associate with different molecules by electrostatic and/or hydrophobic interactions (Gamboa et al., 2006). In this thesis, it is proposed that in the presence of bitumen, HA should be adsorbed onto bitumen surfaces due to the strong hydrophobic forces involved, and make bitumen surface more hydrophilic. This means

that bitumen should become more able to interact with water than with quartz surfaces, enhancing bitumen liberation and reducing slurry viscosity. However, it must be pointed out that if bitumen is too hydrophilic then bitumen flotation recovery will be poor.

3 Experimental program

3.1 Experimental conditions

As mentioned in section 2.3, a typical oil sand ore contains on average 10 wt% bitumen, 80 wt% of solids and 10 wt% of water. Solids are composed of 90 wt% quartz and 10 wt% clays, of which kaolinite is the most important.

In this thesis, rheological measurements with two different types of slurries were done:

- Quartz slurries: measurements were done using pure quartz and bitumen-coated quartz (synthetic oil sand ores) slurries.
- Actual oil sands ores slurries: suspensions prepared with four different types of actual oil sand ores were tested.

Testing conditions of rheological measurements were:

- Temperature: values range between 25 and 50 °C, where 50 °C represents the temperature of an oil sand process and 25 °C was chosen in order to perform a test a low temperature condition.
- pH: pH tested were natural pH (7-8), 8.5 and 10.5. Typical values of pH in industrial operations range between 8.5 and 10.5. Natural pH was chosen as a base case.
- Solids concentration: pure quartz slurries were tested at 35 and 45 wt% solids, and actual oil sand ores slurries at 45 wt% solids. It must be noted that the solids content was calculated based on the combined mass of minerals, water and bitumen.
- Salts concentration: NaCl and KCl concentrations were 0.01M; $CaCl_2$ concentration was 0.001M. These concentrations are very similar to those reported for typical industrial operations (Masliyah et al., 2004).
- Bitumen concentration: bitumen concentrations of 1, 5 and 10 wt% were tested for bitumen-coated quartz. It must be pointed out that bitumen concentration was calculated based on the combined mass of minerals and bitumen.
- Humic acids: some experiments with bitumen-coated quartz ore at 10 wt% bitumen were done with addition of humic acids at concentrations of 100 and 200 g humic acid per ton of ore.
- Bitumen emulsion: some experiments with a mixture of quartz and a bitumen emulsion were done in order to simulate a suspension where bitumen is fully liberated. In these tests bitumen was added in order to meet a bitumen concentration of 1 wt%. Higher bitumen

concentrations were not tested because of the difficulty for preparing more concentrated emulsions of bitumen.

Table 3.1 shows the experimental tests considered in this thesis.

Table 3.1: Experimental conditions. (1) Calculated on mass of solid+bitumen+water (2) Calculated on mass of solid+bitumen+water (3) Testing conditions for bitumen-coated quartz (4) Humic acids were tested with a slurry of bitumen-quartz mixture at 10 wt% bitumen.

	Bitumen	**T**	**pH**	**Solid Concentration**	**NaCl, KCl**	**$CaCl_2$**	**Humic Acid**
Slurry	**wt%(1)**	**°C**		**wt%(2)**	**mol/L**	**mol/L**	**g/t**
Quartz	0-1-5-10	25-35-50	Natural-8.5-10.5	35-45(3)	0-0.01	0-0.001	100-200(4)
Actual Ores	Variable	25-50	Natural-10.5	45	0.01 NaCl	0.001	-

3.2 Materials

3.2.1 Equipment

Rheological measurements were conducted using a Haake Rotovisco VT550 rotational viscometer which was connected to an elongated fixture (Klein, 1992; Klein et al., 1995) specifically designed to measure properties of suspensions likely to settle. The elongated fixture consists of a concentric cylinder, bob-in-cup, and double-gap arrangement with gap sizes of 2.5 mm and 3.03 mm for the inner and outer gaps respectively. Figure 3.1 shows a representation of the elongated fixture utilized in this thesis.

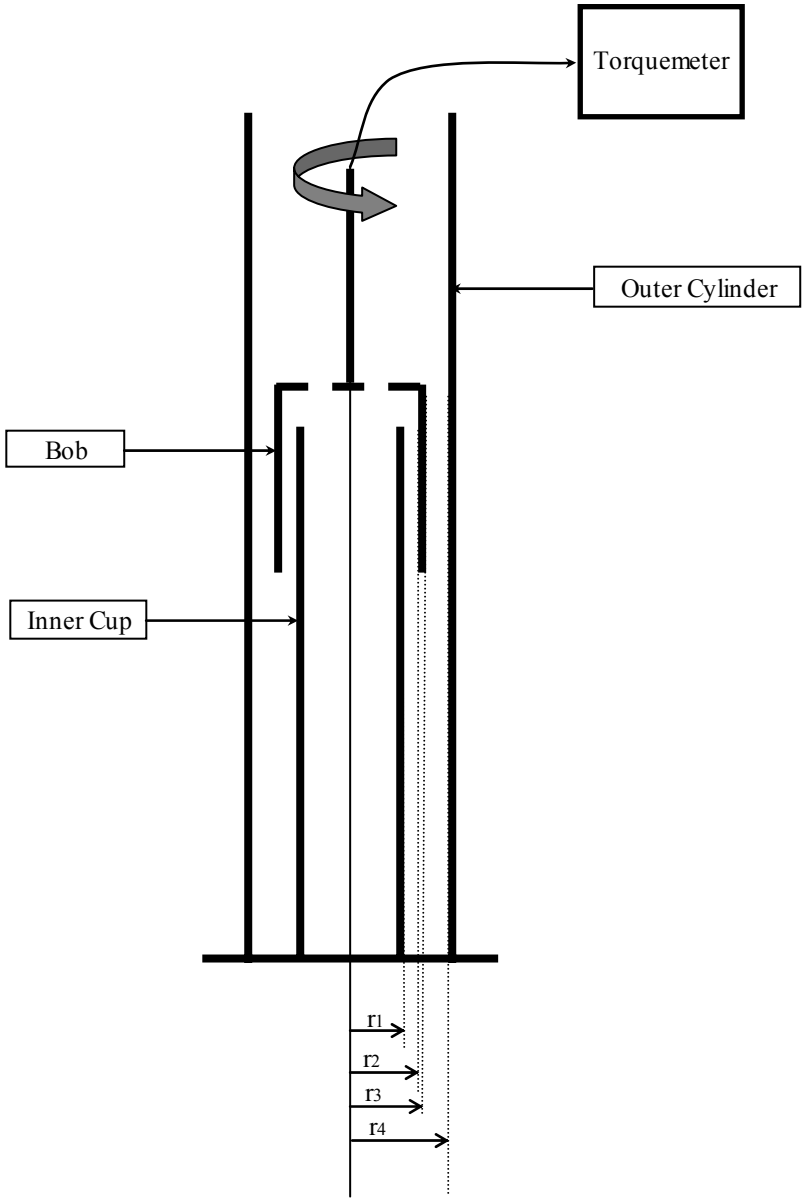

Figure 3.1: Representation of the elongated fixture used to perform the rheological measurements. r_1= 16.5 mm, r_2= 19.0 mm, r_3= 20.0 mm, r_4= 23.03 mm.

The Haake Rotovisco VT550 applies a rotation speed, Ω, to the bob. For Newtonian fluids the rotation speed is directly proportional to shear rate, $\dot{\gamma}$, according to Equation 3.1.

$$\dot{\gamma} = M\Omega \qquad (3.1)$$

M is a fixture constant which depends on the fixture dimensions and that can be calculated from Equation 3.2.

$$M = \frac{\pi}{6}\left(\frac{r_1^2}{r_2^2 - r_1^2} + \frac{r_4^2}{r_4^2 - r_3^2}\right) \qquad (3.2)$$

The units of Ω are $\%_{max}$ (percent of viscometer maximum speed) while the units of M are $(1/s)/(\%_{max})$.

The resulting torque, T, produced after the application of shear rate is measured by the Haake Rotovisco VT550. T is proportional to shear stress, τ, according to Equation 3.3.

$$\tau = A\,T \qquad (3.3)$$

Where A, is a constant which can be determined by testing viscosity standards. The units of T are $\%\ T_{max}$ (percent of the viscometer maximum torque) while the units of A are $(Pa)/(\%\ T_{max})$. Two viscosity standards were used in this calibration, CANNON N75 and CANNON N415, whose viscosities are 125.0 mPas and 828.3 mPas respectively at 25 °C.

The critical angular velocity at which the onset of the Taylor vortices starts can be determined from Equation 3.4 (Taylor, 1923).

$$V_\theta = \frac{41.3\mu_p}{\rho R_c (1-\kappa)\sqrt{\frac{(1-\kappa)}{\kappa}}} \qquad (3.4)$$

Where μ_p is the slurry viscosity, ρ the slurry density, R_c the radius of the cup and κ is the ratio between the radius of the cup and the radius of the bob. It is expected that almost all the slurries to be tested in this thesis will have viscosity values higher than 15 mPs; in addition the slurry density values will be lower than 1.2 g/cm^3 and, considering the outer gap from Figure 3.1, the calculated critical shear rate at which turbulence should appear is 180 s^{-1}. This value is greater than the maximum shear rate considered in the experiments, 114 s^{-1}, assuring that the experiments will be carried out in laminar flow.

For additional information about considerations and restrictions of the elongated fixture the reader is referred to Klein (1992).

Some rheological measurements were also performed on pure bitumen using the VT550 equipped with the standard Haake MV1-P sensor (single gap, bob-in-cup geometry). The relationship between rotational speed and shear rate is obtained also from the geometry of fixture with an inner cup diameter of 40.08 mm and a gap of 0.96 mm. The viscometer was calibrated using the N75 CANNON Viscosity Standard.

Particle size distributions of solid samples were determined using a Malvern Mastersizer 2000, a laser-based instrument that allows measurements to be carried out in the range from 0.02 to 2,000 μm, on different types of samples, including emulsions, suspensions and dry powders.

A Quantasorb sorption system was used to measure the specific surface area of all solid samples. In this system the surface area of particles is determined from the adsorption/desorption process of nitrogen molecules using the BET (Brunauer, Emmett, Teller) equation.

3.2.2 Pure quartz sample

Figure 3.2 shows the particle size distribution of the quartz sample used in this work. Quartz was obtained from Alfa Aesar Company. The commercial product is 99.5 wt% silicon (IV) oxide whose measured specific gravity is 2.45 g/cm^3. The measured mean particle size for this type of quartz is 3.6 μm and 100 v/v% of particles have a size finer than 17.6 μm. The measured specific surface area is 6 m^2/g. An x-ray diffraction analysis confirmed that the material is quartz indeed.

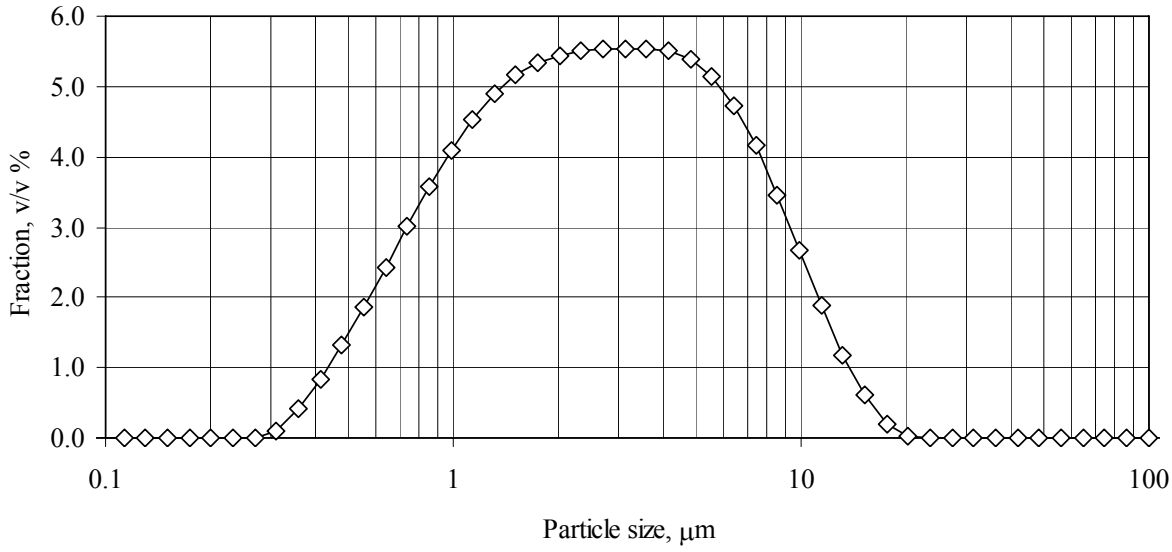

Figure 3.2: Malvern particle size distributions of the sample of pure quartz.

3.2.3 Bitumen sample

An important part of this thesis considers using synthetic mixtures of bitumen-quartz. These synthetic ores were prepared by coating pure particles of quartz with bitumen at different concentrations. Bitumen used for coating was recovered from an actual good processing ore (obtained from Alberta Research Council) by applying three flotation stages at 50 °C (1 rougher and 2 cleaner with distilled water).

It is well known that bitumen viscosity increases sharply as temperature decreases and that the absolute value is dependent on the origin and extraction method used to recover the bitumen (Helper and Smith, 1994; Seyer and Gyte, 1989). Helper and Smith (1994) proposed an exponential equation (Equation 3.5) to correlate bitumen viscosity (μ_B) with temperature (T).

$$\mu_B = A_B \, \mathrm{Exp}\left(\frac{C_B}{T}\right) \qquad (3.5)$$

Where A_B and C_B are constants and T is temperature in Kelvin.

Figure 3.3 shows experimental bitumen viscosity values obtained from rheological measurements conducted in a MV1-P bob and cup sensor. Fitting of Equation 3.5 to experimental values gives constant A_B a value of 1.32 x 10^{-10} mPas and C_B of 9,927 K.

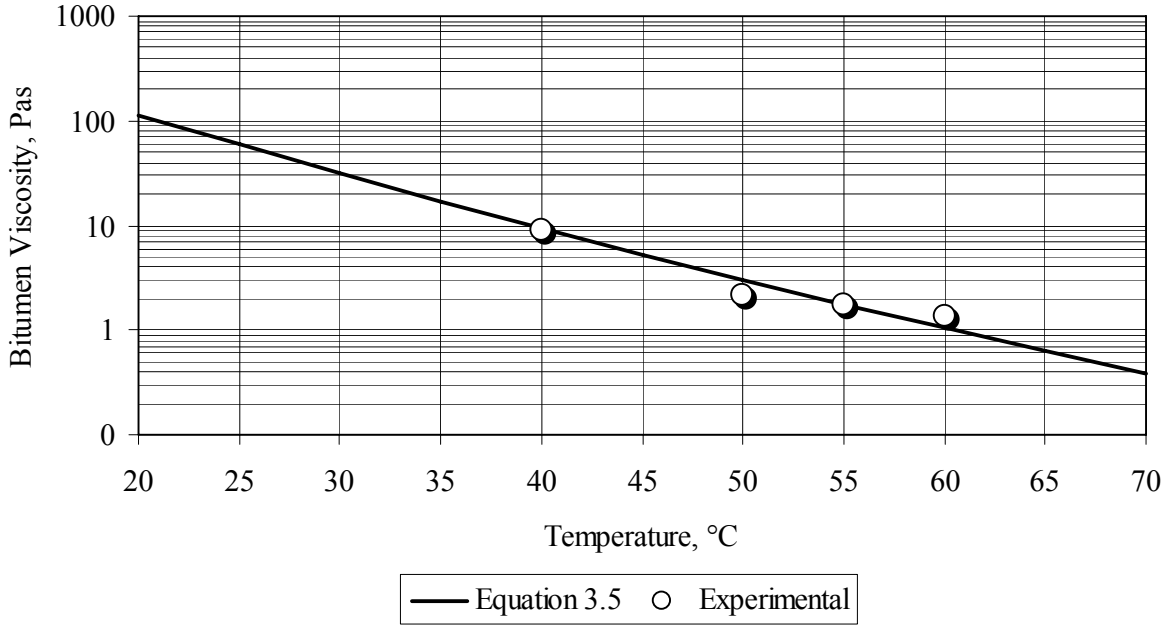

Figure 3.3: Experimental bitumen viscosity and fitting of Equation 3.5 for A_B=1.32 x 10^{-10} mPas and C_B=9,927 K. Experimental data was obtained by testing in a MV1-P bob and cup sensor.

3.2.4 Actual oil sands ores

Four actual oil sand ores were tested in this thesis. The samples were obtained from Canadian Natural Resources Ltd. (CNRL, Calgary, Alberta) and came from a developing operation. Table 3.2 shows a characterization of these ores in terms of bitumen grade, water and solids percentage. It can be seen that bitumen grade ranges between 3.6 and 9.2 wt% bitumen which means that these ores are medium-low grade ores. The results presented in Table 3.2 were obtained from the standard Dean-Stark analysis (Bulmer and Starr, 1979).

Table 3.2: Bitumen, water and solid concentrations of actual oil sand ore samples. Results were obtained from the standard Dean-Stark analysis.

	Bitumen	Water	Solids
Oil sand ore	**wt%**	**wt%**	**wt%**
Ore 1	9.2	4.6	86.2
Ore 2	3.6	8.2	88.2
Ore 3	6.3	5.6	88.1
Ore 4	6.4	4.3	89.3

Figure 3.4 shows particle size distributions of the solids obtained from the oil sands ores, while Table 3.3 summarizes the mean size, fraction of particles finer than 44 and 3 μm, specific gravity and specific surface area of solids. Bitumen-free solid samples were obtained by washing representative ore samples of 50 g with toluene (ratio toluene:ore 2:1) in 5 consecutive stages with a filtering stage between every stage of washing. It can be seen from Table 3.3 that the fraction of particles with a size smaller than 44 μm is greater than 20 v/v% for all the ores tested. Besides, this fraction is far greater than the upper limit set for a good processing ore (20 v/v%). Therefore, all oil sand ores tested in this thesis can be classified as poor processing ores because of the exceptionally high content of fines.

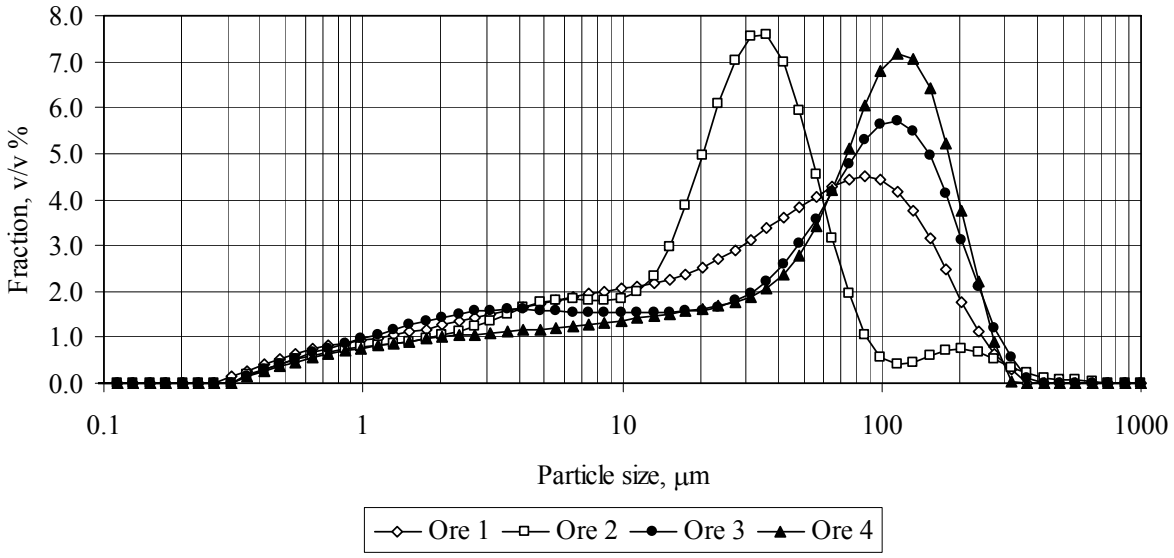

Figure 3.4: Malvern particle size distributions of solids obtained from the four actual oil sand ores tested.

Table 3.3: d_{50}, fraction finer than 44 μm and 3 μm, specific gravity and specific surface area of the solids obtained from the four actual oil sand ores.

	d_{50}	<44 μm	< 3 μm	Specific Gravity	Specific Surface Area
Oil sand sample	**μm**	**v/v %**	**v/v %**	**g/cm^3**	**m^2/g**
Ore 1	27	58	10	2.53	2.23
Ore 2	27	80	13	2.43	1.86
Ore 3	54	47	16	2.46	1.22
Ore 4	73	40	12	2.45	0.52

Table 3.4 shows the mineralogical characterization of the solids obtained from the oil sand ores. Three samples were characterized for every ore: a total sample (whole range of sizes), the size fraction coarser than 44 μm, and the fines below 44 μm. The analysis of the total samples show that quartz grade is greater for ores 3 and 4 which is inversely proportional to the fraction finer than 44 μm for these two ores; this relationship is very common in oil sands ores and it is the basis for the definition of good and poor processing ores. A second observation is that the content of aluminosilicates minerals is greater in the fine fraction, and that kaolinite is predominant in the first two ores.

Table 3.4: Mineralogical characterization of the solids obtained from actual oil sand ores.

Ore 1		**Total Sample**	**> 44 µm Size Fraction**	**< 44 µm Size Fraction**
Quartz	wt%	89.3	93.5	83.6
Kaolinite	wt%	4.2	2.1	6.4
Anatase	wt%	-	-	-
K-feldspar	wt%	3.6	3.5	5.0
Muscovite	wt%	2.9	0.9	5.0
Plagioclase	wt%	-	-	-
Pyrite	wt%	-	-	-
Ore 2		**Total Sample**	**> 44 µm Size Fraction**	**< 44 µm Size Fraction**
Quartz	wt%	85.3	87.4	78.5
Kaolinite	wt%	5.7	5.1	9.4
Anatase	wt%	0.4	0.2	0.6
K-feldspar	wt%	4.4	3.2	4.8
Muscovite	wt%	4.3	3.2	5.7
Plagioclase	wt%	0.0	0.9	1.0
Pyrite	wt%	-	-	-
Ore 3		**Total Sample**	**> 44 µm Size Fraction**	**< 44 µm Size Fraction**
Quartz	wt%	92.3	93.7	85.2
Kaolinite	wt%	2.0	1.6	4.5
Anatase	wt%	0.1	0.0	0.4
K-feldspar	wt%	2.9	2.8	4.1
Muscovite	wt%	1.9	1.1	4.3
Plagioclase	wt%	0.8	0.9	1.0
Pyrite	wt%	0.0	0.0	0.5
Ore 4		**Total Sample**	**> 44 µm Size Fraction**	**< 44 µm Size Fraction**
Quartz	wt%	94.1	93.6	88.1
Kaolinite	wt%	2.0	1.9	3.7
Anatase	wt%	0.0	0.0	0.3
K-feldspar	wt%	2.6	3.2	4.5
Muscovite	wt%	1.3	1.3	3.4
Plagioclase	wt%	-	-	-
Pyrite	wt%	-	-	-

3.2.5 Reagents

Technical grade reagents sodium chloride (NaCl), potassium chloride (KCl) and calcium chloride ($CaCl_2 \cdot 2H_2O$) from Fisher Scientific were used to prepare solutions. pH was adjusted with a 3M sodium hydroxide (NaOH) solution. A sodium salt of humic acids of technical grade was provided by Aldrich Chemical.

3.3 Methods

3.3.1 Rheological measurements

Suspensions tested in this study were expected to show time dependent behaviour (thixotropy or rheopexy). For this reason all slurries were prepared under controlled conditions of mixing time, impeller speed and slurry volume to ensure consistent shearing and to minimize time dependent effects. All the experiments consider stirring of 550 mL of slurry for 25 minutes at an impeller speed of 500 rpm; stirring speed was chosen arbitrarily while a mixing time of 25 minutes was found to produce a constant pH value. After 25 minutes, the impeller was stopped and the slurry was poured into the rheometer. In all experiments, the time interval between stoppage of the impeller and initialization of the rheometer was between 20 and 30 s. Standard rheological flow curves were obtained by increasing the shear rate between 0 and 114 s^{-1} in 50 s, and decreasing the shear rate from 114 s^{-1} and 0 s^{-1} in 50 s. Figures 3.5 and 3.6 show pictures of the mixer and the Haake Rotovisco VT550 used in this thesis. In order to estimate the reproducibility of the obtained flow curves, duplicate tests under one set of conditions were done for every type of suspension (Appendix I).

Figure 3.5: Picture of the mixer.

Figure 3.6: Picture of the Haake Rotovisco VT550.

3.3.2 Coating of pure solids with bitumen

To achieve a good coating of bitumen onto particles of pure quartz, bitumen was first dissolved in toluene at a ratio of 3 mL toluene per 1 g bitumen. Then, the organic solution of bitumen was mixed with particles of pure solids. This mixture was then homogenized in order to spread the bitumen solution over all the particles of pure solids. In order to allow toluene to evaporate, the mixture was kept under a fume hood for 1 week. In order to avoid the formation of lumps, and to produce a homogeneous feed for the experiments, the toluene-ore mixture was passed through a 4.76 mm sieve.

3.3.3 Specific gravity measurements

Specific gravity measurements were conducted by pouring 60 g of solid sample in a 500 mL flask. 400 mL of distilled water were added and then the slurry was placed on a hot plate at 50 °C for 30 minutes so that water could reach all the pores present in the solid. After 30 minutes, the flask was removed from the hot plate and filled with distilled water to complete 500 mL. The slurry was weighed and the mass of water was determined. The volume of solid is the difference between the volume of the flask (500 mL) and the volume of water. As the mass of solid is known, the specific gravity can also be calculated.

4 Results and discussion

4.1 Flow curves presentation

The main results from this thesis will be reported in charts as pseudo-equilibrium flow curves (most likely the equilibrium between shear stress and shear rate is not reached). Every chart will display values of apparent viscosity evaluated at a shear rate of 114 s^{-1} (η_{app114}), yield stress (ys) and hysteresis of the pseudo-equilibrium flow curves (H).

Apparent viscosity at 114 s^{-1} will be calculated from the values of shear stress and shear rate. Yield stress values will be obtained by using the Bingham, Herschel-Bulkley and Casson models from which average and maximum values will be taken and presented in every chart.

In order to quantify the time dependency of the pseudo-equilibrium flow curves, a simple model which considers the time dependent nature of slurries was developed by the author of this thesis. In this model, shear stress is considered to originate from a combination of elastic/plastic variables: elastic variables are related to the relationship between shear rate and shear stress and can be expressed by any of the models mentioned in Chapter 2.1.3: plastic variables consider the time dependent nature of slurries.

The model can be mathematically expressed by Equation 4.1.

$$\tau = \tau(\dot{\gamma})S(t) \qquad (4.1)$$

Where $\tau(\dot{\gamma})$ represents the relationship between shear stress and shear rate, which will be described in this thesis by the Casson model. S(t) is a structure factor which considers the plastic variables; the structure factor S(t) will be represented by the following first order kinetic equation:

$$\frac{dS(t)}{dt} = -\frac{H}{\tau(\dot{\gamma}_{max})}S(t) \qquad (4.2)$$

Where H is the hysteresis constant and $\tau(\dot{\gamma}_{max})$ is the Casson shear stress at the maximum shear rate tested. H can be positive or negative depending on the occurrence of thixotropy (+) or rheopexy (-).

After integrating Equation 4.2, Equation 4.3 is obtained.

$$S(t) = S(0)Exp\left(-\frac{H}{\tau(\dot{\gamma}_{max})}t\right) \qquad (4.3)$$

It will be considered that the structure factor has a value of 1 at time 0, which means that the structure of the slurry is not affected. The constant H is calculated from the fitting of the model to the experimental data. Figure 4.1 shows the fitting of the model for cases of low-high shear stress and strong thixotropy. From values of R^2, it can be seen that the fitting of the model is very good. It is interesting to note that the constant H is proportional to the area between the increasing and the decreasing parts of the flow curves, and also to the ratio between the shear stress evaluated at a shear rate of 50 s^{-1} of the increasing and the decreasing branches.

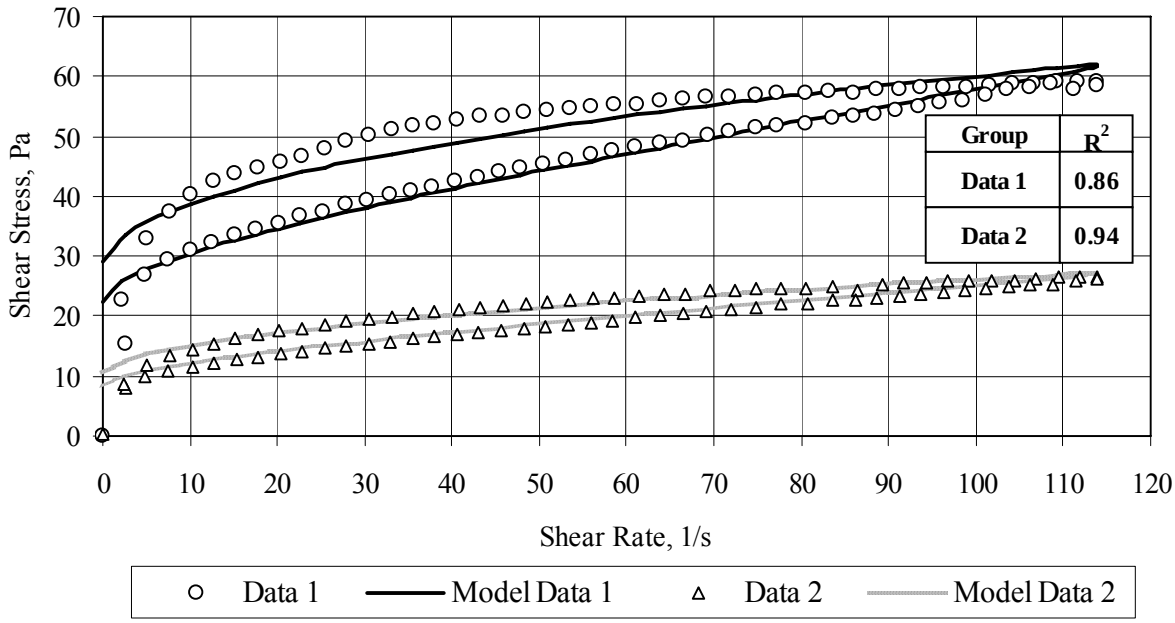

Figure 4.1: Model applied to cases of high and low shear stress flow curves. Fitting constant Data 1: τ_{CY}=28.9 Pa, η_C=0.081 Pas and H=181 mPa/s. Fitting constant Data 2: τ_{CY}=10.4 Pa, η_C=0.047 Pas and H=70 mPa/s. 50 seconds rump-up, 50 seconds rump down.

4.2 Rheological results for quartz-bitumen mixtures

4.2.1 Results for pure quartz slurries

The data obtained for pure quartz suspensions served as the baseline rheological response for comparison with the results collected for quartz-bitumen slurries.

4.2.1.1 Effects of pH, temperature and solids content

Figure 4.2 shows the effect of pH on the rheology of pure quartz slurries tested at 35 wt% solids, 50 °C, in solutions containing 0.01M NaCl/0.001M $CaCl_2$ and 0.01M KCl/0.001M $CaCl_2$. The results for both types of solutions show that a reduction of pH from 10.0 to 6.0 produces a change of flow curve patterns from slightly shear thickening to shear thinning, an increase in apparent viscosity and the occurrence of yield stress. These results can be explained by the reduction of quartz surface charge as pH changes from 10.0 to 6.0 (Scott, 1982; Savarmand et al., 2003; Franks, 2000). These experiments also show that KCl produces more aggregation than NaCl, an effect that was reported previously by some authors (Franks, 2002; Farrow et al., 1989) for dilute quartz suspensions, and was explained by the poorly hydrated nature of K^+ compared to Na^+, which leads K^+ to be adsorbed onto quartz in a greater amount than Na^+, causing a stronger reduction in quartz surface charge. It is interesting to note that flow curve patterns at pH 10.0 are slightly shear thickening, a result that was also reported previously by some authors (Scott, 1982; Savarmand et al., 2003) and explained by an increase in particle aggregation produced by shearing.

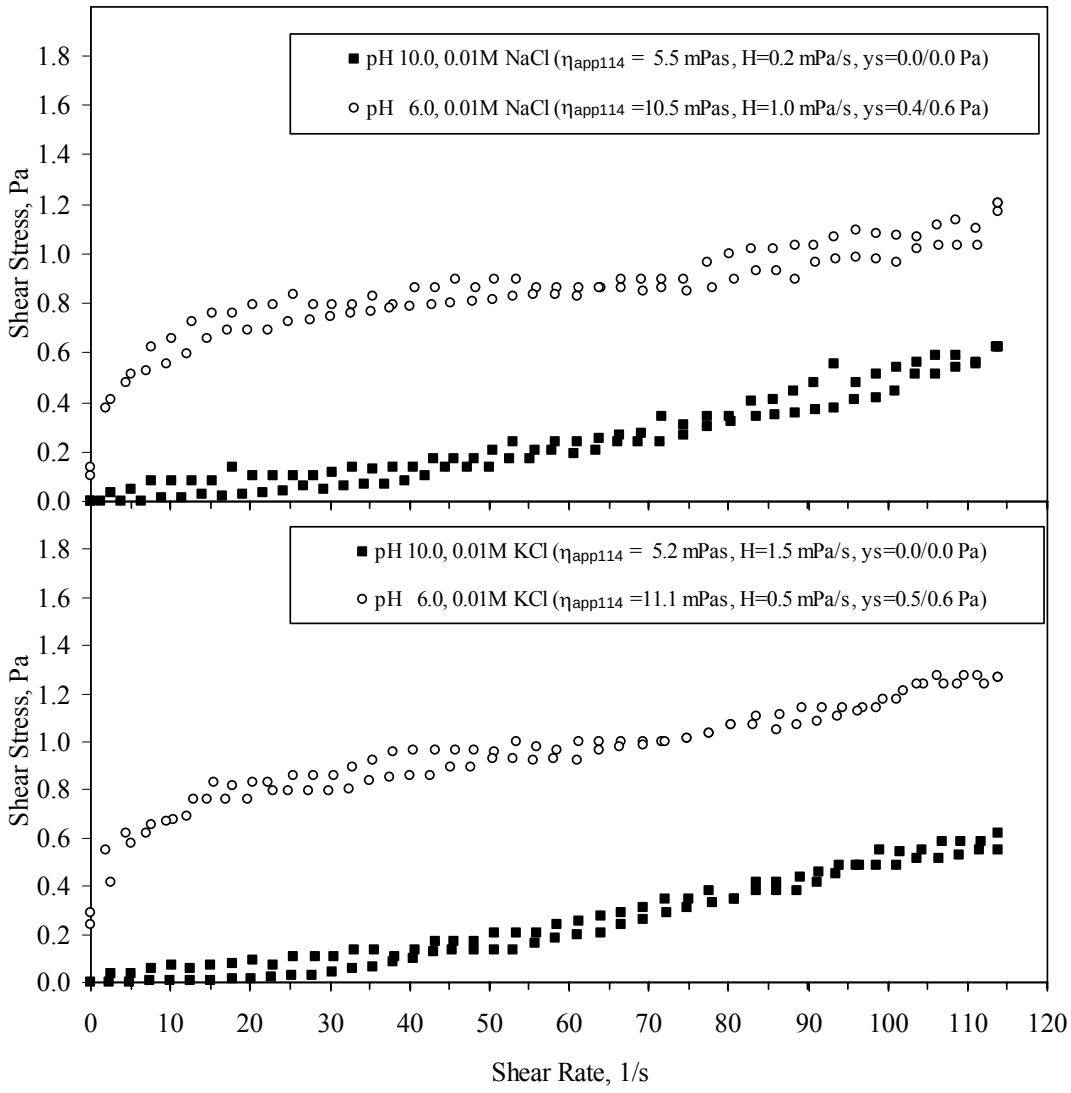

Figure 4.2: Effect of pH and salts on rheological flow curves for slurries of pure quartz. General testing conditions: 35 wt% solids, 50 °C and solutions containing 0.001M $CaCl_2$.

Figure 4.3 shows the effect of temperature on the rheology of pure quartz slurries tested at 35 wt% solids, pH 10.0, in solutions containing 0.01M NaCl/0.001M $CaCl_2$ and 0.01M KCl/0.001M $CaCl_2$. The results for both types of solutions show that a reduction of temperature from 50 to 25 °C increases apparent viscosity (no yield stress is observed at 25 °C). However, the effect is much smaller than the effect of pH. From a theoretical point of view, a reduction of temperature increases the carrier fluid viscosity and reduces the surface charge of quartz (Rodriguez and Araujo, 2006), both changes being promoters of aggregation. However, the experimental results show only a small effect.

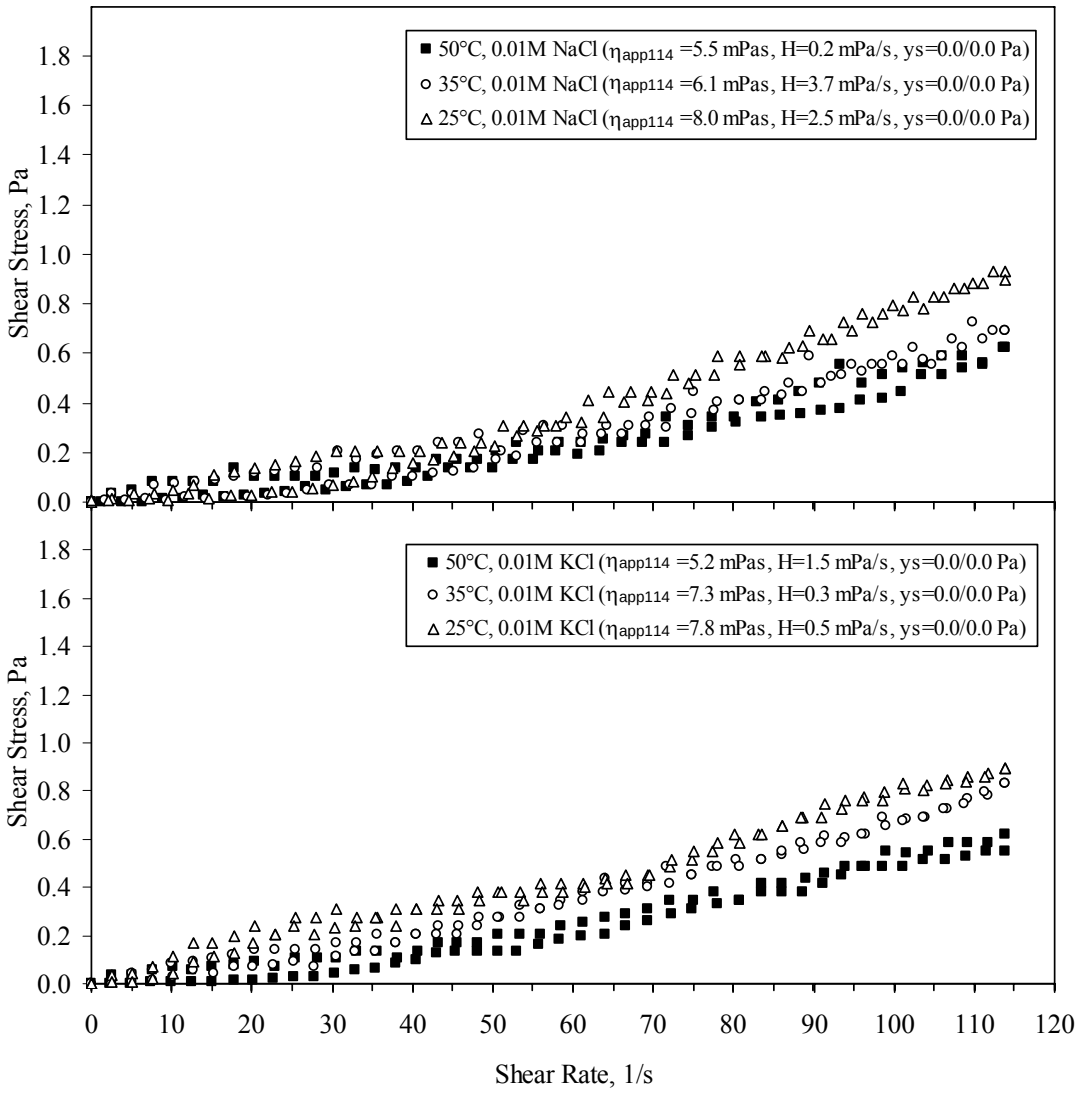

Figure 4.3: Effect of temperature and salts on rheological flow curves for slurries of pure quartz. General testing conditions: 35 wt% solids, pH 10.0 and solutions containing 0.001M $CaCl_2$.

Figure 4.4 shows the effect of solid concentration on the rheology of pure quartz slurries tested at 50 °C, pH 10.0, in solutions containing 0.01M NaCl/0.001M $CaCl_2$ and 0.01M KCl/0.001M $CaCl_2$. The results show that an increase of solid concentration from 35 to 45 wt% increases apparent viscosity (no yield stress is observed at 45 wt%) to a similar level that a reduction of temperature from 50 to 25 °C does.

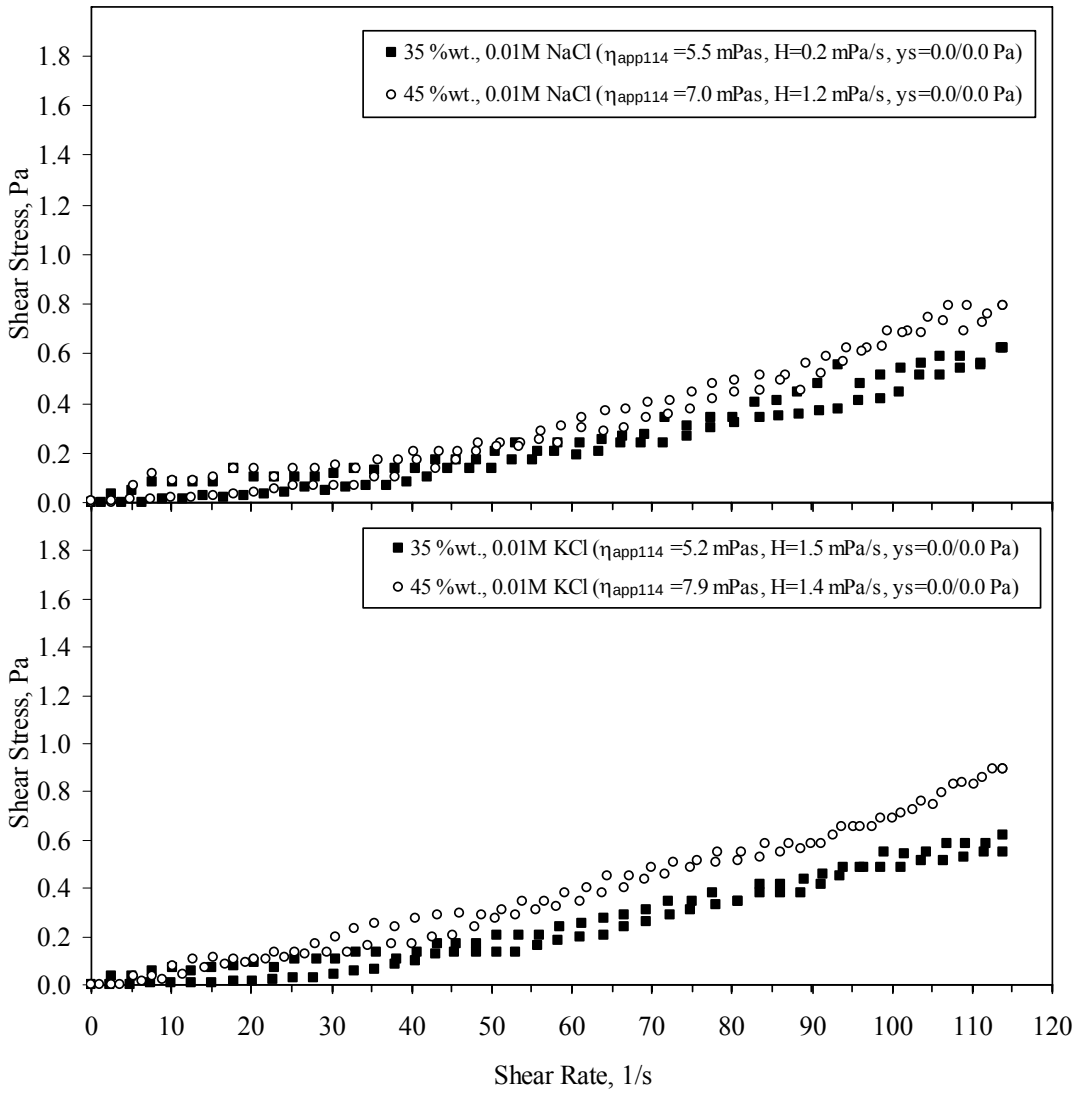

Figure 4.4: Effect of solid concentration and salts on rheological flow curves for slurries of pure quartz. General testing conditions: 50 °C, pH 10.0 and solutions containing 0.001M $CaCl_2$.

The results concerning the effect of pH and temperature presented in Figures 4.2 and 4.3 were obtained by testing slurries at 35 wt% solids. In order to explore the effect of pH and temperature in more aggregated conditions, slurries of pure quartz at 45 wt% solids concentration were also tested.

Figure 4.5 shows the effect of temperature and pH on the rheology of pure quartz slurries at 45 wt% solids, in solutions containing 0.01M NaCl/0.001M $CaCl_2$. Figure 4.6 shows the results obtained under the same conditions as in Figure 4.5 but using KCl instead of NaCl. The results for both types of solutions show that apparent viscosity decreases with increase of pH, flow curve patterns switch from slightly shear thickening at pH 10.0 to shear thinning at pH 6.0 and 8.5, and yield stress is only displayed at pH 8.5 and 6.0. It can be seen that the effect of temperature is smaller than the effect of pH, which was also observed at 35 wt% solids.

At pH 6.0, aggregation of quartz appears to be so advanced that manipulation of temperature is not sufficient to change the conditions of the system. Under weakly alkaline conditions (pH 8.5), when quartz should partly be dispersed, the effect of temperature is most pronounced. At even higher pH, the full dispersion of quartz now controls the rheology of quartz suspensions and again a change in temperature has a small effect on rheology. Interestingly, it is pH 8.5 that is most frequently used during the hot water extraction process, and at this pH, temperature has a beneficial effect on quartz dispersion in terms of lowering slurry viscosity.

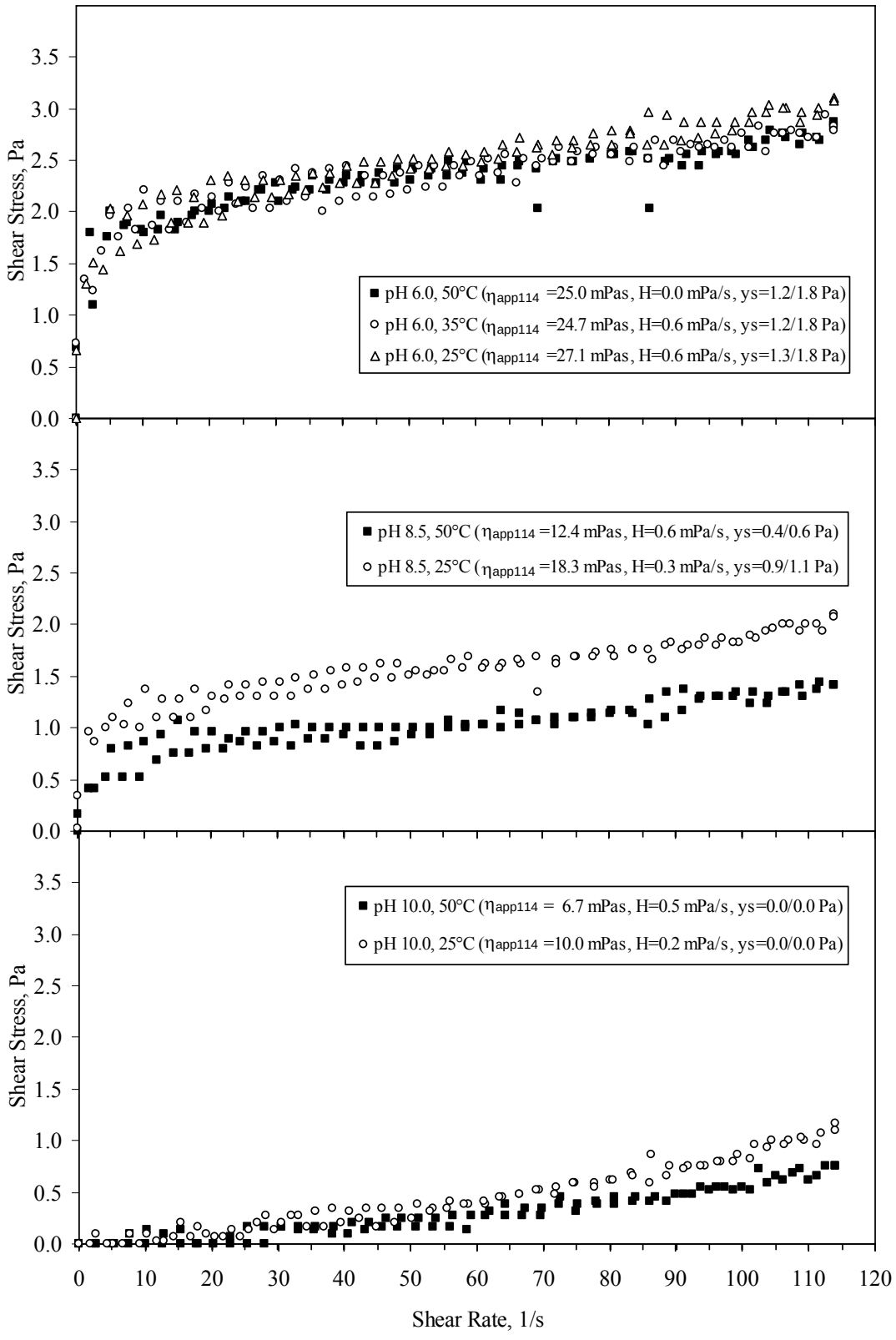

Figure 4.5: Effect of temperature and pH on rheological flow curves for slurries of pure quartz. General testing conditions: 45 wt% solids and solutions containing 0.01M NaCl/0.001M $CaCl_2$.

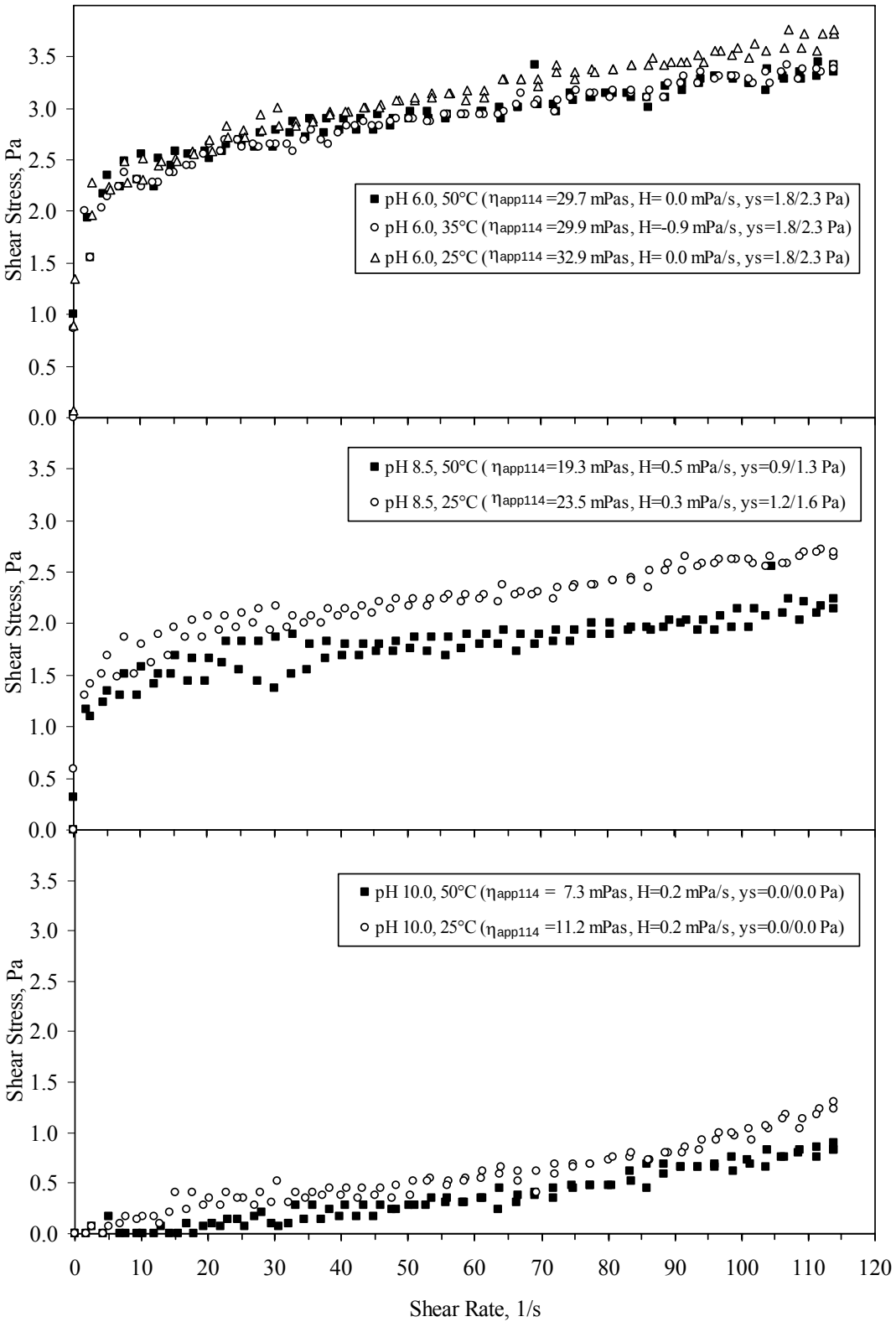

Figure 4.6: Effect of temperature and pH on rheological flow curves for slurries of pure quartz. General testing conditions: 45 wt% solids and solutions containing 0.01M KCl/0.001M $CaCl_2$.

4.2.1.2 Effects of NaCl, KCl and $CaCl_2$

Figure 4.7 shows the effect of NaCl, KCl and $CaCl_2$ on the rheology of pure quartz slurries tested at 35 wt% solids, pH 10.0 and 50 °C. The background solutions for these experiments contain 0.01M NaCl/0.001M $CaCl_2$ and 0.01M KCl/0.001M $CaCl_2$. The results show that 0.01M NaCl, 0.01M KCl and 0.001M $CaCl_2$ do not significantly affect the rheological behavior of quartz suspensions under the testing conditions. In theory, these salts increase particle aggregation because they reduce the surface charge of quartz (Ma and Pawlik, 2005; Franks, 2002; Farrow et al., 1989). However, the absence of an effect of the salts observed from these experiments can be explained by the small change that these salts generate on the zeta potential, compared to the strong repulsive forces present at pH 10.0 between the negatively charged quartz particles.

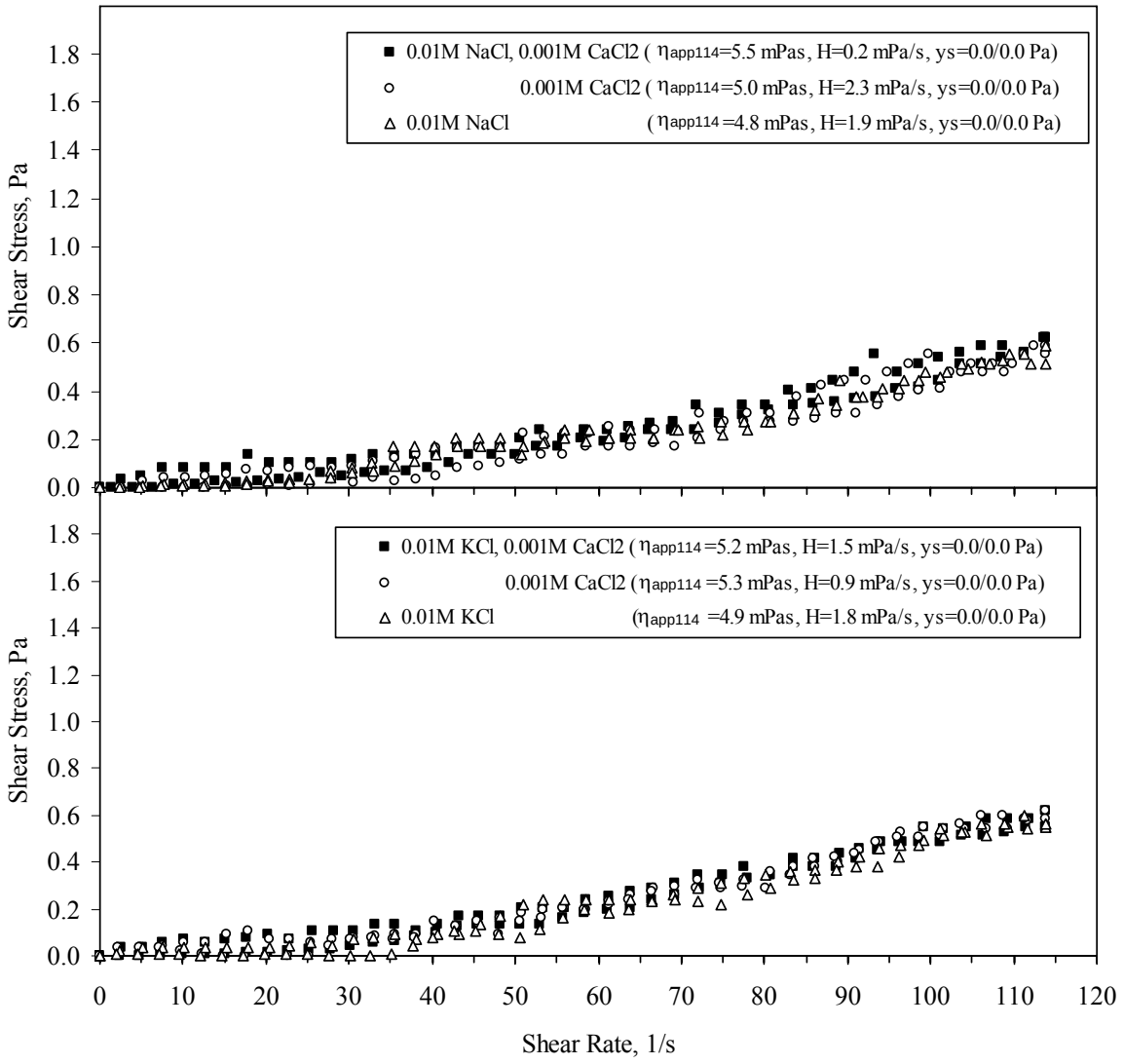

Figure 4.7: Effect of NaCl, KCl and $CaCl_2$ on rheological flow curves for slurries of pure quartz. General testing conditions: 35 wt% solids, pH 10.0 and 50 °C.

Figure 4.8 shows the effect of NaCl and $CaCl_2$ on the rheology of pure quartz slurries tested at 45 wt% solids, 50 °C and at different pH values. The background solution for these experiments contains 0.01M NaCl/0.001M $CaCl_2$. The results show that 0.01M NaCl and 0.001M $CaCl_2$ increase apparent viscosity only at pH 6.0 and 8.5 (not at pH 10.0, which is coincident with the results in Figure 4.7) with $CaCl_2$ producing a stronger effect than NaCl. It is possible that because of the stronger electrostatic forces existing between Ca^{2+} (divalent ion) and quartz the amount of Ca^{2+} adsorbed onto quartz was greater than the amount of Na^{+}.

Figure 4.9 shows the effect of KCl and $CaCl_2$ on the rheology of pure quartz slurries tested at 45 wt% solids, 50 °C and at different pH values. The background solution for these experiments contains now 0.01M KCl/0.001M $CaCl_2$. The results show that 0.01M KCl and 0.001M $CaCl_2$ increases apparent viscosity only at pH 6.0 and 8.5 but not at pH 10.0, which again agrees with the results in Figures 4.7 and 4.8. It is interesting to note that KCl has a stronger effect than $CaCl_2$ showing that the poorly hydrated nature of K^{+} plays an important role in its adsorption capacity on quartz.

Overall, the data for different salt types show that any differences between the salts can most clearly be observed at lower pH values, with potassium showing the greatest effect on the rheology of quartz slurries.

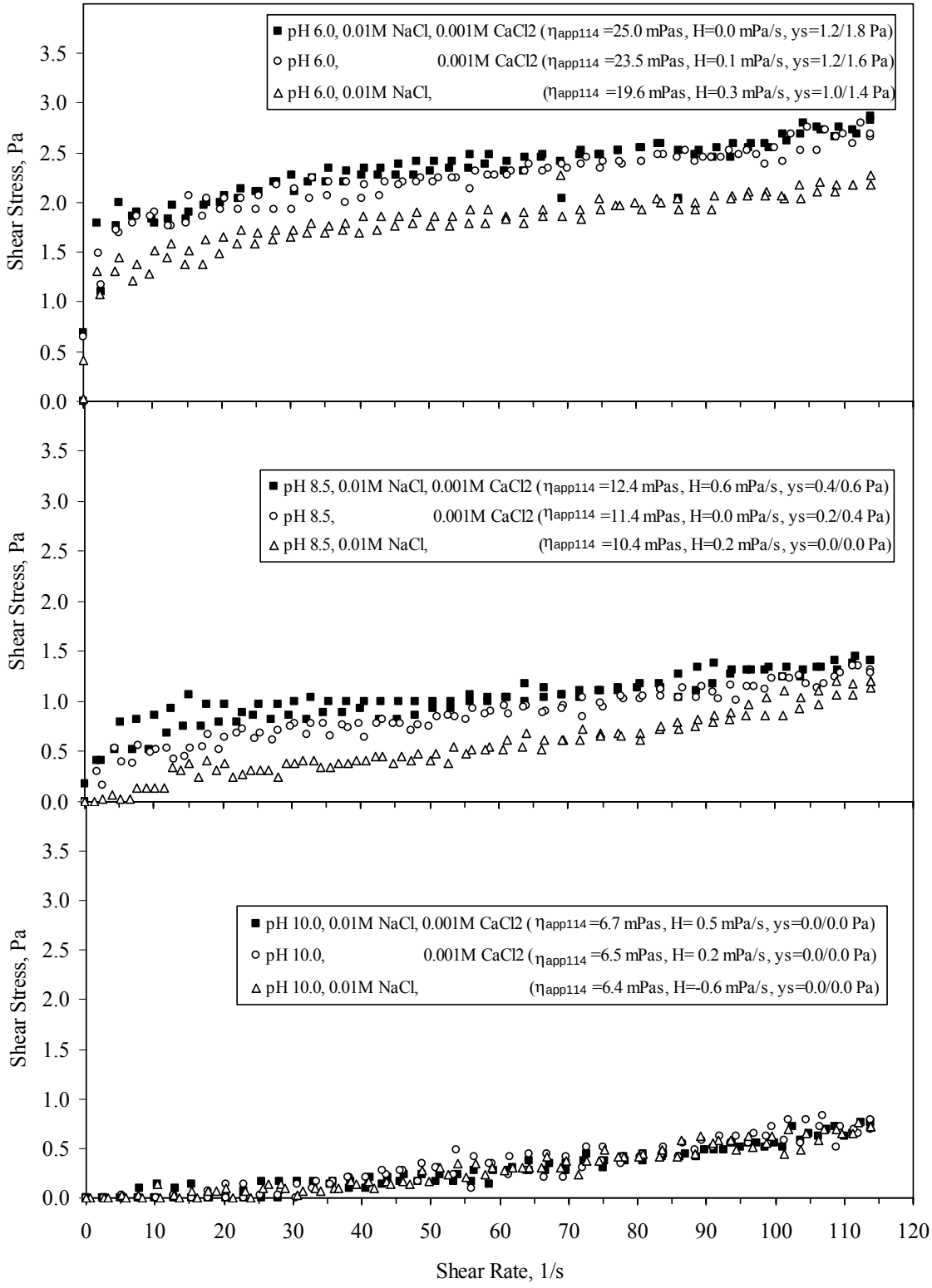

Figure 4.8: Effect of pH, NaCl and $CaCl_2$ on rheological flow curves for slurries of pure quartz. General testing conditions: 45 wt% solids and 50 °C. Background solutions of 0.01M NaCl/0.001M $CaCl_2$.

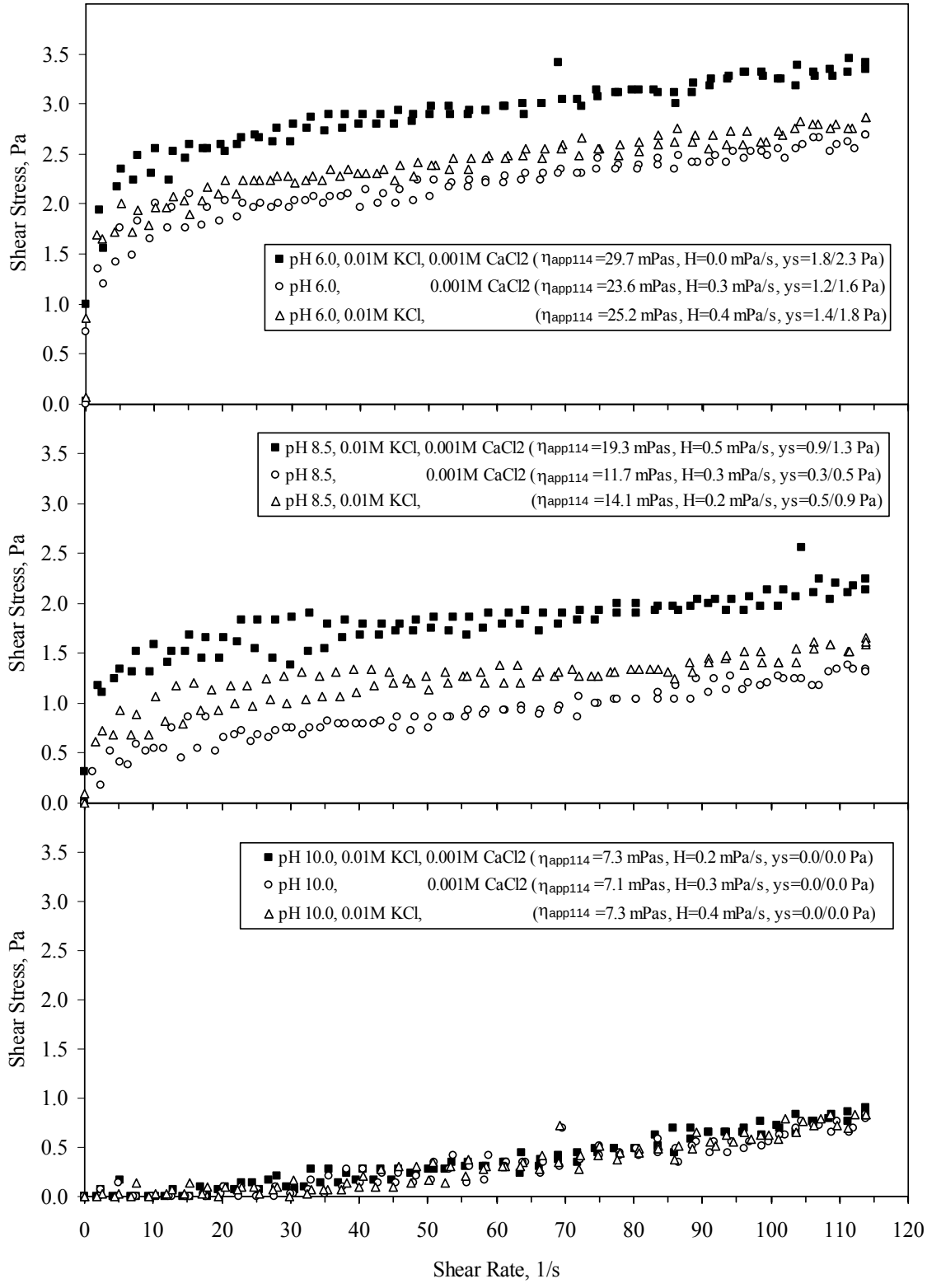

Figure 4.9: Effect of pH, KCl and $CaCl_2$ on rheological flow curves for slurries of pure quartz. General testing conditions: 45 wt% solids and 50 °C. Background solutions of 0.01M KCl/0.001M $CaCl_2$.

4.2.2 Results for slurries of bitumen-coated quartz

The risk that bitumen forms thick coatings on the shearing surfaces of the fixture walls represented an important concern when doing experiments with bitumen in a bob and cup fixture. As it was mentioned in chapter 3, the fixture constant M depends on fixture dimensions and determines the relation between the rotational speed applied by the Haake Rotovisco, and the shear rate. If bitumen covers the fixture walls, the fixture dimensions and M value is changed, and the results will not represent the genuine rheological behavior of tested slurries. A simple way to minimize this problem is to conduct a test as quickly as possible. The total measuring time in all the experiments conducted in this thesis was 100 s.

Figure 4.10 shows pictures of the rotary bob after 100 s of rheological testing for two different slurries: a slurry of synthetic oil sand ore 10 wt% bitumen tested at pH 10.0 and 25 °C, and another slurry tested at pH 10.0 and 50 °C. Both pictures show that some bitumen drops were attached to the bob surface and that the amount of bitumen left on the bob was greater in case B (high temperature) which could be expected because bitumen liberation should increase at high temperature. As a rough estimation it is possible to say that less than 20 % of the total bob surface was covered by bitumen which is quite acceptable from the point of view of the rheological measurements. Moreover, it is possible that these drops of bitumen were attached only after the bob was taken out from the outer cylinder which means that they were not attached to the bob during the test itself.

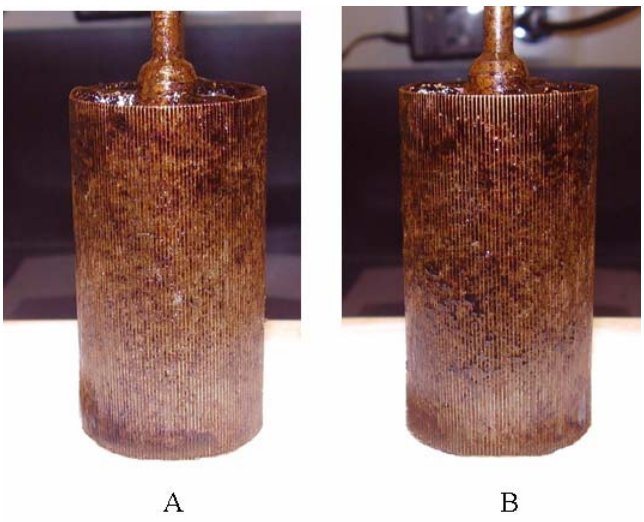

Figure 4.10: Bob pictures after 100 s of rheological testing for two different slurries. A: suspension of bitumen-quartz mixture at 10 wt% bitumen, pH 10 and 25 °C; B: suspension of bitumen-quartz mixture at 10 wt% bitumen, pH 10 and 50 °C.

4.2.2.1 Effect of pH

Figure 4.11 shows the effect of pH on the rheology of slurries of pure quartz and quartz-bitumen mixtures at 1 wt% bitumen and at a solids content of 45 wt%, 50 °C, in solutions containing 0.01M NaCl/ 0.001M $CaCl_2$. Figure 4.12 shows the effect of pH on slurries of bitumen-coated quartz containing 5 and 10 wt% bitumen under the same testing conditions as in Figure 4.11. Figure 4.13 shows apparent viscosity at a shear rate of 114 s^{-1} as a function of bitumen concentration at different values of pH.

The results from Figures 4.11 to 4.13 show that the apparent viscosity of all tested slurries increases with bitumen concentration of the synthetic ore. As it was mentioned in section 2.3.1, Liu et al. (2005) found that the Hamaker constant of interaction between two bitumen surfaces is around $100x10^{-21}$ J, twenty times greater than the Hamaker constant of interaction between silica surfaces. These authors explained that hydrophobic forces lead to strong bitumen-bitumen attractions and that a way to reduce these forces would be to add surfactants to make bitumen less hydrophobic. Comparing the values of the Hamaker constant of silica-silica and bitumen-bitumen surfaces, it is possible to conclude that if pure particles of quartz were coated with bitumen, attraction forces between bitumen-coated particles should be stronger and suspension viscosity should be higher compared to interactions and suspension viscosity for pure quartz particles in the absence of bitumen, an effect which is enhanced at higher bitumen concentrations.

It should be pointed out that the effect of bitumen concentration decreases with pH, in particular at pH 10.0 the difference between η_{app114} at 5 wt% and 10 wt% bitumen is very small (Figure 4.13). A reasonable explanation for this behavior is that as bitumen liberation from quartz surfaces increases with increasing pH, it is possible that, regardless of the bitumen concentration in the mixture, quartz surfaces at high pH have a very similar amount of residual bitumen adsorbed.

Another very important observation from Figures 4.11 to 4.13 is that apparent viscosity decreases with increasing pH for all bitumen concentrations. These results can be explained by an increase in bitumen liberation obtained at high pH. As it was explained before, this increase in bitumen liberation caused by high pH reduces the amount of strong attractive bonds between bitumen surfaces (adsorbed onto quartz surfaces) compared to the amount of weak attractive bonds between quartz surfaces. In addition, the zeta potential of both quartz and bitumen become

more negative at high pH enhancing quartz-quartz and quartz-bitumen dispersion through electrostatic repulsion.

These results represent evidence that there is a relationship between bitumen liberation and the rheological behavior of oil sands slurries.

A final observation about the results from Figures 4.11 to 4.13 is that at pH 6.0 and for mixtures containing 5 wt% and 10 wt% bitumen, the flow curves show very strong thixotropy (H=125 Pa/s at 5 wt% bitumen and H=200 Pa/s at 10 wt% bitumen) and H increases sharply with bitumen concentration. These results show that although an increase in bitumen concentration increases the amount of attractive bitumen-bitumen and bitumen-particle bonds, an important number of them are broken-down by shearing, which also suggests that bitumen liberation and dispersion are enhanced by the shearing action of the viscometer itself.

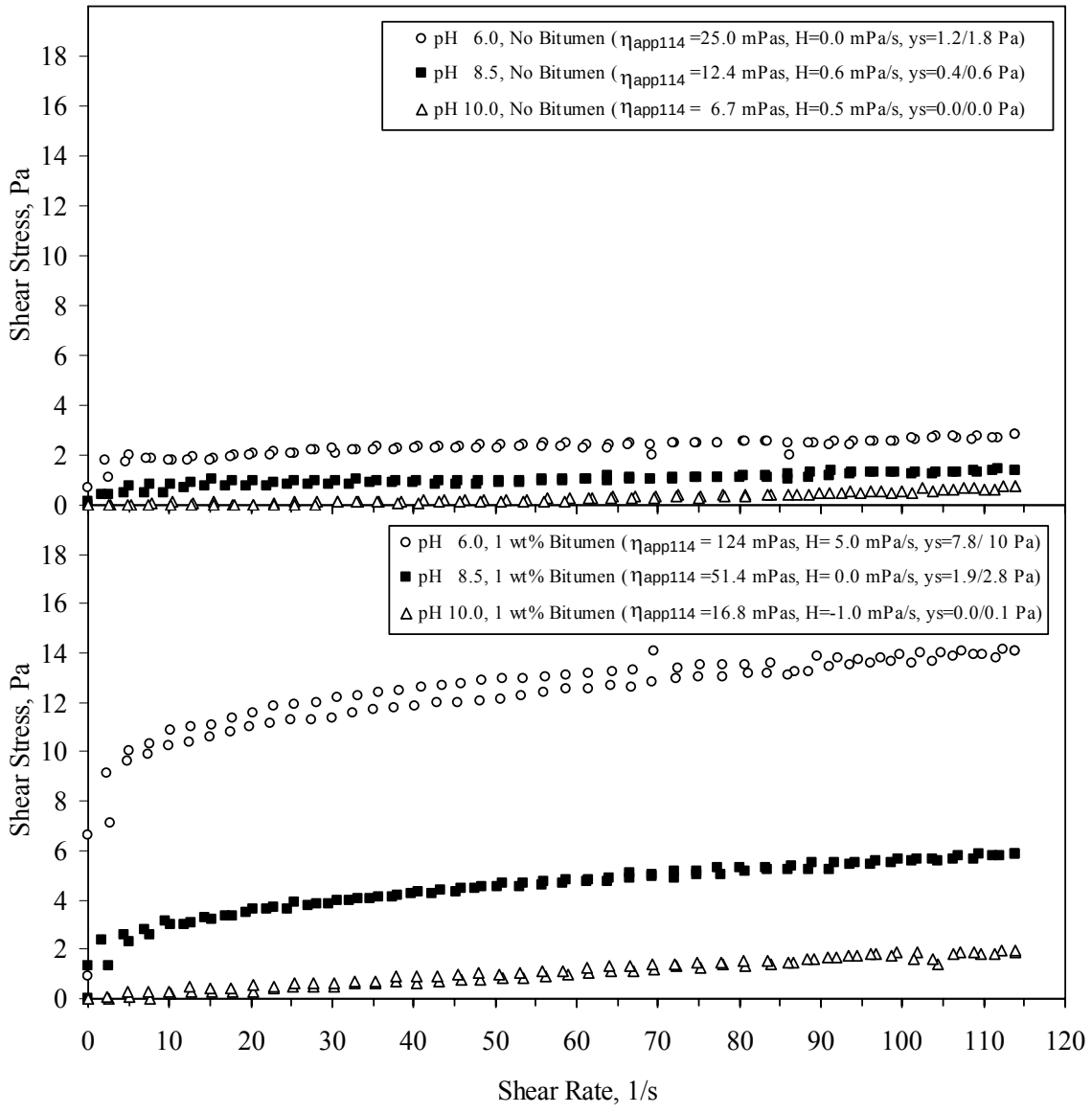

Figure 4.11: Effect of pH on rheological flow curves for slurries of pure quartz (Top Figure) and bitumen-quartz mixtures at 1 wt% bitumen (Bottom Figure). General testing conditions: 45 wt% solids, 50 °C and solutions containing 0.01M NaCl/0.001M $CaCl_2$.

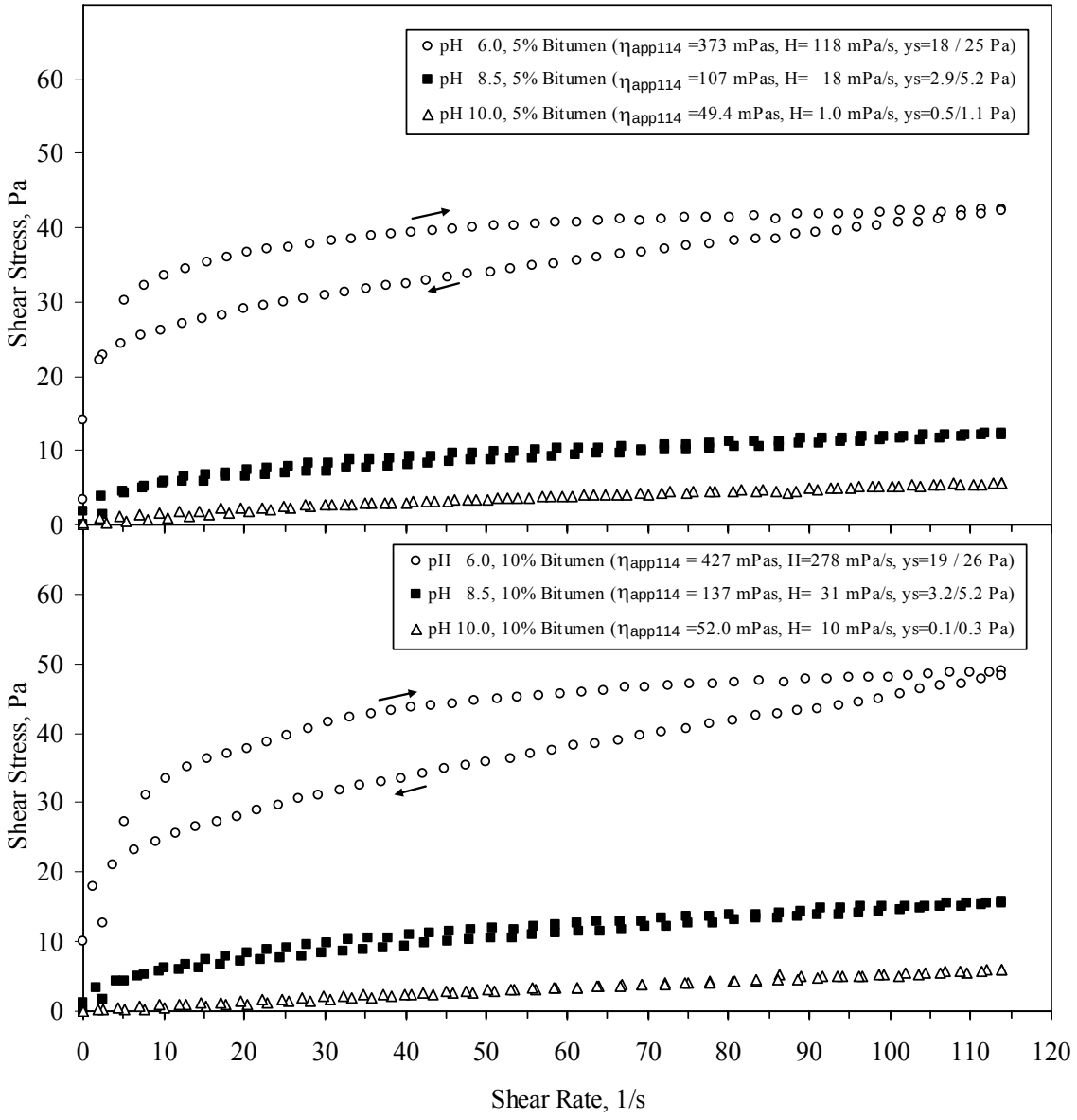

Figure 4.12: Effect of pH on rheological flow curves for slurries of bitumen-quartz mixtures at 5 wt% bitumen (Top Figure) and at 10 wt% bitumen (Bottom Figure). General testing conditions: 45 wt% solids, 50 °C and solutions containing 0.01M NaCl/0.001M $CaCl_2$.

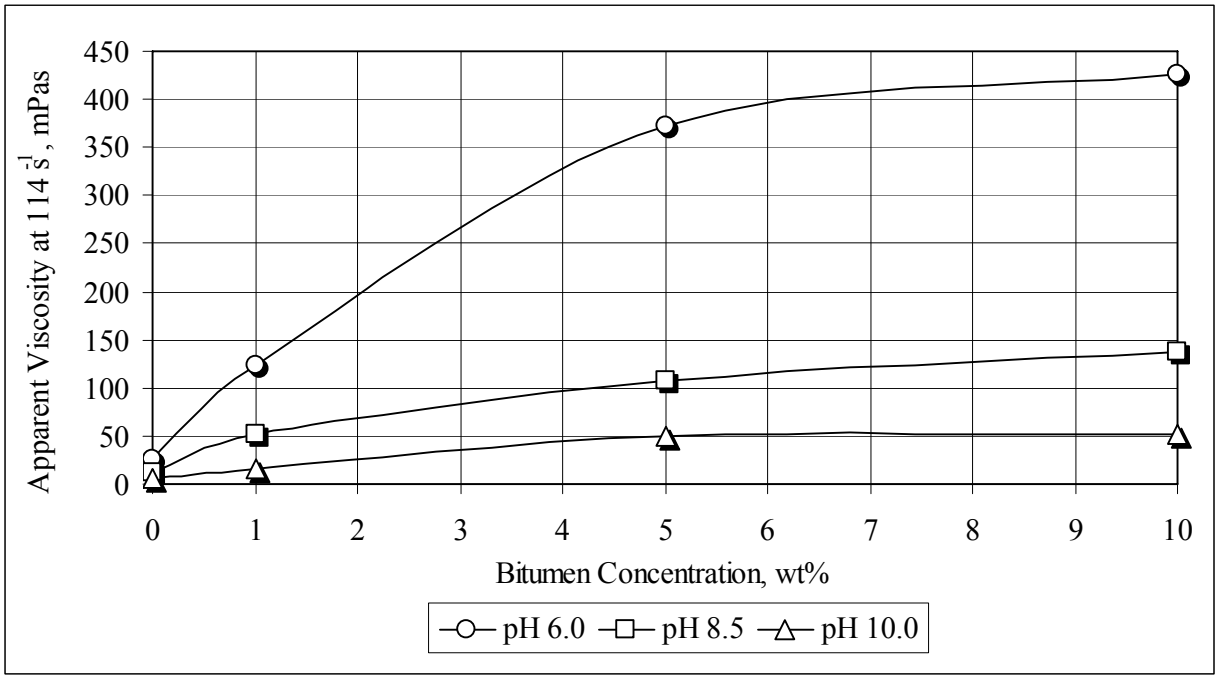

Figure 4.13: Apparent viscosity at a shear rate of 114 s^{-1} (η_{app114}) as a function of bitumen concentration and pH. General testing conditions: slurries of bitumen-quartz mixtures tested at 45 wt% solids, 50 °C and using solutions containing 0.01M NaCl/0.001M $CaCl_2$.

In order to support the statement that bitumen liberation increases with pH, pictures of the bitumen layer displayed on the top surface of slurries were taken just before they were poured into the rheometer. Figure 4.14 shows three pictures of slurries of bitumen-coated quartz containing 10 % bitumen tested at pH 6.0, 8.5 and 10.0. It can be seen that the amount of free bitumen in the surface layer increases as pH increases from 6.0 to 10.0 which confirms that bitumen liberation increases with pH.

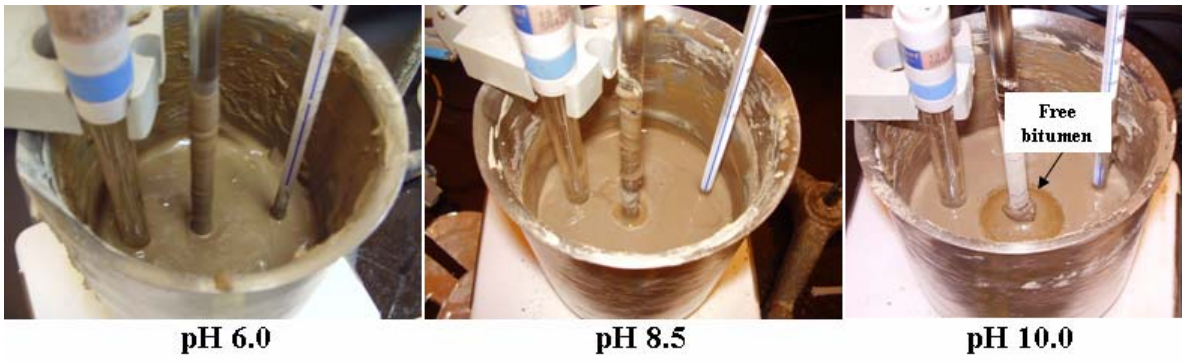

Figure 4.14: Bitumen layer formed on the surface of slurries of bitumen-quartz mixtures at different pH values, after 25 min of mixing (just before rheological measurement). General testing conditions: 10 wt% bitumen, 45 wt% solids, 50 °C and solutions containing 0.01M NaCl/0.001M $CaCl_2$.

4.2.2.2 Effect of temperature

Figure 4.15 shows the effect of temperature on the rheology of slurries of pure quartz and bitumen-quartz mixtures at 1 wt% bitumen, 45 wt% solids, pH 8.5, in solutions containing 0.01M NaCl/0.001M $CaCl_2$. Figure 4.16 shows the effect of temperature on slurries of bitumen-coated quartz at 5 and 10 wt% bitumen concentrations, under the same testing conditions as Figure 4.15. Figure 4.17 shows the parameter η_{app114} as a function of bitumen concentration at different temperatures.

The results from Figures 4.15 to 4.17 show that the apparent viscosity of all slurries decreases with increasing temperature, an effect that can be explained by an increase in bitumen liberation obtained at high temperature. It is interesting to note that the effect of temperature is very significant at high bitumen concentrations, which indicates that bitumen liberation from quartz particles is an important variable controlling the rheological properties of these types of high-bitumen slurries. Other variables affected by temperature, such as reduction of solution viscosity and increase of quartz surface charge, affect the rheological behavior to a much smaller extent and, in this case, they do not explain changes observed in the results from Figures 4.15 to 4.17. These results are also an important demonstration that there is a strong relationship between bitumen liberation and the rheological behavior of oil sands slurries.

It is also noteworthy in the results from Figures 4.15 to 4.17 that at 25 °C and for 5 wt% and 10 wt% bitumen mixtures, the flow curves show very strong thixotropy (H=98 Pa/s at 5 wt% bitumen and H=281 Pa/s at 10 wt% bitumen) and H increases sharply with bitumen concentration. These results show again that although an increase in bitumen concentration increases the number of inter-particle aggregates, a large number of them are broken-down by shearing during the test.

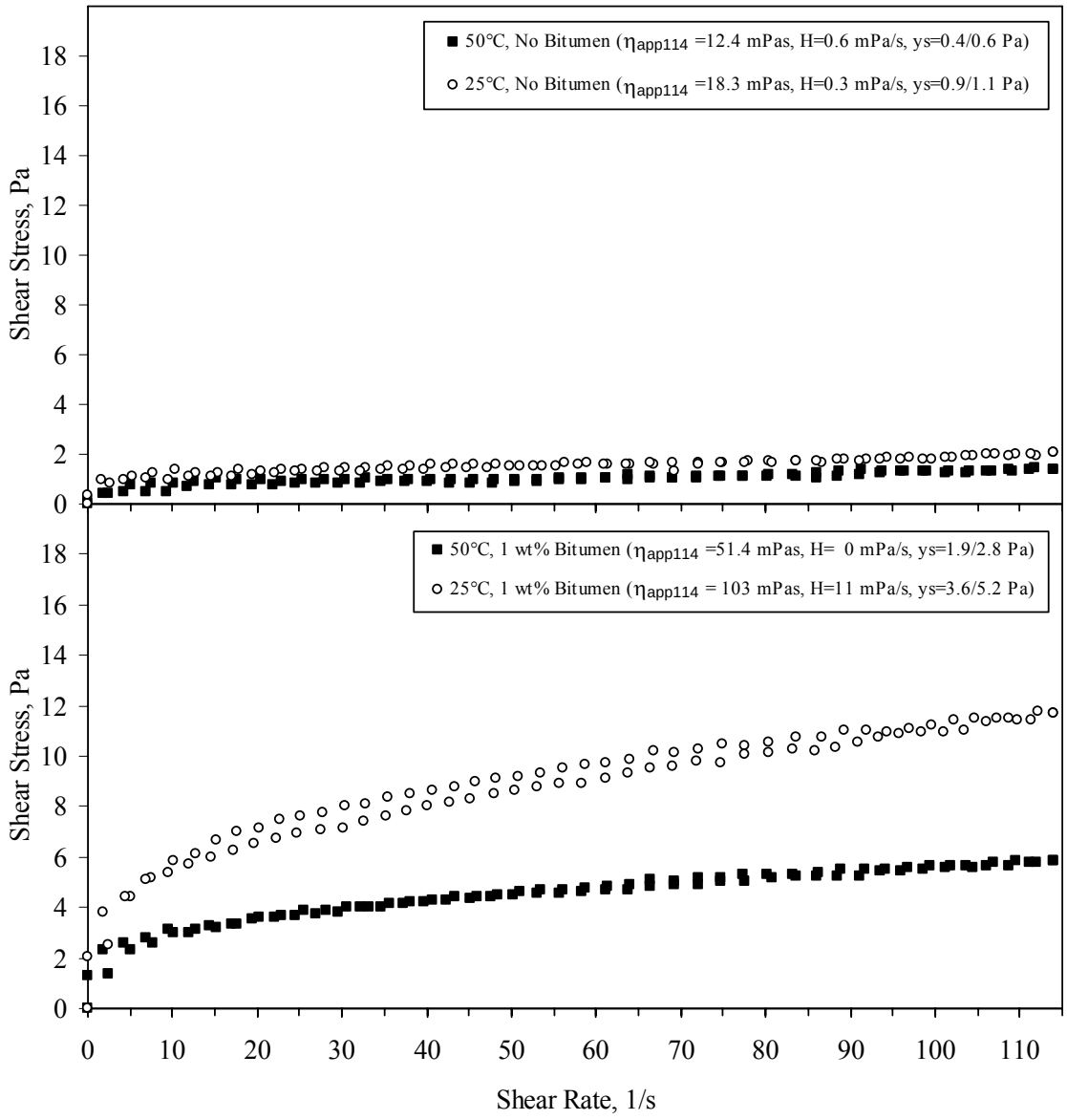

Figure 4.15: Effect of temperature on rheological flow curves for slurries of pure quartz (Top Figure) and bitumen-quartz mixtures at 1 wt% bitumen (Bottom Figure). General testing conditions: 45 wt% solids, pH 8.5 and solutions containing 0.01M NaCl/0.001M $CaCl_2$.

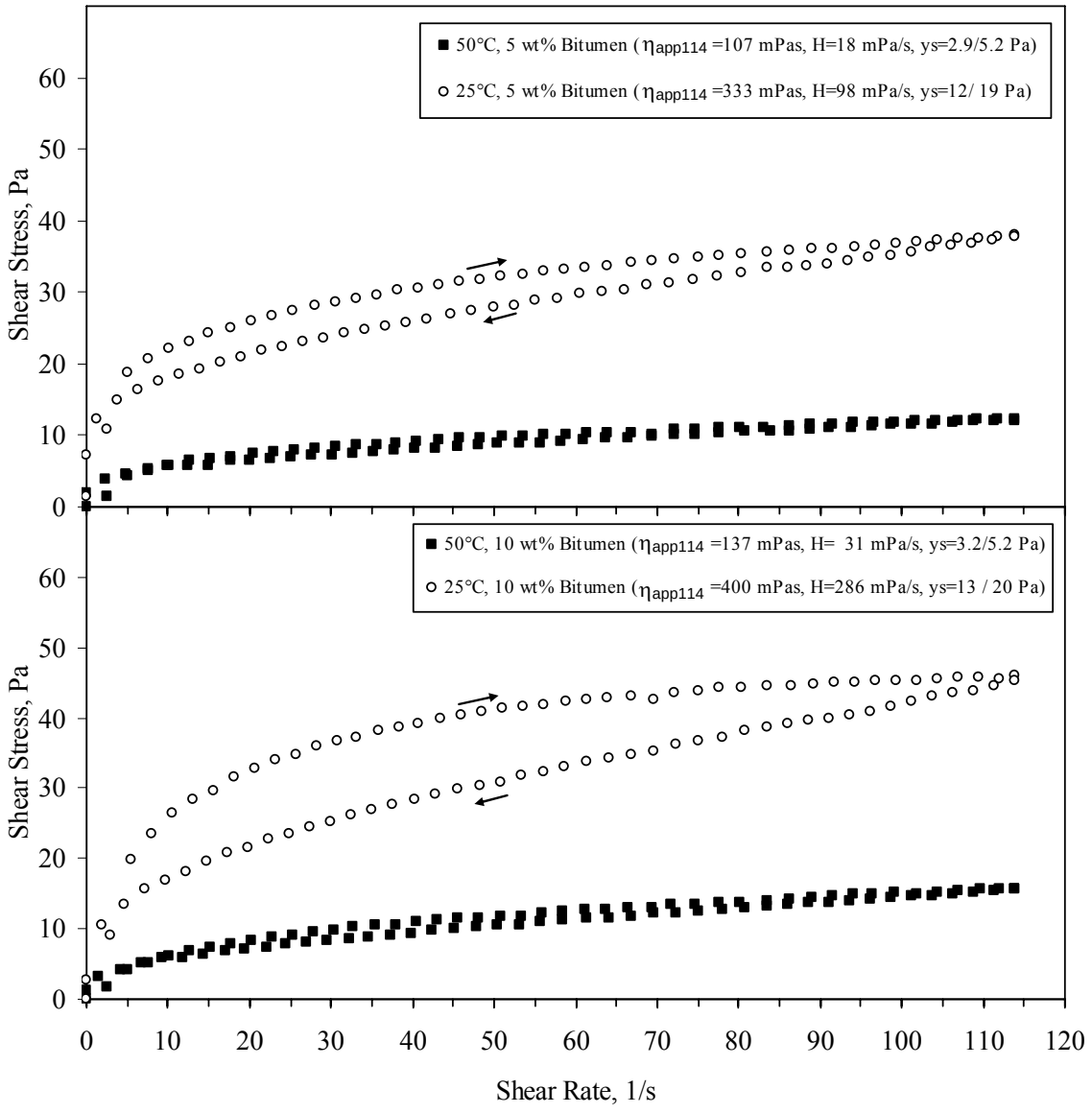

Figure 4.16: Effect of temperature on rheological flow curves for slurries of bitumen-quartz mixtures at 5 wt% bitumen (Top Figure) and at 10 wt% bitumen (Bottom Figure). General testing conditions: 45 wt% solids, pH 8.5 and solutions containing 0.01M NaCl/0.001M $CaCl_2$.

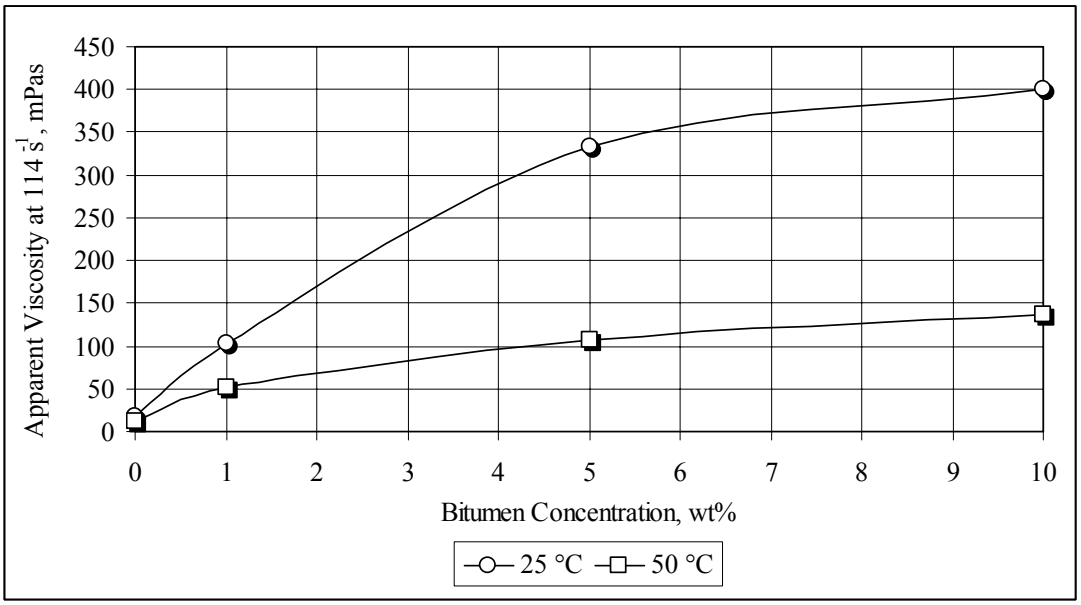

Figure 4.17: Apparent viscosity at a shear rate of 114 s^{-1} (η_{app114}) as a function of bitumen concentration and temperature. General testing conditions: slurries of bitumen-quartz mixtures tested at 45 wt% solids, pH 8.5 and using solutions containing 0.01M NaCl/0.001M $CaCl_2$.

Figure 4.18 shows two pictures of slurries of bitumen-quartz mixtures at 10 % bitumen tested at 25 and 50 °C. It can be seen that the size of the free bitumen layer increases with temperature, which indicates that bitumen liberation from quartz increases with temperature under the testing conditions.

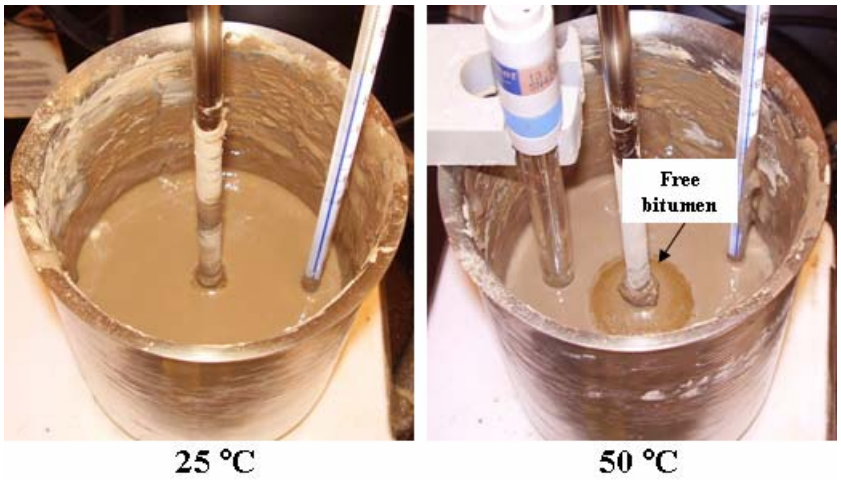

Figure 4.18: Bitumen layer formed on the surface of slurries of bitumen-quartz mixtures at different temperature, after 25 min of mixing (just before rheological measurement). General testing conditions: 10 wt% bitumen, 45 wt% solids, pH 8.5 and solutions containing 0.01M NaCl/0.001M $CaCl_2$.

4.2.2.3 Effects of NaCl, KCl and $CaCl_2$

Figure 4.19 shows the effect of NaCl, KCl and $CaCl_2$ on the rheology of slurries of bitumen-coated quartz containing 1, 5 and 10 wt% bitumen. The background condition for these tests is 45 wt% solids, pH 8.5, 50 °C and a solution containing 0.01M NaCl/0.001M $CaCl_2$.

The results show that 0.01M NaCl and 0.001M $CaCl_2$ slightly increase apparent viscosity at all bitumen concentrations tested. The adsorption of these types of ions onto surfaces of bitumen and quartz reduces the surface charge of quartz (Ma and Pawlik, 2005; Franks, 2002; Farrow et al., 1989; Masliyah et al., 2004) causing aggregation in dilute suspensions. However, the experimental results show that these effects are not significant at the concentration levels tested.

It can be seen that when KCl is used instead of NaCl apparent viscosity measurably increases and this difference due to the presence of KCl is significantly greater than the increase observed with pure quartz slurries. These results indicate that the poor hydration of K^+ enhances its adsorption onto quartz and bitumen surfaces causing a strong reduction of surface charge of these materials. The fact that the potassium effect is stronger in the presence of bitumen than in pure quartz slurries suggests that this ion also strongly interacts with bitumen.

Figure 4.20 shows pictures of slurries of bitumen-quartz mixtures at 10 wt% bitumen tested in solutions with and without 0.001M $CaCl_2$, and with and without 0.01M KCl. It can be seen that the slurry without 0.001M $CaCl_2$ shows a bitumen layer slightly darker and larger than the suspension with 0.001M $CaCl_2$. This result suggests that bitumen liberation is only slightly lower when a small amount of $CaCl_2$ is present, which is in agreement with the slight change in the obtained apparent viscosity values. In the case of KCl, it can be seen that when 0.01M KCl is present, the bitumen layer is not observed, implying a very low level of bitumen liberation, which is in agreement with the high apparent viscosity observed in the absence of KCl.

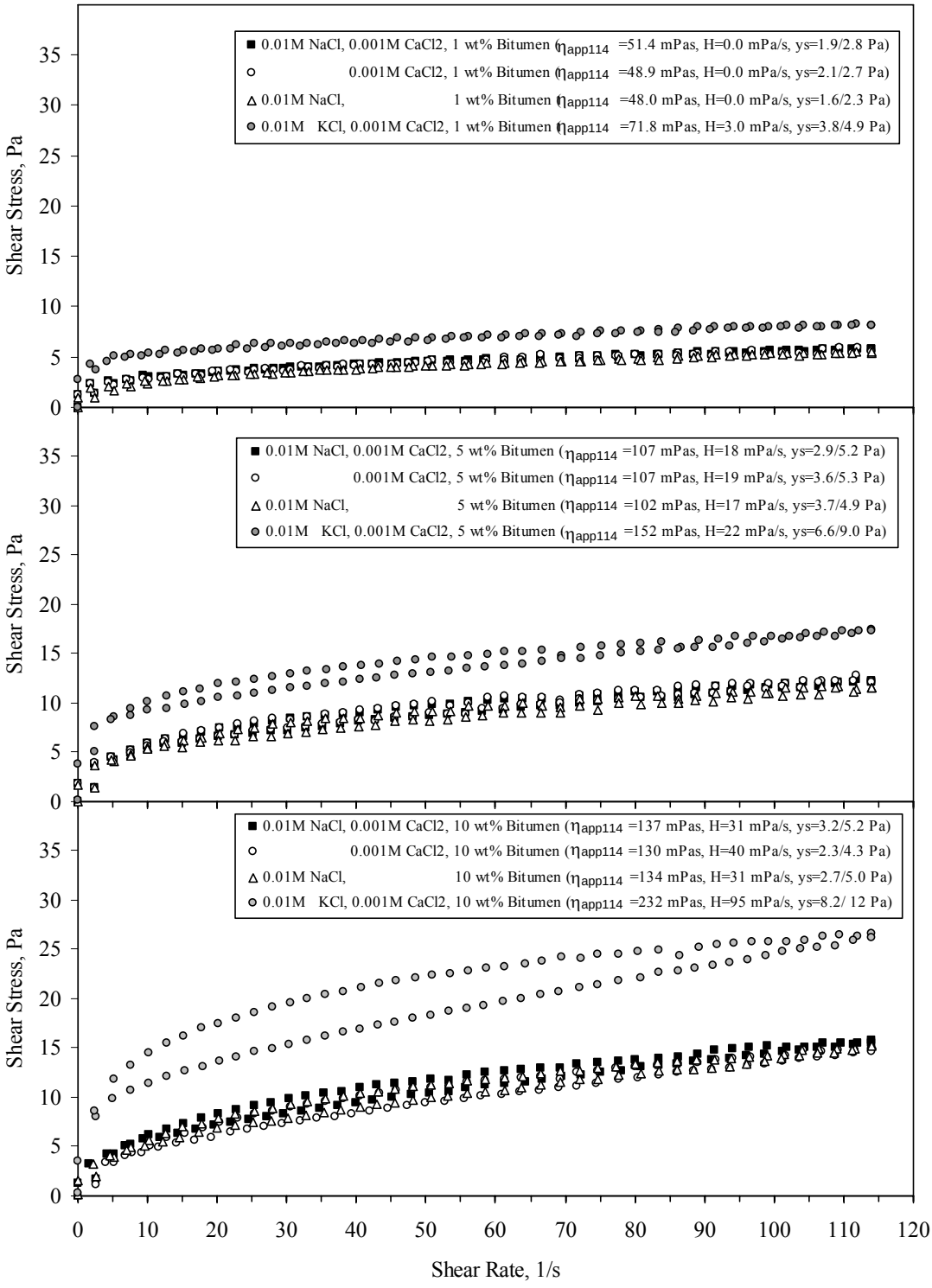

Figure 4.19: Effect of NaCl, KCl and $CaCl_2$ on rheological flow curves for slurries of bitumen-quartz mixtures at 1 wt% bitumen (Top Figure), 5 wt% bitumen (Middle Figure) and 10 wt% of bitumen (Bottom Figure). General testing conditions: 45 wt% solids, pH 8.5 and 50 °C.

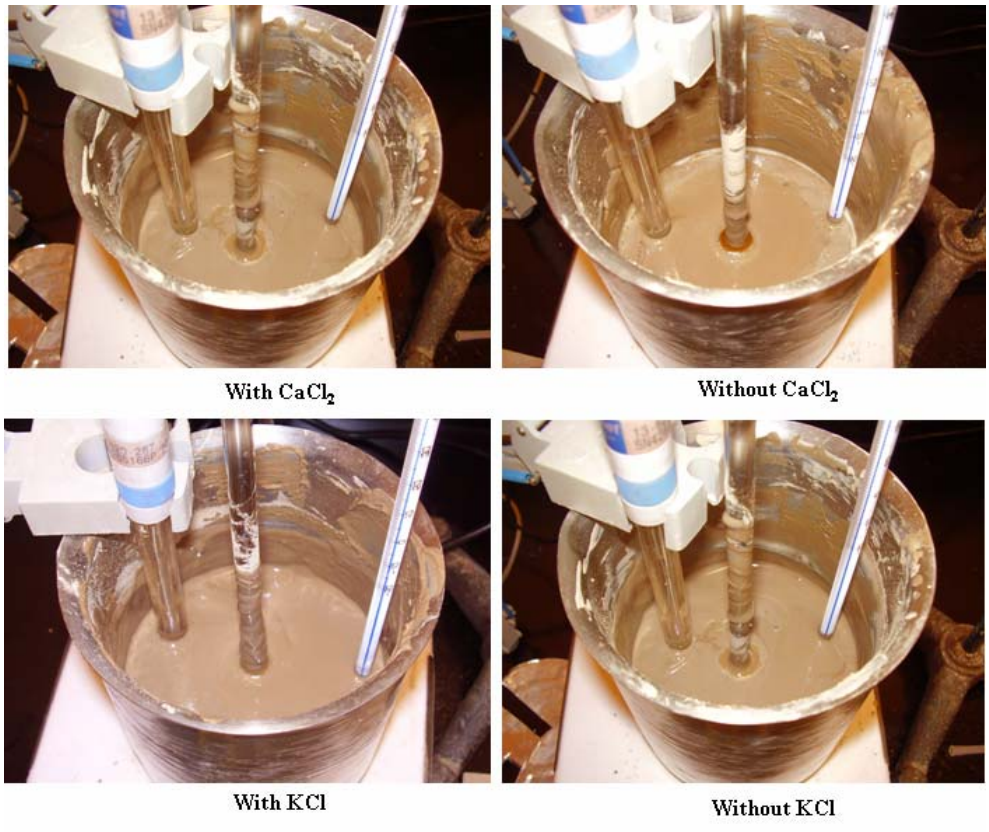

Figure 4.20: Bitumen layer formed on the surface of slurries at different solution composition, after 25 min of mixing (just before rheological measurement). General testing conditions: 10 wt% bitumen, 45 wt% solids, pH 8.5 and 50 °C.

4.2.2.4 Effects of temperature, pH and ions on rheology of slurries of bitumen-coated quartz at 10 wt% bitumen

In order to explore the effects of temperature and salts at different pH values, additional experiments were conducted with slurries of one bitumen-quartz mixture containing 10 wt% bitumen.

Figure 4.21 shows the effects of temperature and pH on slurries tested at 45 wt% solids, in solutions containing 0.01M NaCl/0.001M $CaCl_2$. The results show that the effect of temperature seems to be stronger at pH 8.5, an observation which is in agreement with results obtained with pure quartz slurries. It is interesting to note that these results, obtained with synthetic ores, show that the effect of temperature at different pH values follows the same trend as the results obtained with pure quartz slurries, which suggests that the surface charge characteristics of quartz are not affected by bitumen. This conclusion correlates with the known observation that the iep values for bitumen and quartz are very similar (pH 2-3) which means that at a given pH value both bitumen and quartz will similarly be charged promoting mutual repulsion and dispersion. It is also known that hydrophobicized quartz (methylated quartz) has the same iep at pH around 2 as pure hydrophilic quartz (Laskowski and Kitchener, 1969).

Figure 4.22 shows the effect of NaCl, KCl and $CaCl_2$ at different pH values. These results show that 0.01M NaCl does not have a significant effect at any pH tested which can be explained by the small change in the surface charge of quartz and bitumen generated by this salt under the testing conditions. 0.01M KCl and 0.001M $CaCl_2$ increase the apparent viscosity of these types of slurries which can be explained by a reduction in bitumen liberation, and the differential effect of these salts is more pronounced at lower pH.

It is noteworthy that a slurry with the lowest viscosity is obtained at high pH and high temperature, basically under the conditions that should produce the highest degree of bitumen liberation.

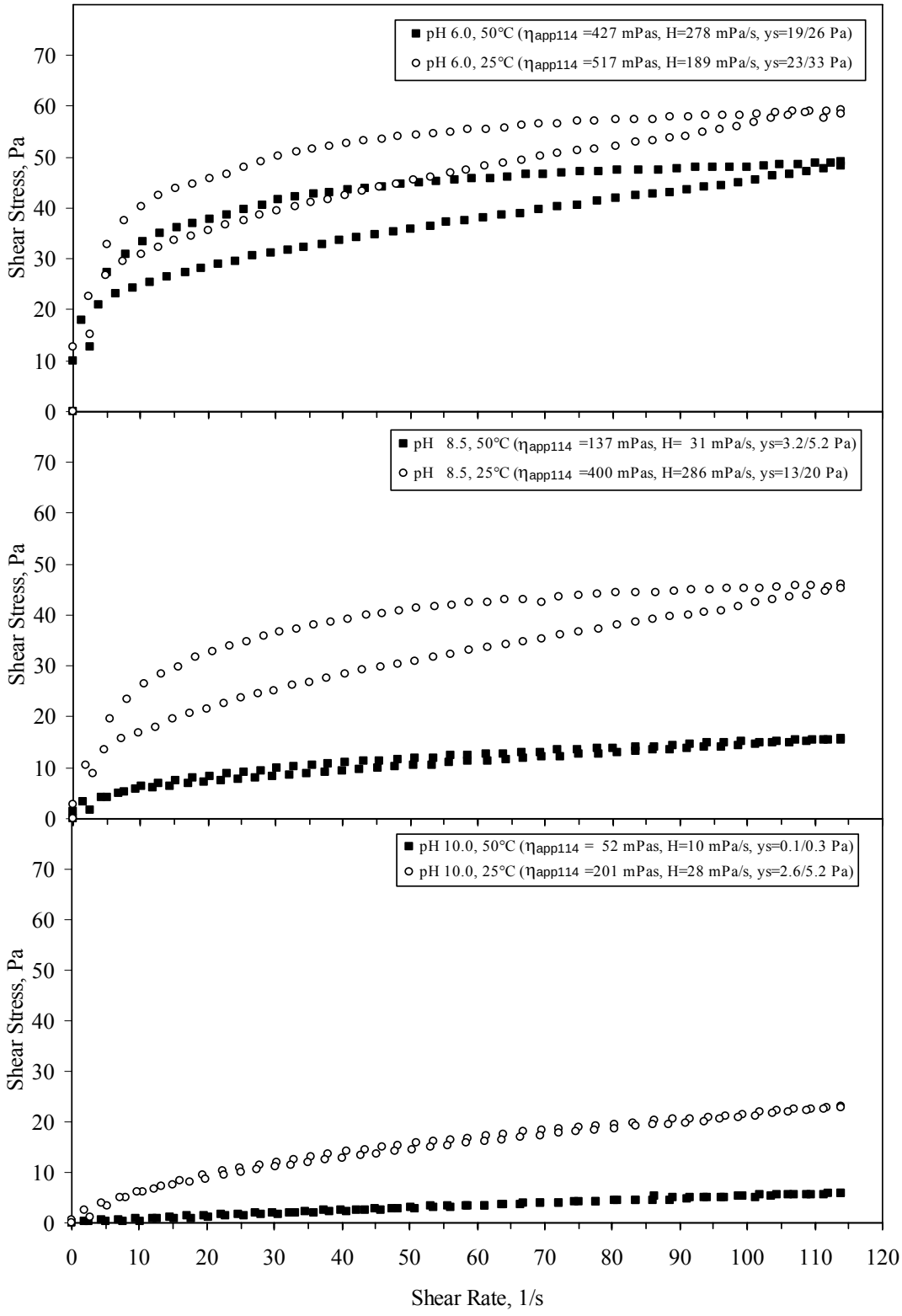

Figure 4.21: Effect of pH and temperature on rheological flow curves for slurries of bitumen-quartz mixture at 10 wt% bitumen. General testing conditions: 45 wt% solids and solutions containing 0.01M NaCl/0.001M $CaCl_2$.

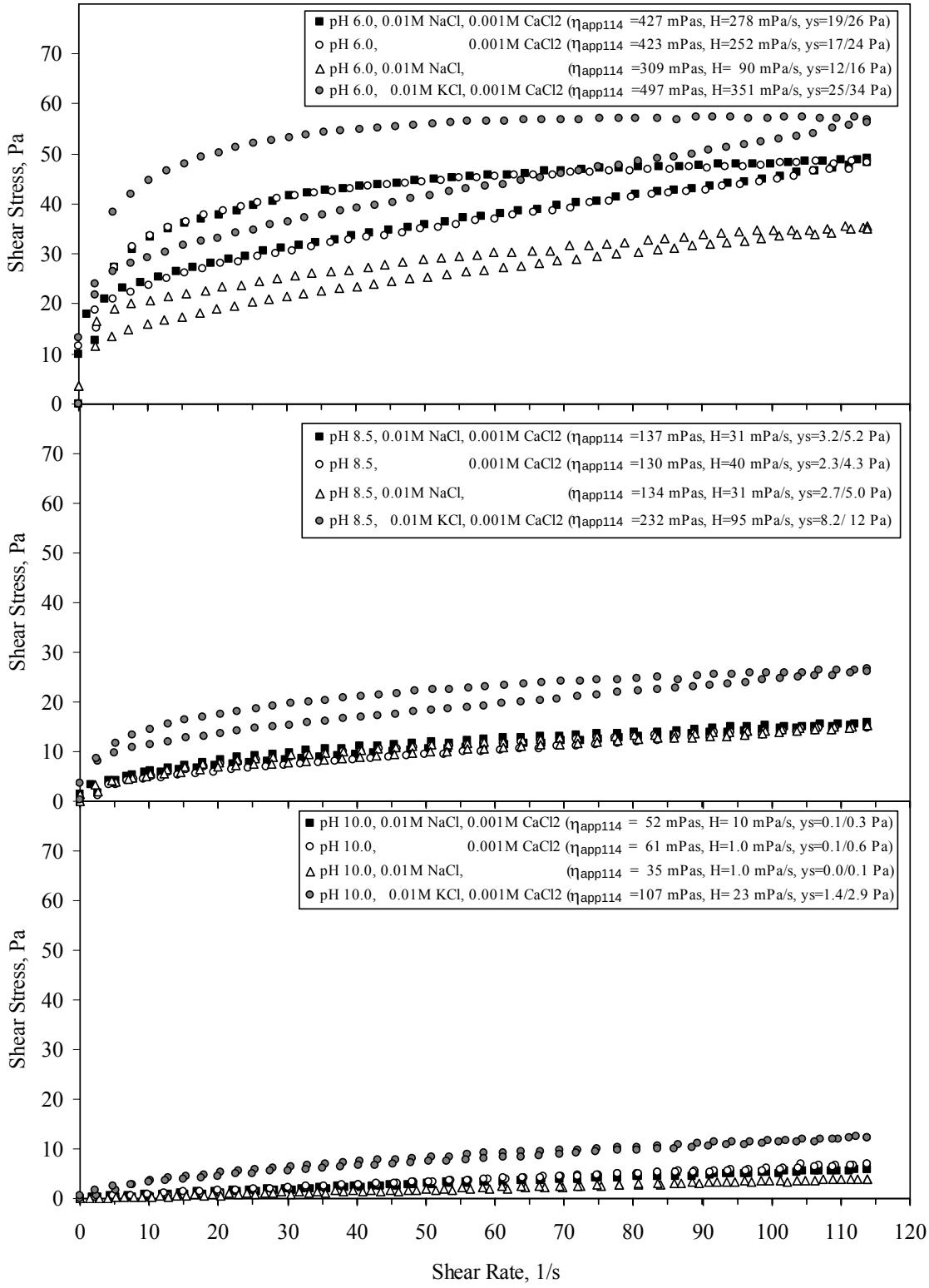

Figure 4.22: Effect of pH, NaCl, KCl and $CaCl_2$ on rheological flow curves for slurries of bitumen-quartz mixtures at 10 wt% bitumen. General testing conditions: 45 wt% and 50 °C.

4.2.2.5 Results with bitumen emulsions (bitumen fully liberated)

In order to confirm the hypothesis that the apparent viscosity of oil sand ore slurries decreases with increasing bitumen liberation, results from two experiments are compared: in the first experiment, a slurry of a bitumen-quartz mixture containing 1 wt% bitumen at 45 wt% solids was tested; in the second experiment the slurry was prepared by pouring an emulsion of bitumen (bitumen fully liberated) into a slurry of pure quartz adding the mass of bitumen required to meet a bitumen concentration of 1 wt% (based on solid + bitumen). In the first test, bitumen was attached to quartz particles, while in the second test bitumen was well liberated in the form of emulsion.

Figure 4.23 shows the results obtained at pH 6.0, pH 10.0 and 50 °C. It can be seen that apparent viscosity is significantly reduced as bitumen is added as an emulsion of free droplets. It is interesting to note also that the flow curve for the fully liberated system at pH 10.0 is almost the same as for a slurry of pure quartz. This is no longer the case at pH 6.0 most likely due to coagulation between bitumen droplets and quartz particles.

Figure 4.24 shows the results obtained under the same testing conditions as the results in Figure 4.23 but at 25 °C. At low temperature, apparent viscosity is also significantly reduced as bitumen is fully liberated. In this case the difference between the flow curves obtained for the fully liberated system and for pure quartz suspensions is slightly greater, maybe due to some attachment of bitumen to quartz obtained at low temperature.

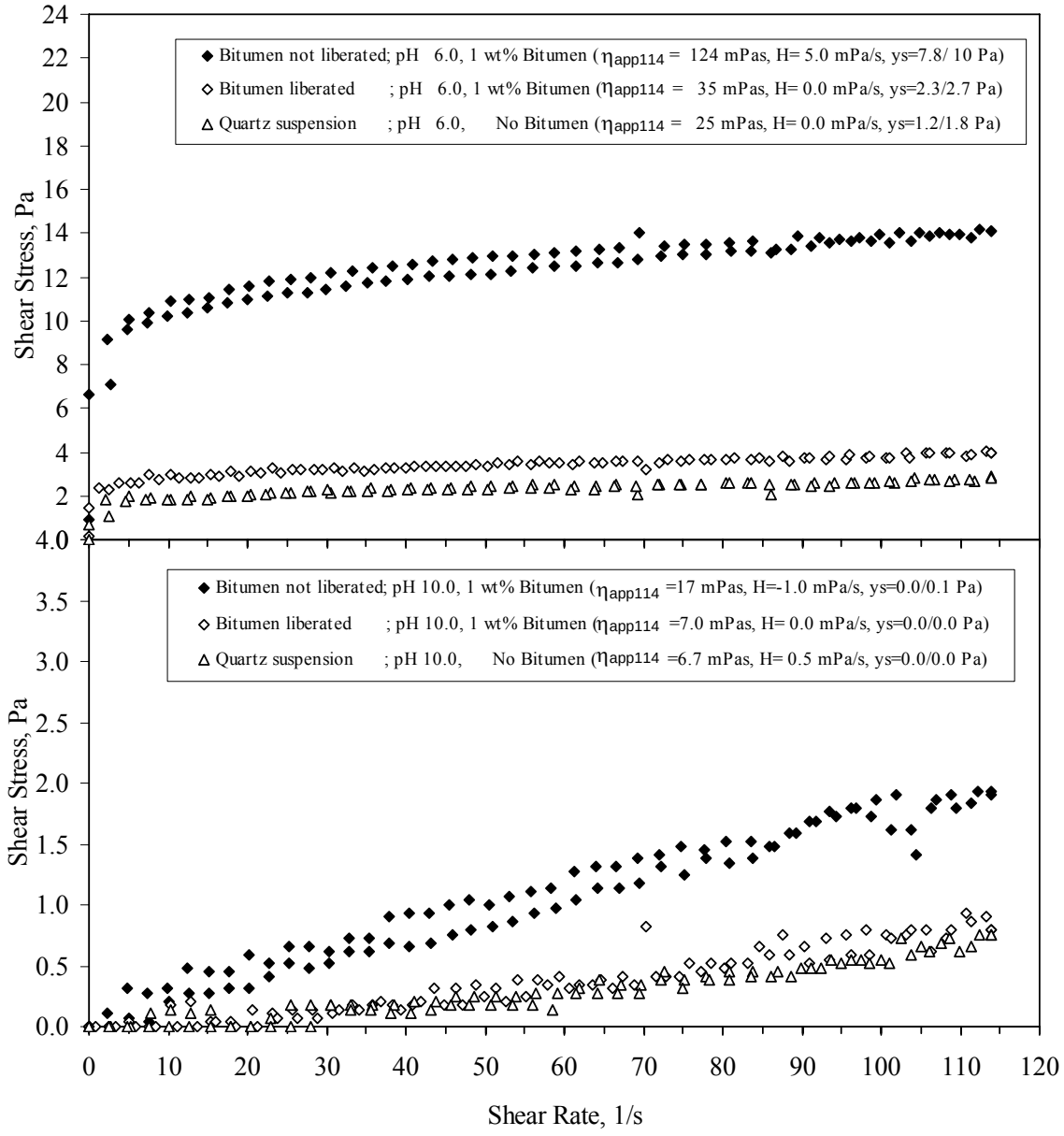

Figure 4.23: Comparison of rheological behavior for slurries of pure quartz, bitumen liberated and bitumen not liberated. General testing conditions: 45 wt% solids, 1 wt% bitumen content, 50 °C and solutions containing 0.01M NaCl/0.001M $CaCl_2$.

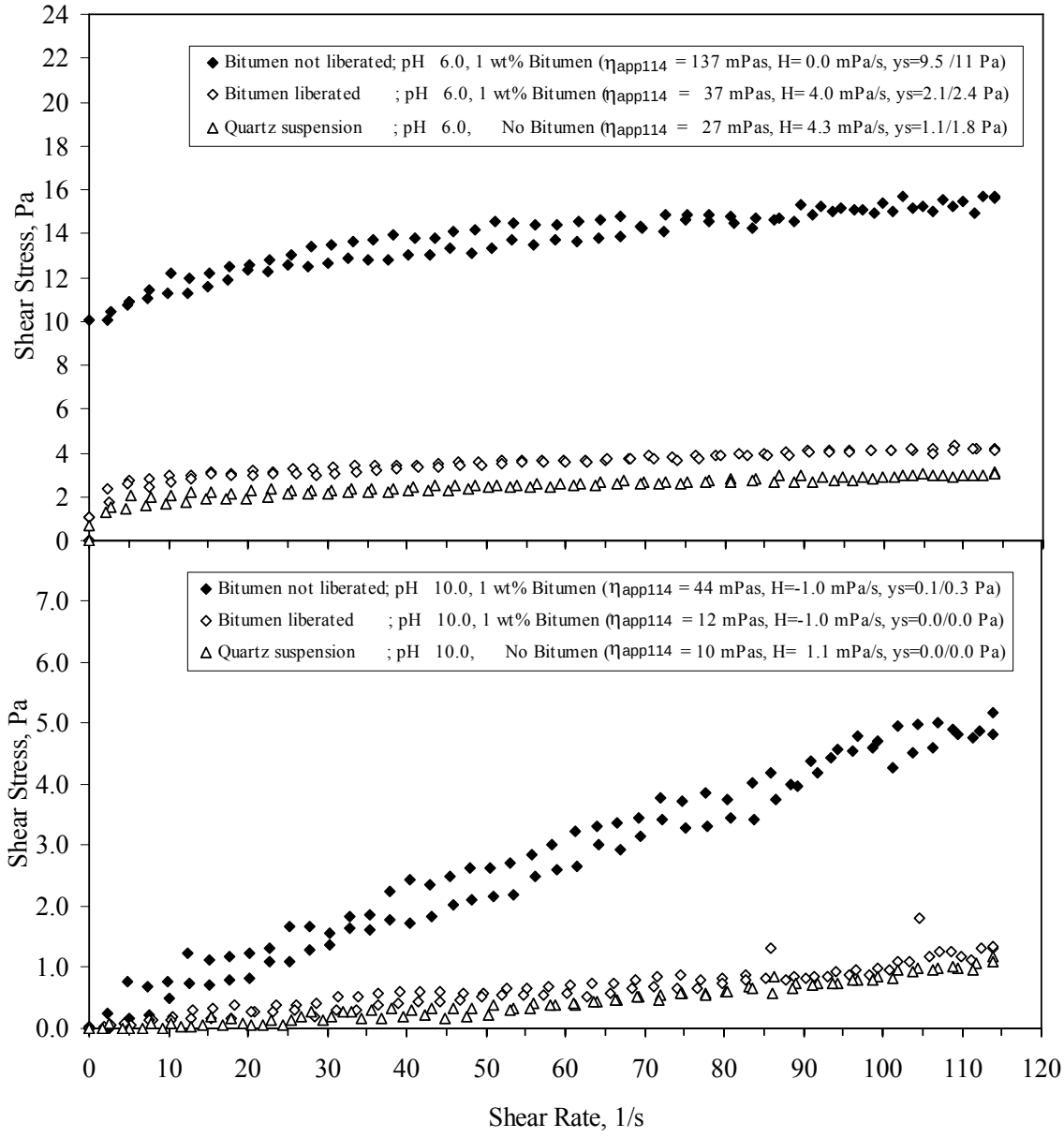

Figure 4.24: Comparison of rheological behavior for slurries of pure quartz, bitumen liberated and bitumen not liberated. General testing conditions: 45 wt% solids, 1 wt% bitumen content, 25 °C and solutions containing 0.01M NaCl/0.001M $CaCl_2$.

4.2.2.6 Effect of humic acids

Figure 4.25 shows results for slurries of bitumen-coated quartz containing 10 wt% bitumen, at two different dosages of humic acid: 100 g/t and 200 g/t. Dosages are calculated with respect to the mass of the bitumen-quartz mixture. It can be seen that humic acids reduce apparent viscosity and that the most important effect is obtained at a dosage of 100 g/t. A dosage of 200 g/t still improves rheology, however, the effect is marginal. As it is explained in section 2.3.4, humic acids are likely to be adsorbed onto bitumen surfaces making them more hydrophilic and more charged, an effect which should enhance bitumen dispersion from quartz particles thus leading to higher liberation.

It must be pointed out that oil sands processing involves a flotation stage after conditioning, so it is of critical significance to investigate how humic acids affect bitumen recovery during flotation. This topic will not be studied in this thesis.

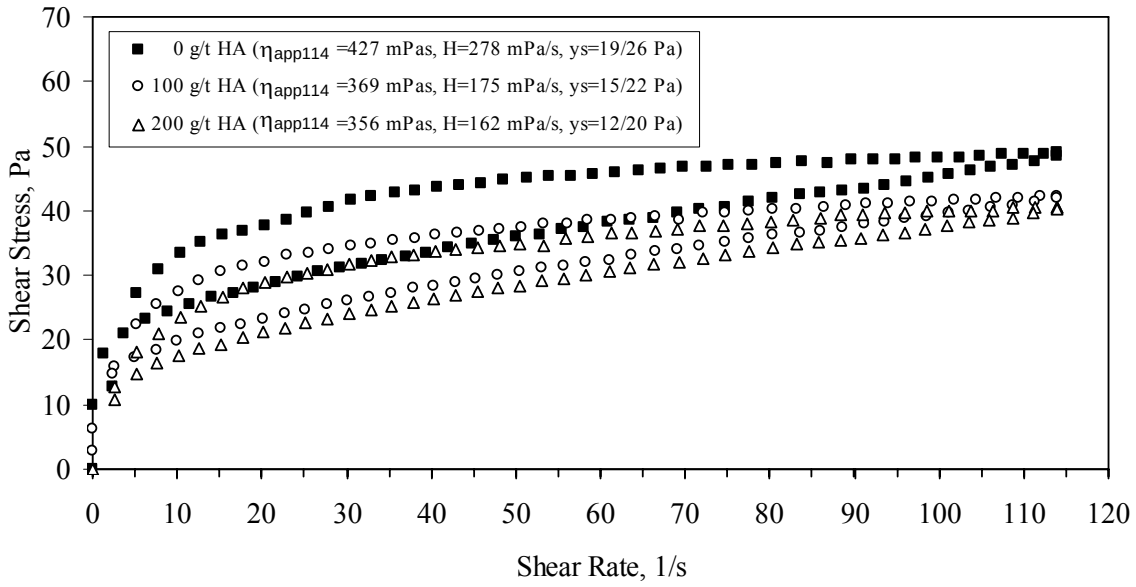

Figure 4.25: Effect of humic acid on the rheological behavior of slurries of a bitumen-quartz mixture at 10 wt% bitumen. General testing conditions: 45 wt% solids, pH 6.0, 50 °C and solutions containing 0.01M NaCl/0.001M $CaCl_2$.

4.3 Rheological results for slurries of actual oil sand ores

4.3.1 Effects of pH and temperature

Figures 4.26 and 4.27 show the effect of pH on the rheology of slurries of four actual oil sand ores: ore-1, ore-2, ore-3 and ore-4. The results show that apparent viscosity decreases with increasing pH for all ores tested, which can be explained by a greater bitumen liberation obtained at high pH. It is important to note that the pH effect for actual ore slurries is very small compared to synthetic ores most likely because of the difference in the particle size distribution of both types of materials which makes the colloidal interaction less important than in the case of fine quartz. The actual ores were much coarser than the model bitumen-quartz sample. It can also be seen that the flow curve patterns are slightly shear thickening in the range of the shear rates explored, which is in agreement with the results reported for pure quartz slurries by Scott (1982) and Savarmand et al. (2003), and with the results presented in the earlier section of this thesis.

Figure 4.28 and 4.29 show the effect of temperature on the rheological behavior of slurries prepared with the same four actual oil sand ores. It can be seen that an increase in temperature produces a reduction in apparent viscosity, which can be explained also by a greater bitumen liberation obtained at high temperature.

Figure 4.30 shows a relation between the apparent viscosity at a shear rate of $114s^{-1}$ and bitumen content. The general trend indicates that the apparent viscosity of the actual ore slurries decreases with increasing bitumen content, which correlates with industrial observations that bitumen liberation increases with bitumen grade.

Figure 4.31 and 4.32 show a relation between apparent viscosity and the fraction of particles finer than 44 μm and 3 μm respectively. It can be seen that the degree of correlation is better when the fraction finer than 3 μm is used. These results suggest that the ultra-fines content (<3 μm) plays an important role in the rheology of oil sand ores. The negative effect of ultra-fines on the processing of oil sands was reported previously by Tu et al. (2004). It is also important to note that the correlations shown in Figures 4.30 through 4.32 were obtained under the conditions of highest bitumen liberation and strongest particle dispersion. As it was shown in the section on quartz-bitumen mixtures, the rheology of completely dispersed, highly liberated quartz-bitumen slurries does not depend on bitumen content (in the range investigated), and is very similar to the rheology of pure quartz suspensions. This observation suggests that only the

particle size distribution of the solids should be the most significant variable in the absence of inter-particle interactions. As the data for the ores show, this is indeed the case although the presence of ultra-fines is far more important than the overall particle size distribution. No other property of the ores seems to correlate with slurry rheology

These results represent a good confirmation of the main working assumption of this thesis that the rheology of oil sand slurries is affected by the liberation of bitumen from sand grains, at least under the testing conditions corresponding to the industrial conditions of optimum bitumen recovery (high pH and high temperature).

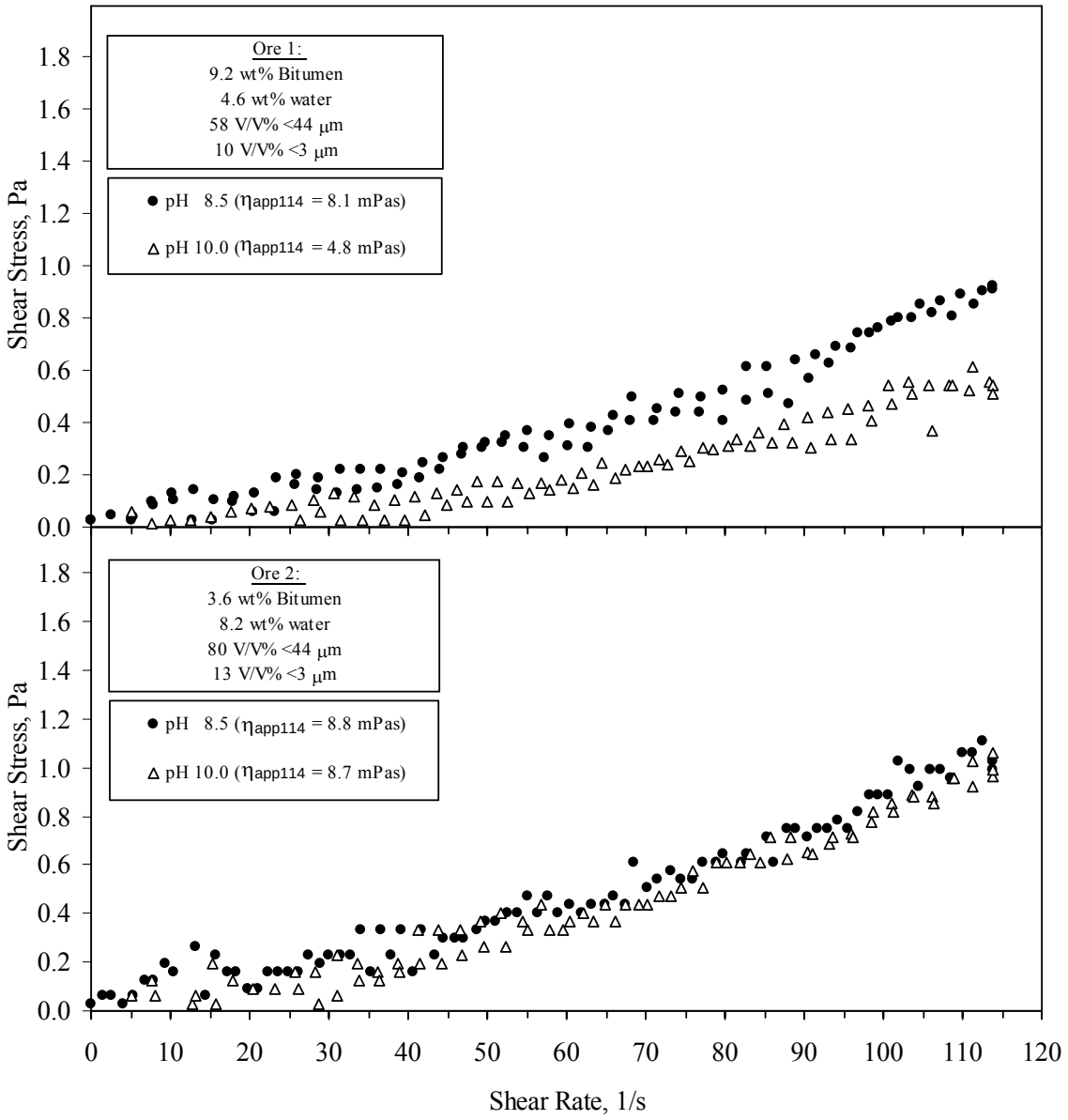

Figure 4.26: Effect of pH on the rheological behavior for slurries of two actual oil sand ores, ore-1 and ore-2, tested at 45 wt% solids, 50 °C and using solutions containing 0.01M NaCl/0.001M $CaCl_2$.

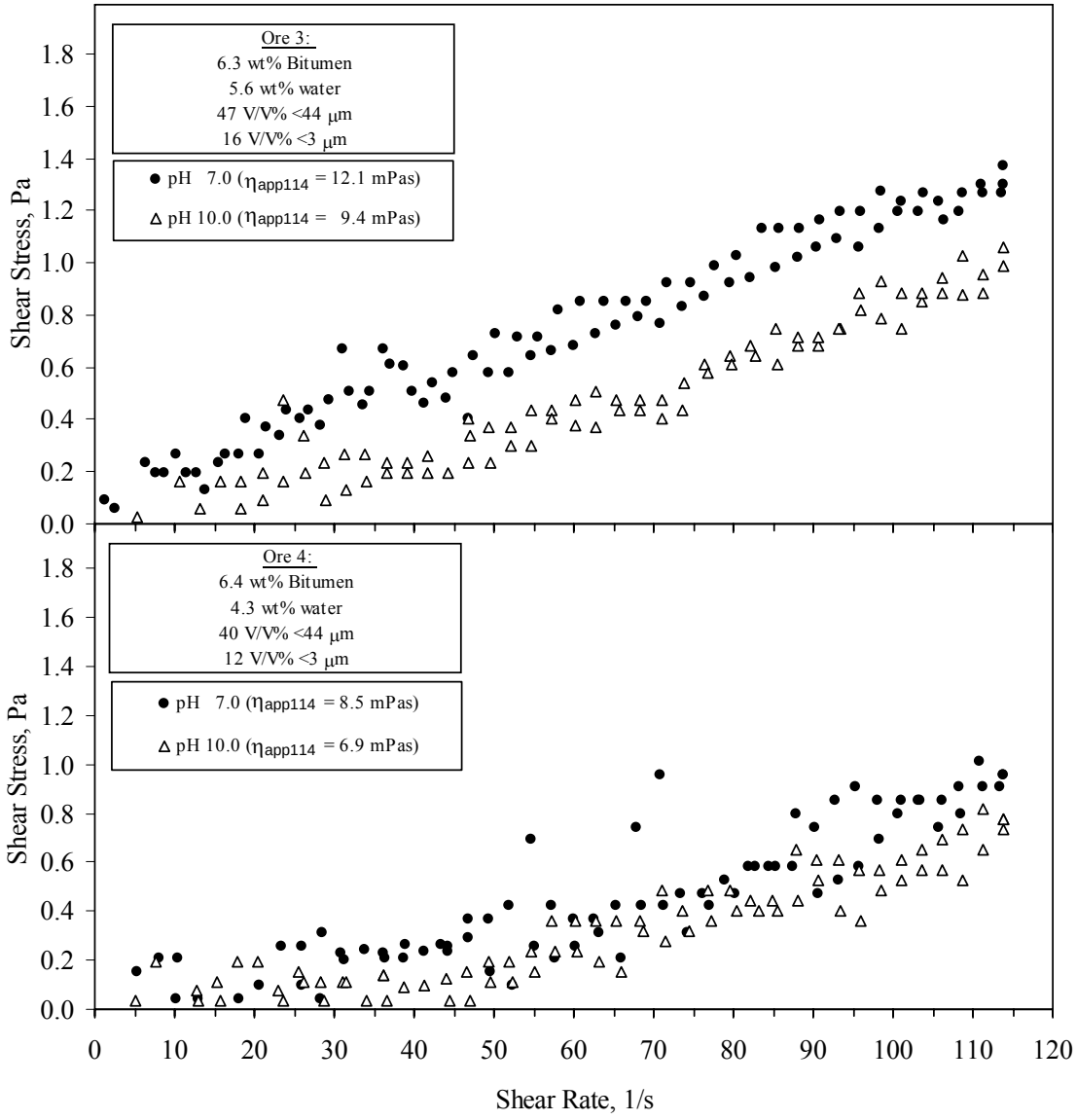

Figure 4.27: Effect of pH on the rheological behavior for slurries of two actual oil sand ores, ore-3 and ore-4, tested at 45 wt% solids, 50 °C and using solutions containing 0.01M NaCl/0.001M $CaCl_2$.

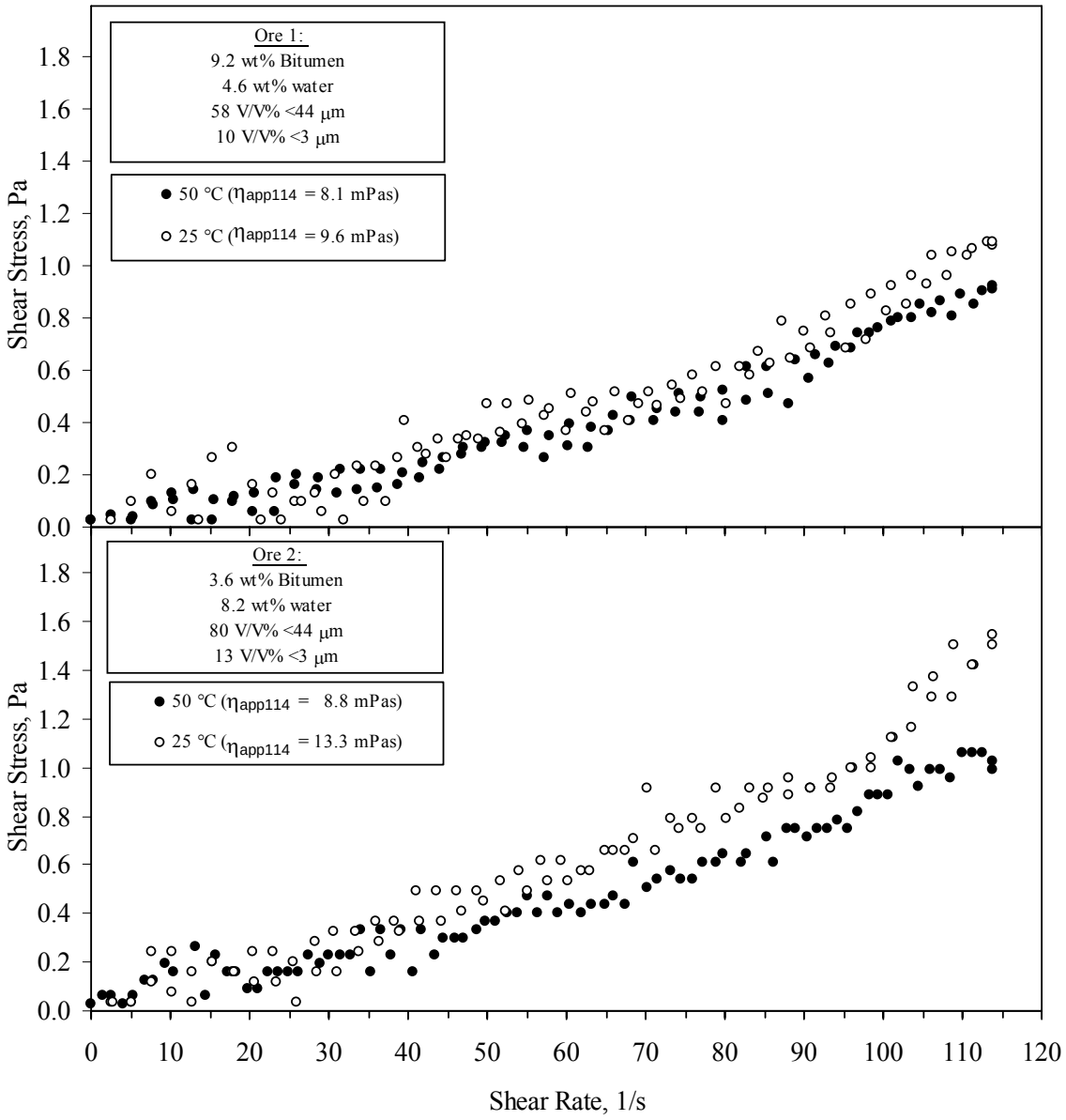

Figure 4.28: Effect of temperature on the rheological behavior for slurries of two actual oil sand ores, ore-1 and ore-2, tested at 45 wt% solids, pH 8.5 and using solutions containing 0.01M NaCl/0.001M $CaCl_2$.

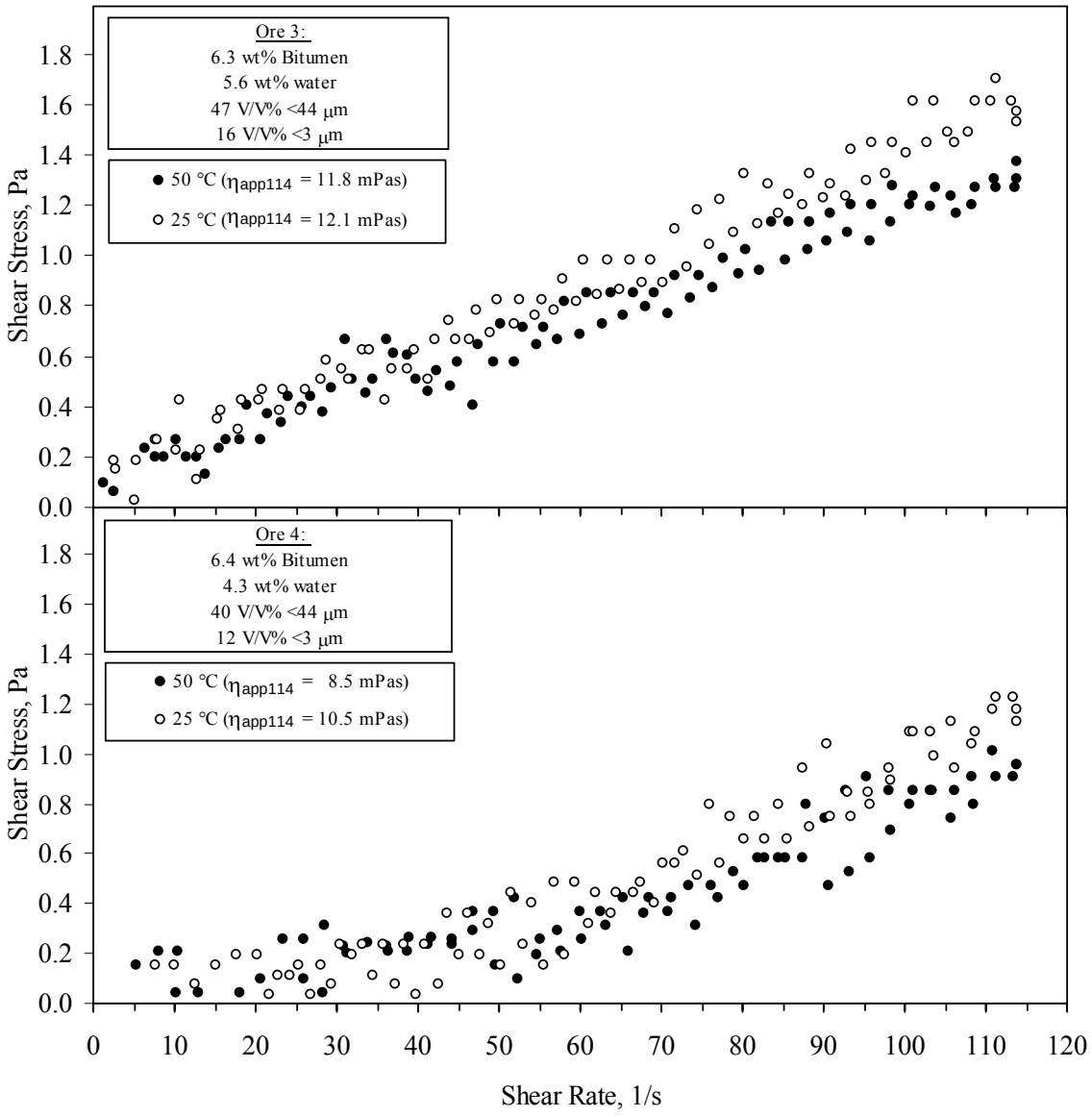

Figure 4.29: Effect of temperature on the rheological behavior for slurries of two actual oil sand ores, ore-3 and ore-4, tested at 45 wt% solids, pH 8.5 and using solutions containing 0.01M NaCl/0.001M $CaCl_2$.

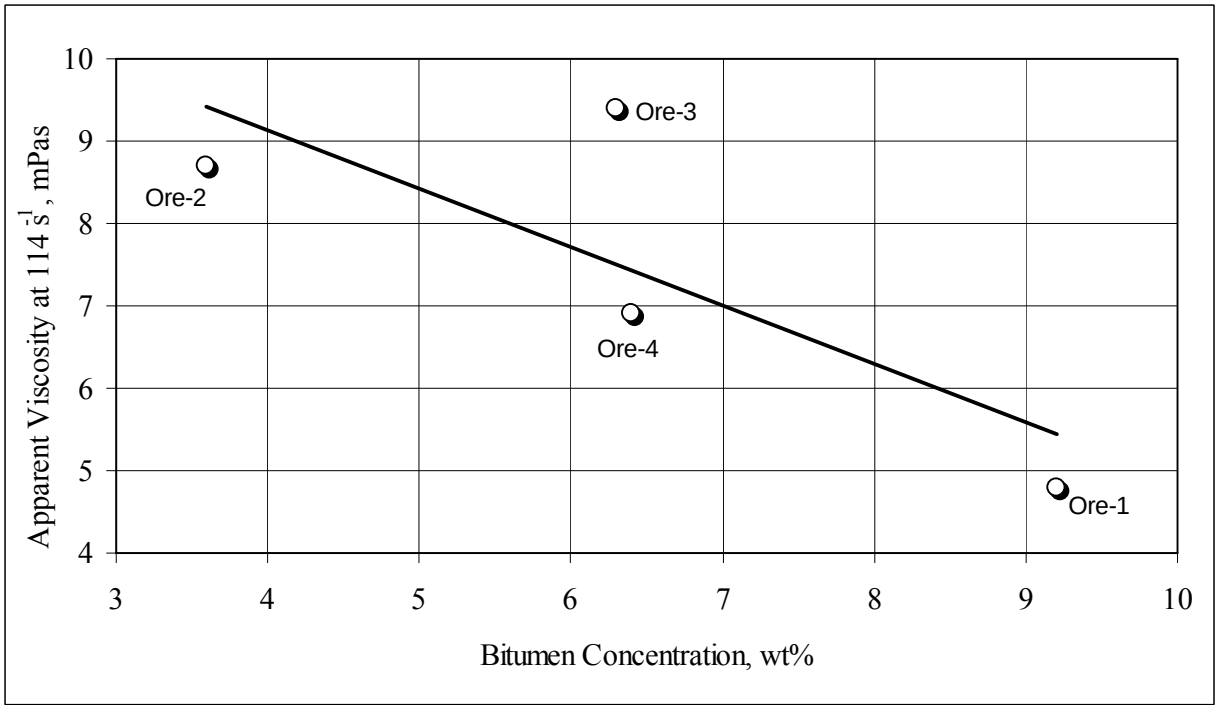

Figure 4.30: Relationship between the apparent viscosity at a shear rate of 114 s^{-1} and bitumen content for the four actual ores tested. Testing conditions: pH 10.0 and 50 °C.

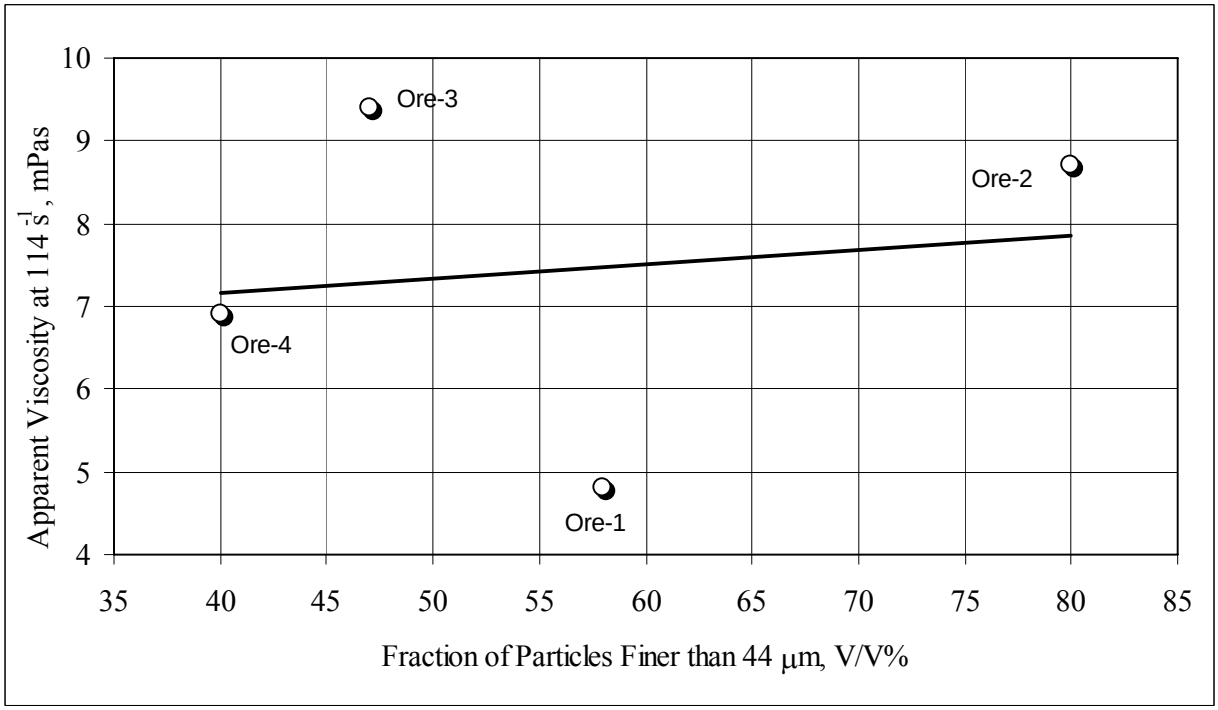

Figure 4.31: Relationship between the apparent viscosity at a shear rate of 114 s^{-1} and fraction of particles finer than 44 μm. Testing conditions: pH 10.0 and 50 °C.

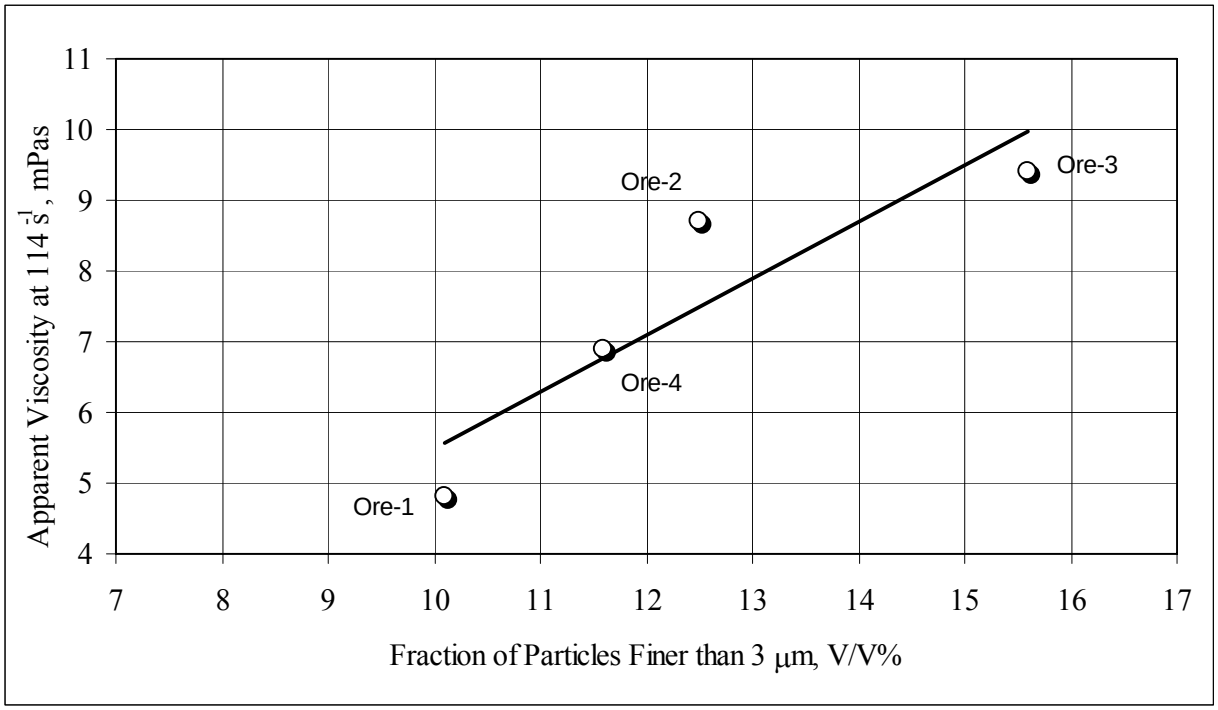

Figure 4.32: Relationship between the apparent viscosity at a shear rate of 114 s^{-1} and fraction of particles finer than 3 μm. Testing conditions: pH 10.0 and 50 °C.

5 Conclusions and recommendations

The rheology of quartz suspensions correlates with the surface properties of quartz under different physicochemical conditions. The pH of the suspensions is the most important factor, and its very strong effect is related to changes in the surface charge of quartz particles. At higher pH values, when quartz particles are strongly negatively charged, the particles are fully dispersed by electrostatic repulsion and this dispersion produces low viscosities of the slurries with basically a Newtonian flow behavior.

As electrostatic repulsion between quartz particles gradually decreases as the pH of the suspension is lowered, both temperature and salts also contribute to the rheological response of the slurries. Higher temperature (50 °C) results in measurably lower viscosities especially under the pH conditions of the actual hot water extraction process (pH 8.5). The effect of temperature diminishes as the extent of quartz aggregation further increases at pH 6. At this pH, and most likely at lower pH values, it is the aggregation of quartz that dominates the system and temperature plays a minor role.

Among the tested salts/ions, potassium tends to produce a stronger aggregation effect than sodium, and this behavior correlates well with the known higher adsorption affinity of potassium towards quartz than that of sodium. However, the differential effect of salts is most visible only at lower pH values when the quartz particles are not fully dispersed by electrostatic repulsion.

The results obtained for quartz-bitumen mixtures show some similarities with the behavior of quartz and also some significant differences. The similarities result from the fact that both quartz and bitumen have very similar surface charge characteristics. These two components in a suspension are negatively charged under a given set of chemical conditions, and this electrostatic repulsion promotes dispersion of bitumen from quartz which is equivalent to the liberation of bitumen droplets from quartz particles. This transition between dispersion and aggregation is reflected in the rheological response of the quartz-bitumen mixtures. Quartz-bitumen slurries prepared at high pH give much lower apparent viscosities than those prepared at lower pH when quartz-bitumen aggregation should be most pronounced. Perhaps the most significant difference is observed in the effect of temperature. At higher bitumen contents (5-10%) in quartz-bitumen mixtures the effect of temperature is much more important in comparison to the effect of temperature for pure quartz suspensions. It seems that higher temperatures promote dispersion of

bitumen and again this liberation effect brings about a significant decrease in the apparent viscosity of the quartz-bitumen mixtures over the entire investigated range of pH values.

The rheology of four different oil sand ore slurries can qualitatively be predicted based on the data obtained for the model quartz-bitumen slurries. Most interestingly, the only property of the different ore types that correlates with the observed rheology is the amount of the finest particle size fractions present in these ores. Under the conditions of most pronounced bitumen liberation (high pH and temperature), only the fines content determines the rheological behavior.

The measurement of bitumen liberation is still based on indirect methods and qualitative observations, even when high speed imaging and analysis are involved. Thus, a need arises to directly quantify the level/degree of bitumen liberation. Such methods exist for mineral ores, but the same techniques cannot be applied to oil sand ores.

As the presented data suggest, there must also be a relationship between pulp rheology, bitumen recovery (by flotation), and energy requirements for mixing. It is therefore recommended that additional studies be performed to correlate bitumen extraction results with the corresponding pulp rheology data. Pulp rheology also affects the ease or difficulty of aerating an oil sand ore slurry during extraction, and a systematic study of gas dispersion phenomena as a function of pulp rheology should also be performed.

Other model systems should also be investigated. Even though quartz is the most dominant component of oil sand ores, clay particles (kaolinite, illite) are known to be present in the finest fractions. It is fair to assume that interactions of bitumen with fine clay particles most likely affect the rheology of clay-bitumen suspensions, but there are no systematic data on the rheology of such systems. The effect of clay particles on rheology is not easy to deduce based only on the presented results for quartz since the surface chemistry of clay particles is much more complex than that of quartz. The anisotropy of clay particles, i.e., the existence of silica-like “faces” and alumina-like “edges”, makes the use of rheology for analysis of aggregation/dispersion phenomena very challenging, and it all probably gets even more difficult in the presence of bitumen.

The role of rheology modifiers (e.g., polymeric dispersants) in affecting bitumen liberation and extraction should also be researched. In this case, however, additional work should be carried out to determine the effect of such additives on the wettability/hydrophobicity of bitumen itself since some of the additives, e.g, humic acids tested in this thesis, are known to depress the flotation of other naturally hydrophobic materials.

6 References

Barnes, H.A., 2000, "A Handbook of Elementary Rheology", Institute of Non-Newtonian Fluid Mechanics, University of Wales.

Basu, S., Nandakumar, K., Masliyah, J.H., 1998, "A Visual Study of High Grade Oil Sand Disintegration Process", *Journal of Colloid and Interface Science,* 205, 201-203.

Bulmer, J.T., Starr, J., 1979, "Syncrude analytical methods for oil sand and bitumen processing", the Alberta Oil Sands Technology and Research Authority, 46-52.

Casson, N., 1959, "A flow equation for pigment-oil suspensions of the printing ink type", in "Rheology of Dispersed Systems", C.C.Mill (Ed.), Pergamon Press, New York, 84.

Dai, Q., Chung, K.H., 1995, "Bitumen-sand interaction in oil sand processing", *Fuel,* 74[12], 1858-1864.

Fagan, M.E., Zukoski, C.F., 1997, "The rheology of charge stabilized silica suspensions", *Journal of Rheology,* 41[2], 373-397.

Farrow, J.B., Horsley, R.R., Meagher, L., Warren, L.J., 1989, "The effect of alkali and alkaline earth cations on the rheology of concentrated quartz suspensions", *Journal of Rheology,* 33[8], 1213-1230.

Franks, G.V., 2002, "Zeta potential and yield stresses of silica suspensions in concentrated monovalente electrolytes: isoelectric point shift and additional attraction", *Journal of Colloid and Interface Science,* 249, 44-51.

Franks, G.V., Zhou, Z., Duin, N.J., 2000, "Effect of inter-particle forces on shear thickening of oxide suspensions", *Journal of Rheology,* 44[4], 759-779.

Gamboa, C., Olea, A.F., 2006, "Association of cationic surfactants to humic acid Effect on the surface activity", *Colloids and Surfaces A: Physicochemical and Engineering Aspects,*278, 241-245.

Helper, L.G., Smith, R.G., 1994, "The Alberta Oil Sands: Industrial Procedures for Extraction and Some Recent Fundamental Research", AOSTRA Tech. Pub. Series #14, Alberta Oil Sands Technology and Research Authority, Edmonton, AB.

Johnson, S.B., Franks, G.V, Scales, P.J., Boger, D.V., Healy, T.W., 2000, "Surface Chemistry-Rheology Relationships in Concentrated Mineral Suspensions", *International Journal of Mineral Processing,* 58, 267-304.

Kasongo, T., Zhou, Z., Xu, Z., Masliyah, J., 2000, "Effect of clays and calcium ions on bitumen extraction from athabasca oil sands using flotation", *Canadian Journal of Chemical Engineering*, 78, 674-681.

Kitchener J.A., 1969, "Colloidal Minerals: Chemical Aspects of Their Dispersion, Flocculation and Filtration", *Filtration and Separation*, 6[5], 553.

Klein, B., Laskowski, J.S., Partridge, S.J. 1995, "A new viscometer for rheological measurements on settling suspensions" *Journal of Rheology,* 39[5], 827-840.

Klein, B., 1992, "Rheology and stability of magnetite dense media" PhD Thesis, The University of British Columbia, Vancouver, Canada.

Klein, B., 2009, "Observations on the rheopectic properties of nickel laterite suspensions" Handout of rheology course, The University of British Columbia, Vancouver, Canada.

Laskowski, J., Kitchener, J.A., 1969, "The hydrophilic—hydrophobic transition on silica", *Journal of Colloid and Interface Science,* 29[4], 670-679.

Lee, J.D., So, J.H., Yang, S.M., 1999, "Rheological behavior and stability of concentrated silica suspensions", *Journal of Rheology,* 43[5], 1117-1140.

Leong, Y.K., Boger, D.V., 1990, "Surface Chemistry Effects on Concentrated Suspension Rheology", *Journal of Colloid and Interface Science,* 136, 249-258.

Liu, J., Xu, Z., Masliyah, J., 2004, "Interaction between Bitumen and Fines in Oil Sands Extraction System: Implication to Bitumen Recovery", *The Canadian Journal of Chemical Engineering,* 82, 655-666.

Liu, J., Zhou, Z., Xu, Z., Masliyah, J., 2002, "Bitumen–Clay Interactions in Aqueous Media Studied by Zeta Potential Distribution Measurement", *Journal of Colloid and Interface Science,* 252, 409-418.

Liu, J., Xu, Z., Masliyah, J., 2005, "Colloidal forces between bitumen surfaces in aqueous solutions measured with atomic force microscope", *Colloids and Surfaces A: Physicochem. Eng. Aspects,* 260, 217-228.

Liu, J., Xu, Z., Masliyah, J., 2004b, "Role of Fine Clays in Bitumen Extraction from Oil Sands", *AICHE Journal,* 50[8], 1917-1927.

Liu, J., Xu, Z., Masliyah, J., 2003, "Studies on bitumen-silica interactions in aqueous solutions by atomic force microscopy", *Langmuir,* 19, 3911-3920.

Long, J., Drelich, J., Xu, Z., Masliyah, J.H., 2007, "Effect of Operating Temperature on Water‐Based Oil Sands Processing", *The Canadian Journal of Chemical Engineering,* 85, 726-738.

Luthra, M., 2001, "A visualization technique for estimating bitumen recovery from oil sands", *M.Sc.thesis, University of Alberta, Edmonton, AB.*.

Ma, X., Pawlik, M., 2005, "Effect of alkali metal cations on adsorption of guar gum onto quartz", *Journal of Colloid and Interface Science,* 289, 48-55.

Masliyah, J., Zhou, Z.J., Xu, Z., Czarnecki, J., Hamza, H., 2004, "Understanding water-based bitumen extraction from athabasca oil sands", *The Canadian Journal of Chemical Engineering,* 82, 628-654.

Ramachandran, R., Somasundaran, P., 1986, "Effect of temperature on the interfacial properties of silicates", *Colloids and Surfaces,* 21, 355–369.

Rodriguez, K., Araujo, M., 2006, "Temperature and pressure effects on zeta potential values of reservoir minerals", *Journal of Colloid and Interface Science,* 300, 788–794.

Somasundaran, P., Kulkarni, R.D., 1973, "A new streaming potential apparatus and study of temperature effects using it", *Journal of Colloid and Interface Science,* 45, 591–600.

Savarmand, S., Carreau, P.J., Bertrand, F., Vidal, D.J.-E., Moan, M., 2003, "Rheological properties of concentrated aqueous silica suspensions: Effects of pH and ions content", *Journal of Rheology,* 47[5], 1133-1149.

Scott, K.J., 1982, "The effect of surface charge on the Rheology of concentrated aqueous quartz suspensions", *Chemical Engineering research Group-Council for Scientific and Industrial Research,* Report CENG 423, Pretoria, South Africa.

Seyer, F.A., Gyte, G.W., 1989, "Viscosity", AOSTRA Tech. Handbook Oil Sands, Bitumen Heavy Oils—AOSTRA Tech. Pub. Series #6, L. G. Helper and C. Hsi, Eds., Alberta Oil Sands Technology and Research Authority, Edmonton, AB.

Taylor, G.I., 1923, "Stability of a viscous liquid contained between two rotating cylinders", Phil. Trans. R.Soc. A223, 289-343.

Terashimaa, M., Fukushimab, M., Tanakaa, S., 2004, "Influence of pH on the surface activity of humic acid: micelle-like aggregate formation and interfacial adsorption", *Colloids and Surfaces A: Physicochemical and Engineering Aspects,*247, 77-83.

Tu, Y., Li, Z., Pleizier, G., Ng, S., Chung, K.H., 2004, "Separation and characterisation of problematic solids from athabasca oil sands and waste unit samples", *The Canadian Journal of Chemical Engineering,* 82, 678-686.

Wallace, D., Tipman, R., Komishke, B., Wallwork, V., Perkins, E., 2004, "Fines/water interactions and consequences of the presence of degraded illite on oil sands extractability", *The Canadian Journal of Chemical Engineering,* 82, 667-677.

Wallwork, V., Xu, Z., Masliyah, J., 2003, "Bitumen recovery with oily air bubbles", *The Canadian Journal of Chemical Engineering,* 81, 993-997.

Wallwork, V., Xu, Z., Masliyah, J., 2004, "Processibility of athabasca oil sand using a laboratory hydrotransport extraction system (LHES)", *The Canadian Journal of Chemical Engineering,* 82, 687-695.

Wallwork, V., 2003, "Laboratory hydrotransport extraction system for oil sand processing" MSc Thesis, The University of Alberta, Edmonton, Canada.

Zhou, Z., Scales, P.J., Boger, D.V., 2001, "Chemical and Physical Control of the Rheology of Concentrated Metal Oxide Suspensions", *Chemical Engineering Science,* 56, 2901-2920.

Appendix I: Reproducibility of rheological measurements

Standard deviation (σ) is a measure of the variability or dispersion of a data set. A low standard deviation indicates that all of the data points are very close to the same value (the mean), while high standard deviation indicates that the data is spread out over a large range of values.

Standard deviation can be calculated from Equation I-1.

$$\sigma = \sqrt{\frac{\sum_{i=1}^{N}(x_i - \mu)^2}{N}} \quad \text{(I-1)}$$

Where x_i is the data point "i", μ is the mean value of all the data and N is the number of data points.

One way to quantify the reproducibility of flow curves is to determine a value of standard deviation of shear stress for every value of shear rate. Afterward, an average value over the whole range of shear rate can be calculated.

Figures I-1, I-2 and I-3 show flow curves of duplicate experiments performed on pure quartz slurries. It can be seen that the maximum value of average standard deviation was 0.04 Pa which can be interpreted as if every rheological measurement performed on these slurries has an error of ±0.04 Pa.

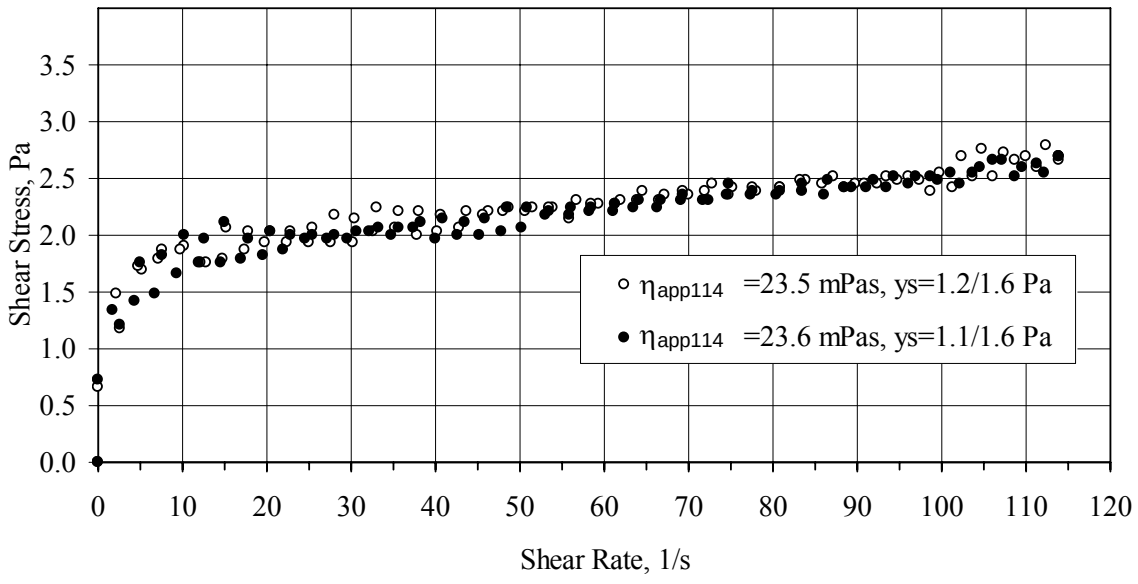

Figure I-1: Reproducibility of flow curves for pure quartz slurries. Testing conditions: 45 wt% solid, pH 6.0, 50 °C, 0.001M $CaCl_2$. Average standard deviation of shear stress= 0.04 Pa.

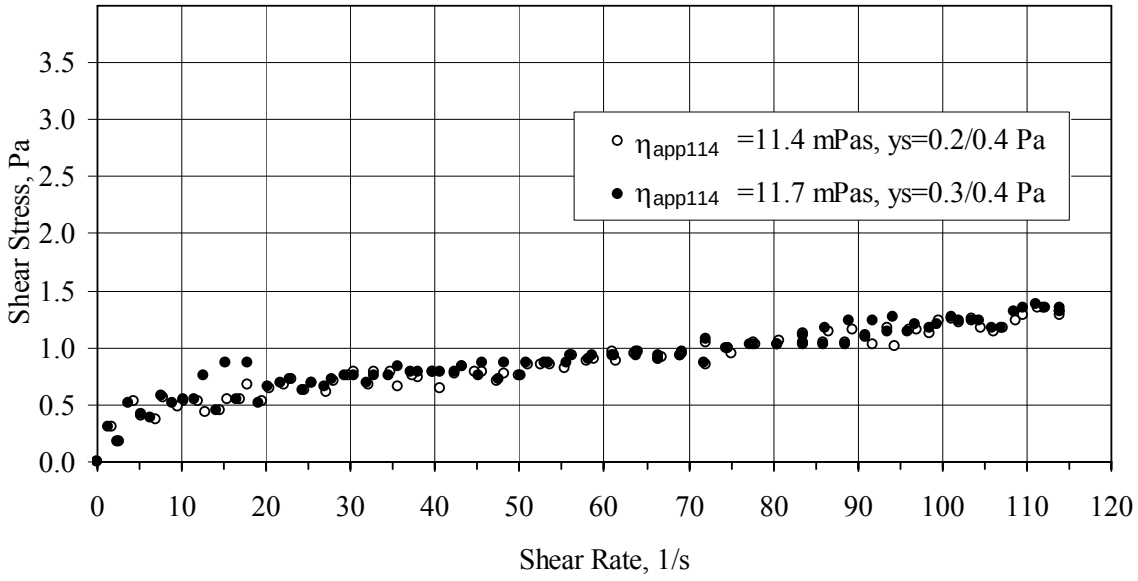

Figure I-2: Reproducibility of flow curves for pure quartz slurries. Testing conditions: 45 wt% solid, pH 8.5, 50 °C, 0.001M $CaCl_2$. Average standard deviation of shear stress= 0.02 Pa.

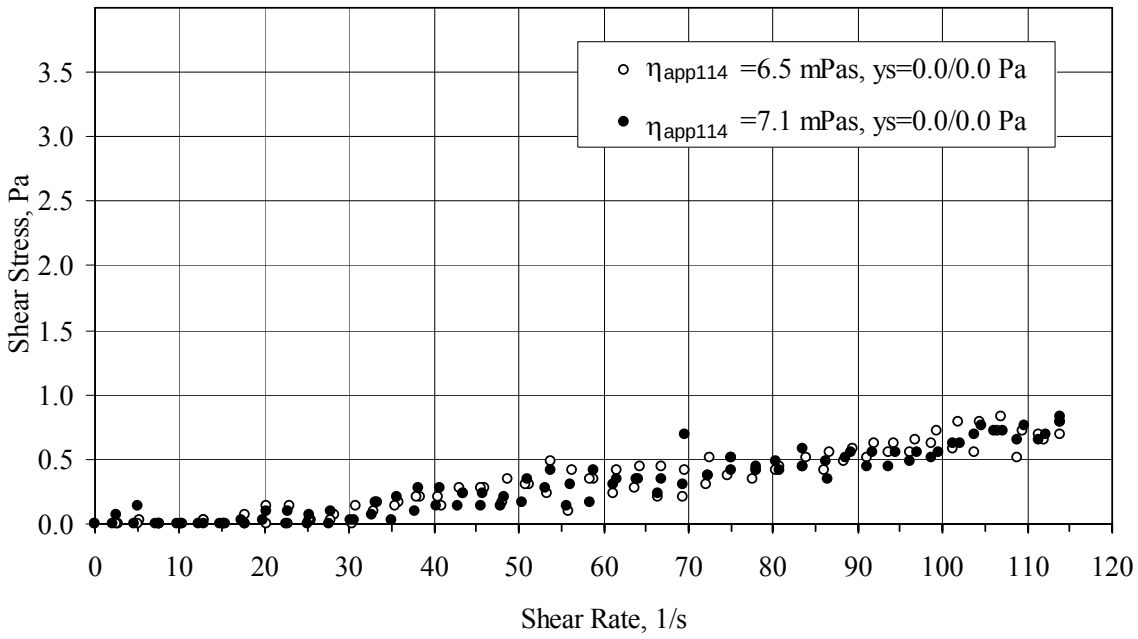

Figure I-3: Reproducibility of flow curves for pure quartz slurries. Testing conditions: 45 wt% solid, pH 10.0, 50 °C, 0.001M $CaCl_2$. Average standard deviation of shear stress= 0.03 Pa.

Figures I-4 shows duplicate flow curves of experiments performed on slurries of bitumen-coated quartz 10 wt% bitumen. It can be seen that the average standard deviation is 0.2 Pa.

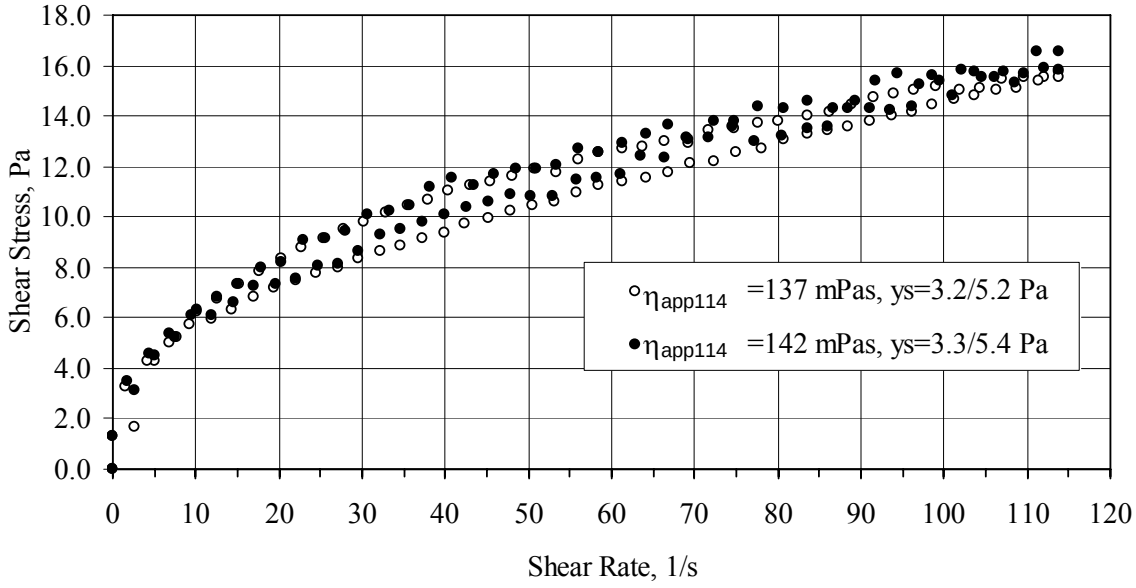

Figure I-4: Reproducibility of flow curves for slurries of bitumen-coated quartz 10 wt% bitumen. Testing conditions: 45 wt% solid, pH 8.5, 50 °C, in solution using 0.01M NaCl and 0.001M $CaCl_2$. Average standard deviation of shear stress= 0.2 Pa.

Appendix II: Constants obtained from flow curve modeling

Table II.1: Bingham, Herschel-Bulkley and Casson parameters obtained from flow curve modeling of pure quartz slurries (Part I).

Solid Conc.	**wt%**	35	35	35	35	45	35	35	35	35	35
NaCl	**mol/L**	0.01	0.01	0.01	0.01	0.01	0	0.01	0	0	0
KCl	**mol/L**	0	0	0	0	0	0	0	0.01	0.01	0.01
$CaCl_2$	**mol/L**	0.001	0.001	0.001	0.001	0.001	0.001	0	0.001	0.001	0.001
pH		10.0	10.0	10.0	6.0	10.0	10.0	10.0	10	10	10
T	**°C**	50	35	25	50	50	50	50	50	35	25
Bitumen Conc.	**wt%**	0	0	0	0	0	0	0	0	0	0
τ_B	Pa	0.0	0.0	0.0	0.6	0.0	0.0	0.0	0.0	0.0	0.0
η_p	Pas	0.005	0.005	0.008	0.005	0.007	0.005	0.005	0.006	0.007	0.008
R^2		0.93	0.94	0.96	0.81	0.95	0.91	0.95	0.95	0.98	0.98
τ_{HB}	Pa	0.0	0.0	0.0	0.2	0.0	0.0	0.0	0.0	0.0	0.0
K_{HB}		0.000	0.001	0.003	0.189	0.002	0.003	0.003	0.003	0.003	0.008
n		1.51	1.40	1.22	0.32	1.29	1.12	1.12	1.12	1.21	1.00
R^2		0.96	0.96	0.98	0.90	0.97	0.92	0.95	0.96	0.99	0.98
τ_{CY}	Pa	0.0	0.0	0.0	0.5	0.0	0.0	0.0	0.0	0.0	0.0
η_C	Pas	0.005	0.005	0.008	0.001	0.007	0.005	0.005	0.005	0.007	0.008
R^2		0.93	0.94	0.96	0.87	0.95	0.91	0.95	0.95	0.98	0.98
ys Average	Pa	0.0	0.0	0.0	0.4	0.0	0.0	0.0	0.0	0.0	0.0
ys Maximum	Pa	0.0	0.0	0.0	0.6	0.0	0.0	0.0	0.0	0.0	0.0

Table II.2: Bingham, Herschel-Bulkley and Casson parameters obtained from flow curve modeling of pure quartz slurries (Part II).

Solid Conc.	**wt%**	35	45	35	35	45	45	45	45	45	45
NaCl	**mol/L**	0	0	0	0	0.01	0.01	0.01	0	0.01	0
KCl	**mol/L**	0.01	0.01	0	0.01	0	0	0	0	0	0.01
$CaCl_2$	**mol/L**	0.001	0.001	0.001	0	0.001	0.001	0.001	0.001	0	0.001
pH		6.0	10.0	10.0	10.0	6.0	6.0	6.0	6	6	6
T	**°C**	50	50	50	50	50	35	25	50	50	50
Bitumen Conc.	**wt%**	0	0	0	0	0	0	0	0	0	0
τ_B	Pa	0.6	0.0	0.0	0.0	1.8	1.8	1.8	1.6	1.4	2.3
η_p	Pas	0.006	0.007	0.005	0.005	0.010	0.010	0.012	0.010	0.008	0.011
R^2		0.90	0.98	0.94	0.93	0.62	0.65	0.75	0.69	0.70	0.64
τ_{HB}	Pa	0.3	0.0	0.0	0.0	0.4	0.5	0.6	0.5	0.5	1.2
K_{HB}		0.122	0.003	0.000	0.000	0.910	0.816	0.703	0.741	0.511	0.600
n		0.41	1.20	1.56	1.56	0.19	0.21	0.26	0.22	0.25	0.27
R^2		0.94	0.99	0.98	0.97	0.87	0.87	0.91	0.90	0.89	0.87
τ_{CY}	Pa	0.5	0.0	0.0	0.0	1.4	1.5	1.5	1.4	1.1	1.8
η_C	Pas	0.002	0.007	0.005	0.005	0.002	0.002	0.002	0.002	0.002	0.002
R^2		0.94	0.98	0.94	0.93	0.73	0.75	0.84	0.78	0.80	0.75
ys Average	Pa	0.5	0.0	0.0	0.0	1.2	1.2	1.3	1.2	1.0	1.8
ys Maximum	Pa	0.6	0.0	0.0	0.0	1.8	1.8	1.8	1.6	1.4	2.3

Table II.3: Bingham, Herschel-Bulkley and Casson parameters obtained from flow curve modeling of pure quartz slurries (Part III).

Solid Conc.	**wt%**	45	45	45	45	45	45	45	45	45	45
NaCl	**mol/L**	0	0	0	0	0.01	0.01	0	0.01	0	0
KCl	**mol/L**	0.01	0.01	0	0.01	0	0	0	0	0.01	0.01
$CaCl_2$	**mol/L**	0.001	0.001	0.001	0	0.001	0.001	0.001	0	0.001	0.001
pH		6.0	6.0	6.0	6.0	8.5	8.5	8.5	8.5	8.5	8.5
T	**°C**	35	25	50	50	50	25	50	50	50	25
Bitumen Conc.	**wt%**	0	0	0	0	0	0	0	0	0	0
τ_B	Pa	2.3	2.3	1.6	1.8	0.6	1.1	0.4	0.0	1.3	1.6
η_p	Pas	0.011	0.014	0.010	0.009	0.007	0.009	0.008	0.010	0.008	0.010
R^2		0.71	0.75	0.71	0.68	0.78	0.80	0.92	0.94	0.65	0.74
τ_{HB}	Pa	1.3	1.4	0.7	0.9	0.2	0.8	0.0	0.0	0.2	0.6
K_{HB}		0.484	0.446	0.533	0.554	0.222	0.102	0.171	0.014	0.766	0.583
n		0.31	0.35	0.27	0.26	0.34	0.51	0.41	0.92	0.19	0.26
R^2		0.90	0.90	0.89	0.89	0.84	0.87	0.94	0.93	0.84	0.91
τ_{CY}	Pa	1.8	1.8	1.3	1.5	0.4	0.8	0.2	0.0	1.1	1.3
η_C	Pas	0.002	0.003	0.002	0.002	0.003	0.002	0.003	0.010	0.002	0.002
R^2		0.81	0.84	0.80	0.78	0.82	0.87	0.94	0.94	0.73	0.83
ys Average	Pa	1.8	1.8	1.2	1.4	0.4	0.9	0.2	0.0	0.9	1.2
ys Maximum	Pa	2.3	2.3	1.6	1.8	0.6	1.1	0.4	0.0	1.3	1.6

Table II.4: Bingham, Herschel-Bulkley and Casson parameters obtained from flow curve modeling of pure quartz slurries (Part IV).

Solid Conc.	**wt%**	45	45	45	45	45	45	45	45	45	45
NaCl	**mol/L**	0	0	0.01	0.01	0	0.01	0	0	0	0
KCl	**mol/L**	0	0.01	0	0	0	0	0.01	0.01	0	0.01
$CaCl_2$	**mol/L**	0.001	0	0.001	0.001	0.001	0	0.001	0.001	0.001	0
pH		8.5	8.5	10.0	10.0	10.0	10.0	10.0	10	10	10
T	**°C**	50	50	50	25	50	50	50	25	50	50
Bitumen Conc.	**wt%**	0	0	0	0	0	0	0	0	0	0
τ_B	Pa	0.5	0.9	0.0	0.0	0.0	0.0	0.0	0.0	0.0	0.0
η_p	Pas	0.008	0.006	0.005	0.008	0.006	0.006	0.007	0.010	0.006	0.006
R^2		0.89	0.70	0.92	0.95	0.90	0.93	0.94	0.93	0.90	0.90
τ_{HB}	Pa	0.1	0.2	0.0	0.0	0.0	0.0	0.0	0.0	0.0	0.0
K_{HB}		0.131	0.379	0.001	0.001	0.001	0.001	0.001	0.012	0.001	0.001
n		0.45	0.26	1.51	1.42	1.36	1.45	1.40	0.95	1.46	1.55
R^2		0.91	0.85	0.95	0.97	0.91	0.95	0.96	0.93	0.91	0.93
τ_{CY}	Pa	0.3	0.5	0.0	0.0	0.0	0.0	0.0	0.0	0.0	0.0
η_C	Pas	0.003	0.003	0.006	0.008	0.006	0.005	0.007	0.010	0.006	0.006
R^2		0.91	0.77	0.92	0.95	0.90	0.93	0.94	0.93	0.90	0.90
ys Average	Pa	0.3	0.5	0.0	0.0	0.0	0.0	0.0	0.0	0.0	0.0
ys Maximum	Pa	0.5	0.9	0.0	0.0	0.0	0.0	0.0	0.0	0.0	0.0

Table II.5: Bingham, Herschel-Bulkley and Casson parameters obtained from flow curve modeling of slurries of bitumen-quartz mixtures (Part I).

Solid Conc.	**wt%**	45	45	45	45	45	45	45	45	45	45	45
NaCl	**mol/L**	0.01	0.01	0	0.01	0	0.01	0.01	0	0.01	0	0.01
KCl	**mol/L**	0	0	0	0	0.01	0	0	0	0	0.01	0
$CaCl_2$	**mol/L**	0.001	0.001	0.001	0	0.001	0.001	0.001	0.001	0	0.001	0.001
pH		6.0	6.0	6.0	6.0	6.0	8.5	8.5	8.5	8.5	8.5	10.0
T	**°C**	50	25	50	50	50	50	25	50	50	50	50
Bitumen Conc.	**wt%**	10	10	10	10	10	10	10	10	10	10	10
τ_B	Pa	26.3	32.6	24.1	16.4	34.1	5.2	19.9	4.3	5.0	12.1	0.3
η_p	Pas	0.224	0.273	0.247	0.184	0.230	0.101	0.259	0.101	0.096	0.139	0.050
R^2		0.65	0.67	0.62	0.84	0.49	0.90	0.70	0.91	0.91	0.80	0.99
τ_{HB}	Pa	9.9	11.8	9.7	6.9	15.0	1.2	5.0	0.0	0.0	4.0	0.0
K_{HB}		8.824	11.06	8.704	4.310	10.03	1.499	7.106	1.699	2.055	3.594	0.099
n		0.31	0.31	0.31	0.40	0.31	0.48	0.37	0.46	0.42	0.39	0.86
R^2		0.83	0.86	0.85	0.94	0.67	0.97	0.84	0.97	0.98	0.90	0.99
τ_{CY}	Pa	19.9	24.6	17.8	11.8	26.8	3.2	13.6	2.5	3.0	8.4	0.0
η_C	Pas	0.062	0.076	0.075	0.059	0.056	0.044	0.093	0.047	0.043	0.047	0.043
R^2		0.75	0.78	0.74	0.91	0.59	0.95	0.79	0.95	0.96	0.87	0.99
ys Average	Pa	18.7	23.0	17.2	11.7	25.3	3.2	12.8	2.3	2.7	8.2	0.1
ys Maximum	Pa	26.3	32.6	24.1	16.4	34.1	5.2	19.9	4.3	5.0	12.1	0.3

Table II.6: Bingham, Herschel-Bulkley and Casson parameters obtained from flow curve modeling of slurries of bitumen-quartz mixtures (Part II).

Solid Conc.	**wt%**	45	45	45	45	45	45	45	45	45
NaCl	**mol/L**	0.01	0	0.01	0	0.01	0.01	0.01	0.01	0
KCl	**mol/L**	0	0	0	0.01	0	0	0	0	0
$CaCl_2$	**mol/L**	0.001	0.001	0	0.001	0.001	0.001	0.001	0.001	0.001
pH		10.0	10.0	10.0	10.0	6.0	10.0	8.5	8.5	8.5
T	**°C**	25	50	50	50	50	50	50	25	50
Bitumen Conc.	**wt%**	10	10	10	10	5	5	5	5	5
τ_B	Pa	5.2	0.3	0.1	2.9	25.0	1.1	5.2	18.7	5.3
η_p	Pas	0.170	0.059	0.034	0.089	0.200	0.042	0.069	0.188	0.070
R^2		0.94	0.99	0.99	0.95	0.57	0.95	0.86	0.80	0.86
τ_{HB}	Pa	0.0	0.0	0.0	0.0	9.6	0.0	0.0	5.0	2.0
K_{HB}		1.837	0.102	0.045	0.954	11.77	0.348	2.544	6.858	1.334
n		0.53	0.89	0.95	0.54	0.22	0.59	0.33	0.33	0.43
R^2		0.99	0.99	0.99	0.99	0.79	0.98	0.97	0.93	0.95
τ_{CY}	Pa	2.6	0.0	0.0	1.4	19.9	0.5	3.5	13.6	3.5
η_C	Pas	0.093	0.052	0.032	0.049	0.045	0.025	0.025	0.058	0.026
R^2		0.98	0.99	0.99	0.98	0.67	0.98	0.93	0.88	0.92
ys Average	Pa	2.6	0.1	0.0	1.4	18.2	0.5	2.9	12.4	3.6
ys Maximum	Pa	5.2	0.3	0.1	2.9	25.0	1.1	5.2	18.7	5.3

Table II.7: Bingham, Herschel-Bulkley and Casson parameters obtained from flow curve modeling of slurries of bitumen-quartz mixtures (Part III).

Solid Conc.	**wt%**	45	45	45	45	45	45	45	45	45
NaCl	**mol/L**	0.01	0	0.01	0.01	0.01	0.01	0	0.01	0
KCl	**mol/L**	0	0.01	0	0	0	0	0	0	0.01
$CaCl_2$	**mol/L**	0	0.001	0.001	0.001	0.001	0.001	0.001	0	0.001
pH		8.5	8.5	6.0	10.0	8.5	8.5	8.5	8.5	8.5
T	**°C**	50	50	50	50	50	25	50	50	50
Bitumen Conc.	**wt%**	5	5	1	1	1	1	1	1	1
τ_B	Pa	4.9	9.0	10.0	0.1	2.8	5.2	2.7	2.3	4.9
η_p	Pas	0.065	0.080	0.041	0.016	0.030	0.063	0.029	0.031	0.032
R^2		0.86	0.81	0.60	0.96	0.86	0.87	0.84	0.89	0.77
τ_{HB}	Pa	2.9	4.0	5.0	0.0	1.1	2.0	1.5	1.0	2.5
K_{HB}		0.697	2.353	3.001	0.034	0.743	1.363	0.507	0.521	1.268
n		0.53	0.36	0.24	0.85	0.39	0.41	0.45	0.46	0.32
R^2		0.94	0.94	0.88	0.97	0.98	0.97	0.95	0.98	0.93
τ_{CY}	Pa	3.3	6.7	8.4	0.0	2.0	3.6	2.0	1.6	3.9
η_C	Pas	0.024	0.023	0.007	0.014	0.010	0.022	0.009	0.011	0.007
R^2		0.92	0.89	0.73	0.97	0.94	0.94	0.92	0.95	0.86
ys Average	Pa	3.7	6.6	7.8	0.0	1.9	3.6	2.1	1.6	3.8
ys Maximum	Pa	4.9	9.0	10.0	0.1	2.8	5.2	2.7	2.3	4.9